



Cairo University

# **INTRA-CORTICAL MICROELECTRODE WITH MEMS TECHNOLOGY**

By

**Hebatullah Hassan Mohamed Draz**

A Thesis Submitted to the  
Faculty of Engineering at Cairo University  
in Partial Fulfillment of the  
Requirements for the Degree of  
**DOCTOR OF PHILOSOPHY**  
in  
**Electronics and Communications Engineering**

FACULTY OF ENGINEERING, CAIRO UNIVERSITY  
GIZA, EGYPT  
2019

# **INTRA-CORTICAL MICROELECTRODE WITH MEMS TECHNOLOGY**

By

**Hebatullah Hassan Mohamed Draz**

A Thesis Submitted to the  
Faculty of Engineering at Cairo University  
in Partial Fulfillment of the  
Requirements for the Degree of  
**DOCTOR OF PHILOSOPHY**

in

**Electronics and Communications Engineering**

Under the Supervision of

**Prof. Dr. Mohamed Fathy Abu El-  
Yazeed El-Barrawy**

**Prof. Dr. Amal Zaki**

Professor  
Electronics & Communication Dept.,  
Faculty of Engineering, Cairo University

Professor  
VLSI  
Electronics Research Institute

**Dr. Hassan Mostafa**

Assistant Professor  
Electronics & Communication Dept.,  
Faculty of Engineering, Cairo University

FACULTY OF ENGINEERING, CAIRO UNIVERSITY  
GIZA, EGYPT  
2019

# **INTRA-CORTICAL MICROELECTRODE WITH MEMS TECHNOLOGY**

By  
**Hebatullah Hassan Mohamed Draz**

A Thesis Submitted to the  
Faculty of Engineering at Cairo University  
in Partial Fulfillment of the  
Requirements for the Degree of  
**DOCTOR OF PHILOSOPHY**  
in  
Electronics and Communication Engineering

Approved by the  
Examining Committee

---

**Prof. Dr. Mohamed Fathy Abu-Elyazeed, Thesis Main Advisor**

---

**Dr. Hassan Mostafa, Advisor**

---

**Prof. Dr. Mohamed Ryad Elghonemy, Internal Examiner**

---

**Prof. Dr. Elsayed Mostafa Saad, External Examiner**  
Electronics department, Helwan University

FACULTY OF ENGINEERING, CAIRO UNIVERSITY  
GIZA, EGYPT  
2019

**Engineer's Name:** Hebatullah Hassan Mohamed Draz  
**Date of Birth:** 21/9/1984  
**Nationality:** Egyption  
**E-mail:** hdraz@eri.sci.eg  
**Phone:** 01005037094  
**Address:** 6090 at 58St. from 9St. Elmokatam  
**Registration Date:** 1/10/2014  
**Awarding Date:** 2019  
**Degree:** Doctor of Philosophy  
**Department:** Electronics and Communication Engineering

Insert photo here

**Supervisors:**

Prof. Mohamed Fathy Abu-Elyazeed.  
Prof. Amal Zaki.  
Dr. Hassan Mostafa.

**Examiners:**

Porf. Mohamed Fathy Abu-Elyazeed.  
Dr. Hassan Mostafa  
Prof. Mohamed Ryad Elghonemy (Internal examiner)  
Prof. Elsayed Mostafa Saad (External examiner)  
Electronics department, Helwan University

**Title of Thesis:**

INTRA-CORTICAL MICROELECTRODE WITH MEMS TECHNOLOGY

**Key Words:**

DBS Electrode; MEMS Fabrication; Optrode; Figure of Merit; Comsol

**Summary:**

In electrophysiological procedures, Microelectrodes are used as main elements in functional electric stimulation (FES) systems. They establish an interface with the individual neurons and record the brain activities and communications, then modulate neuron behavior through stimulation. Several modifications and innovations are progressed through Microelectrode to improve their functionality and usability. In this research, intra-cortical microelectrodes are introduced with design methodology and fabrication processes for capable of achieving a wide range of design requirements and applications.

## **Acknowledgments**

Foremost, all thanks are due to Almighty, the most merciful Allah. Allah blessed me and gave me the strength to finish this study while taking care of my family.

Prof. Amal, Prof. M. Fathey and Dr Hassan Mostafa, my thesis supervisors, have guided my work insightfully and enriched my research with his fruitful experience. Special thanks for trusting me and providing such a flexible working environment.

My parents have supported me with their love, care and prayers. They have always encouraged me and stood by my side taking care of my little children. Owing them my success, I will never be able to thank them enough. To them, I would like to express my sincere thanks.

My husband, Ahmed Abd-Elghafour, deserves a special acknowledgement. He has always encouraged me and stood by my side taking care of our little children. I would never have completed this work without his support. Also my friends (Omnia and Mervat), and my niece Radwa, have supported me unconditionally.

Thanks to all my family members and friends.

# **Dedication**

To my father, and mother.

We did it again, without your unconditional love, support, sacrifice and prayers I wouldn't have gone so far, and yet more to come.

# Table of Contents

<b>ACKNOWLEDGMENTS</b> .....	<b>I</b>
<b>DEDICATION</b> .....	<b>II</b>
<b>TABLE OF CONTENTS</b> .....	<b>III</b>
<b>LIST OF TABLES</b> .....	<b>VI</b>
<b>LIST OF FIGURES</b> .....	<b>VII</b>
<b>LIST OF ABBREVIATIONS</b> .....	<b>IX</b>
<b>ABSTRACT</b> .....	<b>XI</b>
<b>CHAPTER 1 : INTRODUCTION</b> .....	<b>1</b>
1.1.MOTIVATION .....	2
1.2.RESEARCH OBJECTIVE .....	2
1.3.THESIS OUTLINE.....	3
<b>CHAPTER 2 : LITERATURE SURVEY</b> .....	<b>4</b>
2.1.INTRODUCTION .....	4
2.2.NEURO-ENGINEERING.....	4
2.3.ELECTROTHERAPEUTIC TECHNIQUES AND ITS APPLICATIONS .....	7
2.4.INTRA-CORTICAL ELECTRODE DEVELOPMENT .....	9
2.4.1.Glass Micropipettes.....	10
2.4.2.Multisite recording.....	11
2.4.2.1.Micro-wire.....	12
2.4.3.Thin film technology (Micromachined).....	12
2.4.3.1.Single shaft electrode (Silicon based).....	13
2.4.3.2.Needle arrays.....	14
2.4.3.2.1.Utah Electrode Array (UEA).....	16
2.4.3.2.2.Microwire Microelectrode Array.....	16
2.4.3.3.Multi-shaft electrodes.....	16
2.4.3.3.1.Michigan Electrode Array (MEA) .....	17
2.4.3.3.2.Double Side Penetrating Neural Electrode Array.....	18
2.4.3.4.Flexible electrode.....	19
2.4.3.5.Cuff Electrodes.....	22
2.4.3.6.Optrode.....	22
2.4.3.7.Noninvasive Deep Brain Stimulation .....	23
2.5.CONSIDERATION TO CHECK ELECTRODES .....	25
2.5.1.Tissue distortion .....	25
2.5.2.Pads structure.....	25
2.5.3.Mechanical Failure .....	26
2.5.4.Comsol Multiphysics software program.....	26
2.5.5.Materials of electrode.....	29
2.6.MEMS.....	29
2.7.CONCLUSION .....	31
<b>CHAPTER 3 : RATS ELECTRODES</b> .....	<b>32</b>
3.1.ELECTRODE FORCES AND FAILURE MODELS (MECHANICAL ANALYSIS).....	32

3.1.1. Forces acting on the electrode .....	32
3.1.2. Modes of mechanical failure .....	33
3.2. ELECTRODE PROTOTYPES AND MECHANICAL ANALYSIS.....	33
3.2.1. Electrode prototypes .....	33
3.2.2. Electrode mechanical analysis.....	35
3.2.2.1. Buckling analysis .....	35
3.2.2.2. Fracture.....	35
3.3. ANALYSIS RESULTS.....	36
3.3.1. Linear buckling.....	36
3.3.2. Axial loading .....	39
3.3.3. Shear loading .....	40
3.3.4. FOM.....	41
3.3.5. Results of different stages .....	42
3.4. ELECTRICAL SIMULATION .....	48
3.4.1. Pads.....	48
3.5. CONCLUSION .....	51
<b>CHAPTER 4 : HUMAN ELECTRODES .....</b>	<b>52</b>
4.1. ELECTRODE DIMENSIONS AND PROTOTYPE .....	52
4.2. LINEAR BUCKLING ANALYSIS .....	57
4.3. FRACTURE ANALYSIS.....	57
4.3.1. Axial Stress Analysis .....	60
4.3.2. Shear Stress Analysis.....	61
4.3.3. Figure of Merit.....	62
4.3.4. Electrode design insights .....	63
4.4. ELECTRICAL SIMULATION .....	64
4.4.1. One Metal Layer.....	64
4.4.2. Two Metal Layer.....	66
4.5. CONCLUSION .....	66
<b>CHAPTER 5 : OPTRODE .....</b>	<b>67</b>
5.1. OPTRODES.....	67
5.2. DIFFERENT TYPES OF OPTRODE .....	68
5.2.1. $\mu$ LED.....	71
5.3. SIMULATIONS .....	75
5.3.1. $\mu$ LED simulations .....	76
5.4. OVER ALL MODEL SIMULATION .....	83
5.4.1. Electric field.....	83
5.4.2. Thermal Analysis .....	84
5.5. CONCLUSION .....	84
<b>CHAPTER 6 : FABRICATION.....</b>	<b>86</b>
6.1. LAYOUTS.....	86
6.1.1. One Metal Layer .....	86
6.1.1.1. Fabrication Steps .....	88
6.1.1.1.1. RCA cleaning .....	88
6.1.1.1.2. Dielectric Layer.....	89
6.1.1.1.3. Lithography.....	94
6.1.2. Two Metal Layer.....	100
6.1.2.1. Fabrication Steps .....	102



6.2.PCB .....	105
6.3.TEST ON RAT .....	109
<b>DISCUSSION AND CONCLUSIONS.....</b>	<b>112</b>
<b>REFERENCES.....</b>	<b>113</b>
<b>APPENDIX A: ONE APPENDIX .....</b>	<b>119</b>
<b>APPENDIX B: .....</b>	<b>120</b>
<b>APPENDIX C: .....</b>	<b>121</b>
<b>APPENDIX D: .....</b>	<b>122</b>

## List of Tables

Table 3. 1: Safety factor for different layouts: fixed-free linear buckling analysis .....	37
Table 3. 2: Parameters .....	49
Table 3. 3: DC resistance for different materials .....	49
Table 3. 4 Dc Resistance with Several Thickness and Length .....	51
Table 4. 1: Linear Buckling Safety Factor Results .....	59
Table 4. 2: Axial Stress Safety Factor Results .....	60
Table 4. 3 DESIGN E WITH BEZIER POLYGONS .....	62
Table 4. 4: Shear stress safety factor results .....	63
Table 5.1 Properties of the monolithic probe .....	75
Table 5. 2 Voltage vs. Current .....	78

# List of Figures

Figure 2. 1: Physical representation of recording electrodes [19].	6
Figure 2. 2 Glass Micropipette [32].	11
Figure 2. 3 Micro-wire (Niotrode electrode array) [34]	12
Figure 2. 4 Microprobe with 4 channels [39]	13
Figure 2. 5 Two different types of Molybdenum single shaft electrodes [15].	14
Figure 2. 6 Ceramic electrode [15]	14
Figure 2. 7 Left: 3D Pyramid array, Right: Same length of Needles [40]	15
Figure 2. 8 1141 pins of titanium electrode [43]	16
Figure 2. 9 Left: Utah array, Right: 3D microelectrode array [45]	17
Figure 2. 10 Multi-shaft recording electrode [45]	18
Figure 2. 11 Left: Michigan probe: Basic structure of micromachined microelectrode, Right: four-shank electrodes (MEA) [15]	19
Figure 2. 12 Microscale Implantable Neural Interface with single probe [15]	20
Figure 2. 13 Dual sided electrode and multilayer with Caltech [44]	20
Figure 2. 14 Flexible parylene-based electrodes [32].	21
Figure 2. 15 parylene-based multi-sided MEA [34]	21
Figure 2. 16 Nerve Cuff Electrode [53].	22
Figure 2. 17 Effect of A. DBS, B. Optrode on neurons [52]	23
Figure 2. 18 The Optrode system.	23
Figure 2. 19 Noninvasive Deep Brain Stimulation Electrode [54]	24
Figure 2. 20 AC/DC Module.	28
Figure 3. 1 Forces affecting the electrode. There are three mechanical forces acting on the electrode, these forces are outlined on this free body diagram	33
Figure 3. 2: Several layout designs of the electrodes labeled as Prototype a, b, c, d, e, f, g, h and i	34
Figure 3. 3: Illustrates the values of critical loads with different designs and materials with fixed thickness of 100 $\mu\text{m}$	38
Figure 3. 4: The effect of different base width on the critical load (design E with Polyimide material)	39
Figure 3. 5: The distortion with very large base (design E with Polyimide material)	39
Figure 3. 6: The log diagram for safety factor with axial load the different results of safety factors with axial load for different designs with different materials and fixed thickness	40
Figure 3. 7: The log diagram for safety factor with shear load illustrates the different results of safety factors with shear load for different designs with different materials and fixed thickness.	41
Figure 3. 8: FOM for several designs with different materials	42
Figure 3. 9: 4 different prototypes of electrodes	43
Figure 3. 10: Safety Factor with Buckling Analysis	44
Figure 3. 11: Design A with different number of stages	44
Figure 3. 12: Safety Factor with Buckling Analysis of design A	45
Figure 3. 13: Safety Factor with Axial Load of design A	46
Figure 3. 14: Safety Factor with Axial Load	47
Figure 3. 15: Safety Factor with Shear Force	47
Figure 3. 16: model for the electrode metal structure	48

Figure 3. 17 : illustrates the DC resistance of Au with variable thickness and length of track .....	50
Figure 4. 1: The several layout designs of the electrode .....	53
Figure 4. 2: Design B with five stages, each stage wider than the following stage by 40 $\mu\text{m}$ and is double its length.....	54
Figure 4. 3: Left: Filleted Link. Right: Bzier Polygon Link .....	55
Figure 4. 4: Design E with 3 different stages length: a) longest first stage. b) Longest final stage. c) Equal stage lengths.....	56
Figure 4. 5: the max stress in different designs: (Left) Design E with fillet, (Right) Design E with Bezier polygon .....	61
Figure 4. 6: The FOM for several designs with different materials .....	64
Figure 4. 7 Interconnection pad, Stimulation pad, and track .....	65
Figure 5.1: Illustration of injection process .....	68
Figure 5. 2 Partitions of optrode .....	69
Figure 5. 3 Optrode with optical fiber .....	70
Figure 5. 4 Different shapes of fibers .....	70
Figure 5. 5 Fiber-less optrode .....	71
Figure 5. 6 $\mu\text{LED}$ array on a flexible substrate.....	72
Figure 5. 7 Optrode with a polycrystalline diamond (PCD) substrate .....	72
Figure 5. 8 Wireless optrode .....	73
Figure 5.9 Sapphire based $\mu\text{LED}$ probe .....	73
Figure 5. 10 Miniaturized SU-8 Optical Probe .....	74
Figure 5.11 Monolithically Integrated on Silicon probe .....	75
Figure 5. 12 $\mu\text{Led}$ 1D model.....	77
Figure 5. 13 Left: Current vs. voltage @50x50. Right: 200x200 (area) .....	77
Figure 5.14 Emission Rate of the $\mu\text{LED}$ .....	79
Figure 5. 15 The emission rate due to 1 $\mu\text{A}$ .....	79
Figure 5. 16 Emission Spectrum (power per unit volum) .....	80
Figure 5. 17 Power per unit volume with 1 $\mu\text{A}$ .....	80
Figure 5. 18 Emission Power per unit area .....	81
Figure 5. 19 Total Emission Rate .....	82
Figure 5. 20 Efficiency of the device.....	82
Figure 5. 21 Optical Power Density .....	83
Figure 5. 22 Electric field in X and Y component.....	83
Figure 5. 23 Thermal analysis of $\mu\text{LED}$ .....	84
Figure 5. 24 Thermal analysis of $\mu\text{LED}$ with brain model .....	84
Figure 6. 1 The Layout of the electrode .....	87
Figure 6. 2 Snapshot of Contour mask .....	87
Figure 6. 3 Snapshot of Pads Mask.....	88
Figure 6. 4 Opened chamber pump of PECVD .....	90
Figure 6. 5 4inch wafer above 6inch dummy wafer .....	90
Figure 6. 6 The broken wafer after PECVD process.....	91
Figure 6. 7 Pumping window .....	92
Figure 6. 8 The window of the my recipe .....	94
Figure 6. 9 Chamber before plasma cleaning.....	95
Figure 6. 10 Wafer on Spin Coater .....	95
Figure 6. 11 Spread Photoresist .....	96

Figure 6. 12 Wafer on Hot plate .....	96
Figure 6. 13 UV process .....	97
Figure 6. 14 Wafer in developer .....	98
Figure 6. 15 Pattern under microscope.....	99
Figure 6. 16 Photoresist [89] .....	100
Figure 6. 17 Lithography .....	100
Figure 6. 18 Snapshot of the contour mask.....	101
Figure 6. 19 Mask of the first metal layer .....	101
Figure 6. 20 Vias of the layout.....	102
Figure 6. 21 Some graphs of electrode device .....	104
Figure 6. 22 Some trials to adhere wires .....	106
Figure 6. 23 The design of PCB with 2 Layers .....	107
Figure 6. 24 PCB with one metal layer .....	108
Figure 6. 25 The implemented design .....	108
Figure 6. 26 Implemented PCB.....	109
Figure 6. 27 Rat through the surgery .....	109
Figure 6. 28 Rat with cables .....	110
Figure 6. 29 Brain signal from normal rat .....	110
Figure 6. 30 The rat with seizure .....	111
Figure D. 1 Comsol model .....	122
Figure D. 2 Select Physics window .....	123
Figure D. 3 Model Builder bar.....	123
Figure D. 4 The values of the model .....	124
Figure D. 5 Plane Geometry.....	124
Figure D. 6 First step .....	125
Figure D. 7 the tip of shaft .....	125
Figure D. 8 insert the thickness.....	126
Figure D. 9 Boundary Load.....	126
Figure D. 10 Fixed Constrain.....	127

## List of Abbreviations

FDA	U.S Food and Drug Administration
WHO	World Health Organization
DBS	Deep Brain Stimulation
SCS	Spinal cord Stimulation
VNS	Vagus nerve Stimulation
FES	Functional Electrical Stimulation
BMI	Brain Machine Interface
MEMS	Micro-electro-mechanical System
MOEMS	Micro-opto-electro-mechanical System
NEMS	Nano-electro-mechanical System
ECoG	Electrocorticographic
EEG	Electroencephalographic
TMS	Transcranial Magnetic Stimulation
CS	Cortical Stimulation
PNS	Peripheral nerve Stimulation

# Abstract

Neurological disorders are diseases of the spine, brain and the nerves that connect them. There are more than 600 diseases of the nervous system, such as epilepsy, brain tumors, stroke and Parkinson's disease as well as less familiar ones such as frontotemporal dementia. Epilepsy is a brain chronic disorder described by recurrent seizure. According to statistics of the World Health Organization (WHO), more than 50 million people suffer from epilepsy in the world, and almost 80% of them live in low- and middle-income countries (LAMICs). Recently, an estimated 2.4 million people are diagnosed with epilepsy, every year. Some types of Epilepsy cannot be treated by drugs or eradication, so another types of therapy are appeared to treat these brain chronic disorders. Neuro-engineering is a type of science which appears to treat with the neurological disorder, it is also considered as one type of emerging multi-disciplinary domain. It investigates the electrophysiological activities of the nervous system. It explores the functions of the peripheral and central nervous systems, and provides some techniques and procedures to characterize and analyze several functions of the different components of the nervous system, and that allows to manipulate their behavior through intra-cortical recording and stimulation. It also develops unconventional therapeutic techniques for treating several types of neurological disorders and recovering lost sensory or motor functions.

In electrophysiological procedures, Microelectrodes are used as main elements in functional electric stimulation (FES) systems. They establish an interface with the individual neurons and record the brain activities and communications, then modulate neuron behavior through stimulation. Several modifications and innovations are progressed through Microelectrode to improve their functionality and usability. However, moreover developments are progressed to conventional electrode technologies, and enhancement in microelectrodes technology will progress to improve the neuro-interfacing and electrotherapeutic techniques.

This research introduces design methodology for intra-cortical microelectrodes which achieves a wide range of design requirements and applications. The aim of this research is developing and implementing several designs to be suitable for different neuro-interfacing applications. The research illustrates some different deigns to be suitable for rats' brain and humans' brain. It presents a novel design of Deep brain Stimulation electrode (DBS) and shows its mechanical and electrical behaviors.

Another type of intra-cortical microelectrodes – the ‘optrode’ – is introduced which is used in treating with neurological disorders but by using light in the stimulation process for the neurons instead of electrical signal. In this research optrode with  $\mu$ LED is exposed and modified with a new design to be suitable with humans' brain. MEMS technology is used to fabricate the DBS electrode design and some of the fabrication steps are illustrated for two different designs with different materials. Finally, practical considerations including assembly and interconnection to external circuitry are addressed in this research.

The fabrication is made in the Yousef Jamel Science and Technology Research Center (YJ-STRC) of the School of Sciences and Engineering (SSE) in The American University in Cairo. And the testing of the fabricated electrode is made in the faculty of science in Cairo University.

# Chapter 1 : Introduction

The brain is the most complex member in our body. It contains numerous neurons cell which transfer information using electrical signals. These electrical signals are used to understand the functions of neurons in the brain and to study the functional connectivity among brain regions. In the British Medical Journal, in 1875 [1], R. Caton reported continuous electrical wave of the cerebral cortex then in 1924 [2], H. Berger published the first human electroencephalogram (EEG) [3][4]. Developments and discoveries have continued in this field till now. Nowadays, using various measurement techniques to obtain the electrical signals of the brain such as EEG, local field potential (LFP), electrocorticogram (ECoG), single-unit recording and multi-unit recording. On the other hand, the application of electric charges has been used in therapeutic practices ever since discovering features of electricity. The first time of using the chronic clinical electrotherapeutic techniques in cardiac pacemakers was in the 50's. As a result of the enhancement in the experiments on sound perception with electrode implantation, the development of cochlear prosthesis was appeared. In 1966, the stimulation of the visual cortex was started by David Hubel and Torsten Wiesel [5]. They provided a quantum step in understanding the visual system. In the 70's, spinal cord stimulation (SCS) was used to treat the chronic pain [6]. The Neural Prosthesis Program started a multidisciplinary research to develop the technologies which were used to restore motor function to paralyzed individuals and the main goals were to study neural interface development, biomaterials, and electrode-tissue interaction to develop visual and cochlear prosthesis, and also the control of motor functions, in 1972 by Corbin [7][8]. In France 1987 was the first appearance of deep brain stimulation (DBS) by Benabid et.al [9] and research presented the relation between movement disorders and subthalamic-nucleus (STN) in the basal ganglia. In 1997, FDA approved to use the electrodes and stimulators in the stimulation of the thalamus to treat the movement disorders [10]. It was implemented in about 20,000 patients by Medtronic.

Neurophysiologic investigation depends on the studies of the neural system architecture and information processing. It also requires long-term simultaneous recording of cortical neuron populations. At the beginning of the appearance of the exploration of brain functions, recording was limited to single cell recording because of the technological constraints. These constraints prevented producing multi-channel recording electrodes. Then the advancement of silicon microfabrication and microelectronics industry introduced thin-film electrodes which allowed the production of multisite recording microprobes. Deep brain stimulation includes using a pacemaker-like device to transfer constant electrical stimulation to defect areas within the brain. Over 40,000 people with essential tremor and Parkinson's disease has been treated by DBS worldwide and is presently undergoing clinical trials as a treatment for obsessive-compulsive and depression disorder [11]. In this year 2019, The first patient has been treated from epilepsy with a complete Deep Brain Stimulation (DBS) system surgically implanted for [12]. When medicines don't work, DBS can be used to treat people 18 years or older with uncontrolled focal seizures. Uncontrolled seizures is known as drug resistant seizures. They are considered as seizures that do not respond to appropriate trials of seizure medicines [13].



DBS is also considered as a solution for patients whose seizures are not able to be remedied with other types of epilepsy surgery. The mission of the DBS is to overcome the challenges of living with epilepsy and to accelerate therapies to stop seizures, and save lives.

This research presents the electrode design problem from the engineering prospective. The research explores different parameters which allow to find a suitable electrode performance. Several designs are proposed to get reliable long-term recording and stimulation electrodes. Wide range of materials are experimented in fabricating different electrode components, and various electrode geometries are offered to minimize tissue trauma and displacement.

## **1.1. Motivation**

There are some inevitable needs to develop new generation of electrodes that would enhance functionality by adding more capabilities, and improving biocompatibility to create suitable electrodes for vivo and chronic applications. The enhanced electrodes should provide minimal tissue damage when access to neurons, allow high dense multisite stimulation of cortical columns, and provide high positional accuracy [14]. The delivered electrodes should be capable of satisfying the stringent constraints and suitable for chronic implantation to maintain proper functionality and biocompatibility [15].

Intra-cortical electrode design progress through many innovations to develop neuro-interfacing electrodes for recording and stimulation. The lack of knowledge urges to make simultaneous multisite recording of neural activities to study the population dynamics and information coding across ensembles of neurons over extended recording periods.

## **1.2. Research Objective**

The primary goal of this research is to design, fabricate intra-cortical microelectrodes capable of satisfying a wide range of constraints and design requirements. Improving functionality and biocompatibility in the developed electrodes required redesigning the conventional electrode technology through fulfilling the following objectives:

- Develop design methodology for intra-cortical microelectrodes
- Create mechanical models for the electrode to study the electrode electric performance and improve its design
- Create novel electrode layouts and architectures to implement proposed designs.
- Improve one type of intra-cortical electrode which is known as Optrode to enhance the performance of electrodes.
- Design a printed circuit board to connect the DBS with its external circuit.
- Implement the new design of DSB using MEMS technology.

### **1.3. Thesis Outline**

Chapter 1 presents a brief introduction of the brain system and its chronic disorders, then a history of therapy developments and technologies to treat these chronic disorders and the first appearance of the DBS and the diseases which it can treat them. Then outlines the research motivation and finally the objectives of the thesis. Chapter 2 provides an elaborate survey on the evolution of intra-cortical electrode design, demonstrates the history of cortical recording and stimulation electrode, and some information about the MEMS technology which are used in the fabrication process. Chapter 3 presents the structural analysis and mechanical design optimization for the proposed electrode layouts for rats using finite element analysis and modeling (FEM) and its electrical simulations. Chapter 4 exposes the structural analysis and mechanical design optimization for the proposed electrode layouts for human using (FEM) and some electrical simulation for two designs of pads. Chapter 5 introduces different types of optrodes and some simulations of electric field, temperature and the power of one design. Chapter 6 illustrates the electrode fabrication. Finally, the thesis is concluded and the future work is presented in Chapter 7.

# Chapter 2 : Literature Survey

## 2.1. Introduction

One of the chronic disorder of the brain is Epilepsy which is characterized by recurrent seizures. It has no identifiable cause and often affects people of all ages. It is also considered the fourth most common neurological disease. In all world, more than 50 million people suffer from epilepsy, and almost 80% live in low- and middle-income countries (LAMICs). Recently, an estimated 2.4 million people are diagnosed with epilepsy, every year.

Epilepsy medication is inexpensive and is influential for controlling seizures in 70% of all cases [16]. However although, in LAMICs, about three fourths of people with epilepsy do not take the treatment they need.

Antiepileptic medicines are frequently unavailable, in most LAMICs. In the same time, there are very few health care providers who take a suitable training to recognize, diagnose and treat epilepsy, in these countries. Moreover, misperceptions and poor knowledge about epilepsy will affect health-seeking behavior. Patients who have epilepsy may not have the ability to take the treatment from health care facilities and refuge to ask a help from other sources which may be ineffective. They also may not adhere to medications as prescribed or seek regular follow-up care.

Nearly 30 percent of people with epilepsy have seizures which are considered medically intractable. It is also defined as failing to be interrogated to two or more suitable chosen and taken antiseizure medications. Epilepsy surgery is a candidate solution for many of the previous patients. Yet surgical resection of their seizure focus are not good candidates for some of them, for several reasons. For this group, neuromodulation may be considered a treatment option. And to be able to innovate a new therapy which depends on neuromodulation, neuro-engineering science was appeared.

## 2.2. Neuro-Engineering

Brain is a vital part of the nervous system. It contains a large number of interconnected neurons ( $10^{11}$  neurons with  $10^{14}$  synaptic connections for human brain) [17]. Every neuron works as a basic signal processing unit that transmits and modulates information from different parts of the brain or body. The connections and their activity-dependent plasticity which induce the complex and dynamical properties of the neural system, are accepted to be the microscopic basis of many macroscopic phenomena. These properties are ranging from animal behavior to human cognition. One of the simple ways to study this information processing-storage machinery is to disorganize the system and readout its activity.

Mental and Neurological disorders affect individual quality of life by including irreversible damage to the central or peripheral nervous system. Scientists spend a great efforts to understand neurological disorders and to reduce its harm effects, however treatments for these disorders by improving a several impaired central nervous system is not considered a near-term solution. Spinal cord injuries, and Amytrophic Lateral Sclerosis (ALS) form a large part of all paralysis. These consider 17.500 new cases each year [16]. Epilepsy are diagnosed approximately 500,000 new cases each year

[18]. These examples represent a few of many neurological disorders, which affect people today.

Wherefore, Neuro-engineering appears and provides a hope to some by investigate methods for treating neurological disorders and regaining lost function. Neuro-engineering is divided into two main research venues:

1. Neurological functions are studied and some computational and experimental methods are used to quantify and form coding and information processing in motor and sensory systems.
2. Developing therapeutic techniques by using functional electrical stimulation (FES) to treat neurological disorders and provide neuro-modulation and neural augmentation to restore impaired functions.

FES provides treatment for encephalon and psychological disorders and for therapeutic technologies to restore regulate organ functionality and motor functions.

Neuroprostheses, or Neural prosthetic technologies, are designed to restore function for individuals with hearing, vision, or motor impairments. They are devices that can interface with the nervous system to transmit and receive neural information.

Neuroprostheses are used with two different ways to perform these tasks.

1. For sensory prosthetics such as retinal and cochlear implants for the blind and deaf. These prosthetics receive images from wearable cameras, and microphones and then convert it to electrical impulses which stimulate retinal or auditory nerves.
2. For neural activity in the brain of Parkinsonians, epileptic, and depressed patients. These neuroprosthesis uses functional electrical stimulation (FES) to substitute in a therapeutic way the neural activity in the brain.

To study the neural functions and activities there are some different electrodes are used with a Brain Machine Interface (BMI) which is considered an interface with the central nervous system [19]. This BMI contains four processes:

1. Recording neural activity
2. Coding the activity as an intended action
3. Controlling a device that implements the intended action
4. Giving a feedback to the subject.

These electrodes are divided to 3 types: electrocorticographic (ECoG) electrodes, electroencephalographic (EEG) electrodes, or intra-cortical microelectrode. Figure 2. 1 represents an illustration of each type of recording electrodes.

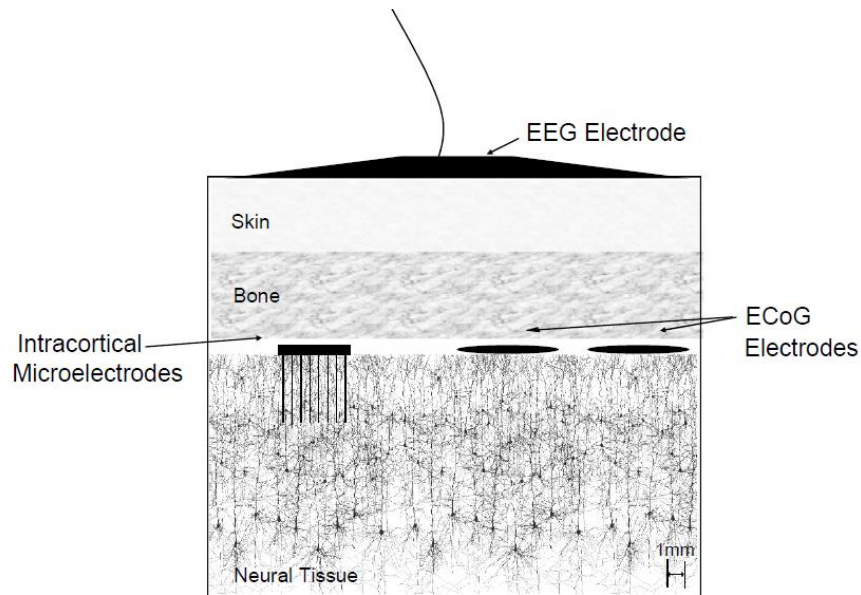


**Figure 2. 1: Physical representation of recording electrodes [19].**

Neuro-modulation is considered as a medical intervention technique. It is developed to stimulate the spinal cord, peripheral nerves, or the brain to adjust the neuron clusters activity. It can be performed by one of three ways:

1. Surgically: by ablating specific regions in the nervous system.
2. Pharmacologically: by drug infusion into cerebrospinal fluid
3. Electrically: through delivering an electric charge to the targeted neurons.

An electrical stimulation of the central, peripheral, and autonomic nervous systems is considered the standard clinical practice. Any stimulation electrode is considered deep brain Stimulation (DBS) electrode because it is implanted intra-cortical inside the brain to reach deep places. Several diseases and disorders are checked and treated by it. It is non-destructive and reversible, contrast conventional neural ablation.

The first form of electric neuro-modulators was the chronic cardiac pacemakers and galvanic [20]. After that, the DBS of the subthalamic nucleus (STN) was appeared and showed improvements in patients with Parkinson's disease, Epilepsy and Torsion Dystonia. It is used to stimulate the cortical, intra-cortical structures, deep brain, and Vagus nerve.

In 1997, vagus nerve stimulation was the first neuromodulatory therapy for epilepsy, which was approved by the FDA. Then it was followed by responsive neurostimulation (RNS), which was approved by the FDA.

DBS is considered the third neuromodulatory procedure for epilepsy treatment. It is an open-loop therapy which depends on placement of tips of DBS in the anterior nucleus of the thalamus deep into the brain for transmitting electrical stimulation on a duty cycle of one minute on and five minutes off. In April 2018, FDA approve for using the first DBS in adult. It is used in conjunction with antiepileptic medications in adults whose suffer frequent and disabling partial-onset seizures, and with patient whose have been unresponsive to three or more antiepileptic drugs.

Initially, there is a thought of as an approach best sufficient for temporal lobe epilepsy, but DBS appears to have provided benefit in patients who have various forms of focal epilepsy. These include people with epilepsy in whom the epilepsy is hard to restrict to one or two specific regions or hard to localize. Whereas RNS is mentioned

for epileptic foci within one or two places, DBS can be a useful treatment of neuromodulation in patients whose have epilepsy is more widely distributed. Similar to RNS, DBS requires placing electrodes within the brain [11].

The main study to evaluate the safety and effectiveness of DBS for epilepsy was made depending on the Stimulation of the anterior nucleus of the thalamus in epilepsy (SANTE) trial. This study implemented on 110 patients who were chosen randomly to receive sham or active stimulation [21]. By the end of three-month of blinded phase (*blinding means that the participants do not know if they are receiving the treatment or the placebo. Blinding is an important aspect of any trial done in order to avoid and prevent conscious or unconscious bias in the design and execution of a clinical trial*) [22] study, medial seizure frequency was decreased by 30 percent in the active stimulation group relative to the sham stimulation (*Sham stimulation is a generic term to indicate an inactive form of stimulation for example a very brief or weak one that is used in research to control for the placebo effect. The subject believes he/she is being stimulated normally, but there should not be any real effects*) [23] group. By the end of the blinded phase, deep brain stimulator was run with active stimulation for all patients over several follow-up years [24].

SANTE trial showed that the efficacy of DBS for seizure reduction is cumulatively growing over time with continued DBS therapy. The first year follow-up showed a median reduction in seizures of 40 percent from baseline among the 83 SANTE trial participants who continued to be followed, rising to 53 percent in three years, 69 percent in five years and 75 percent median seizures reduction in the seven-year follow-up that was presented at the American Epilepsy Society Annual Meeting in 2016. 11 percent of patients seemed seizure-free at the time of last follow-up; also, almost seizures of two-thirds of patients seemed to reduce by half. 8 percent of patients gave the impression of being not respond to DBS therapy and had an increasing in seizures greater than 50 percent through the seventh year of follow-up.

The associated serious adverse effects with DBS comprise harmful effects of surgical, including about 10 percent of patients suffered from site infection through implantation. In the SANTE trial, no patients had symptomatic intracranial hemorrhages through five-year follow-up, and there is no increased rates of unexplained sudden death in epilepsy with patients whose had the DBS device.

The past year has seen a progress in using neuromodulation for epilepsy with the April FDA approval of DBS to be used as an adjunctive treatment of medically intractable seizures in adults. the Medtronic DBS System for Epilepsy is The approved device and it is becoming available to patients at approximately 20 level IV epilepsy centers in the U.S. starting in December 2018.

DBS is one of the electrotherapeutic techniques which are used to treat some brain disorders. The next section introduces some electrotherapeutic techniques with their applications and introduces some disorders which are treated with some stimulators

### **2.3. Electrotherapeutic techniques and its applications**

The devices which are used for nervous system recording and stimulation, provide therapeutic techniques. These therapeutic techniques use neuro-modulation and neural augmentation for the diagnosis and treatment of several disorders.

The cerebral cortex facilitates the entrance to sensory perception and motor intent, and is considered as an interface for restoring neurological functions, which are lost by stroke, degenerative muscular diseases, or spinal cord injury [25]. FES also has the

ability to develop treatments for the restoration of sensory functions as visual, tactile, and vestibular senses, and also treating psychological disorders which includes depression and Obsessive-Compulsive Disorder (OCD).

Some techniques of electrotherapeutic are:

- Deep brain stimulation (DBS)
- Spinal cord stimulation (SCS)
- Vagus nerve stimulation (VNS)
- Peripheral nerve stimulation (PNS)
- Cortical stimulation (CS)
- Transcranial Magnetic Stimulation (TMS) [26]

The current neuro-modulation procedures are divided into two categories:

1. Approved by FDA:

- Pain (SCS)
- Parkinson's disease (DBS)
- Epilepsy (DBS, VNS)
- Dystonia (DBS)
- Essential Tremor (DBS)
- Depression (VNS [27], TMS [26]).

2. Investigational:

- Neuropathic pain (DBS, CS)
- Migraine headache (PNS)
- Occipital neuralgia (PNS)
- Obsessive-compulsive disorder (DBS)
- Cluster headache (DBS)
- Depression (DBS, CS)
- Obesity (DBS, CS)
- Hypertension Stroke rehabilitation (CS)
- Tourette's Disease (DBS)
- Addiction (DBS)
- Minimally-conscious state (DBS)
- Tinnitus (CS, PNS)
- Aphasia (CS)
- Parkinson's disease (CS)
- Tremor (CS).

Neuro-interfacing electrodes has the eminent role in the progress of FES-based therapeutic techniques and neuro-engineering. The improvement in the design of the electrode functionality and biocompatibility enhances the delivered therapy. During the past three decades, cranial and sub-cranial electrodes were developed for neural recording starting with simple glass micropipettes, and followed by metallic needles, and wire electrodes. Finally, micromachined microelectrodes were investigated [28]. Till now, present electrode technologies and electrotherapeutic procedures are far from being mature, so that a milieu for multitude of research activities accommodating diverse fields are created to include the developments in computational neurology, microfabrication, engineering design, material science and neurophysiology.

In the next section, an exposure of the evaluation in intra-cortical electrodes with recording and stimulation which leads finally to the stimulators as DBS.

## 2.4. Intra-Cortical electrode development

Neural electrical activities in the brain should be recorded to be able to study the neural interactions, so that intra-cortical electrodes were designed. Intra-cortical electrode designs started with the form of glass micropipettes which was considered a simple architectures then silicon needles. These designs should be stiff enough to penetrate through the dura and the pia without buckling [15]. Where dura is the tough fibrous membrane covering the brain, spinal cord and the inner surface of the skull and Pia is innermost of the three layers covering the brain and spinal cord. Micro electrodes were investigated to shrink the electrode dimensions to minimize brain tissue trauma, chronic damage, and tissue displacement [25]. The surface of the electrodes should be coated with biologically anti-fouling polymers to counteract the nonspecific affinity of proteins and to prevent cells to attach to surfaces [29]. These modifications were used to reduce tissue adhesion. Moreover, increasing the number of available channels provided more challenges. Other designs aims to improve signal-to-noise ratio (SNR) and signal quality by integrating amplifiers onto the electrode structure to amplify the signal at its source [30]. Other designs uses light sources to stimulate the neurons instead of electrical with the same shape of the intra-cortical electrode.

Several electrode designs were produced with diverse characteristics. The different classifications of the electrodes were defined according to:

- Geometry:
  - Single shaft
    - Glass micropipette
    - Single wire electrode
    - Single shaft thin-film probes
  - Multi-shank
  - Needle array
- Number of channels
  - Single Channel
    - Glass Micropipettes
    - Microelectrode
  - Multisite
    - Single shaft
    - Multi shaft
    - Needle Array
- Function
  - Recording
  - Stimulation
  - Recording and Stimulation
- Anatomical position
  - Brain tissue slice
  - Extra-neural
  - Intra-neural
  - Epidural
  - Intradural
  - Intraspinal
  - Cortical
  - Deep brain structure
- Structure
  - Stiff substrate



- Glass Micropipettes
- Multi-shank probes
- Single shaft probes
- Silicon array electrode
- Flexible substrate
  - Single wire electrodes
  - Single shaft probes
  - Flexible needle array electrode

The earliest technology was glass micropipettes electrodes which provided single channel recording. They are used for recording the brain slice activities because of its low cost and ease of fabrication, but they are not suitable for implantation and long-term applications. Micro-wire bundle electrodes appeared and replaced glass micropipettes in recording primate signal procedures. From the advancement of thin film electrodes and microfabrication technologies, microelectrode design was innovated, as a result of the potential to increase the number of recording spots [15].

### **2.4.1. Glass Micropipettes**

The glass micropipette electrodes were designed to penetrate the brain tissue. The tip had a single recording pad which was used to record a single from deep brain structures. Glass micropipettes were designed to penetrate the cell membrane for intracellular recording and these gave a better signal pickup ( $>10\text{mV}$ ) [31]. Heated glass capillary tubes were pulled into a diameter of 1 to 2 mm to fabricate these electrodes. The electrode is heated and stretched to form its sharp tips and by the temperature and the pulling force, the dimensions can be controlled [32]. The micropipette is poked through the cell membrane and filled with conductive solution such as potassium chloride KCL. Figure 2. 2 illustrated the micropipettes. Its work depended on a negative pressure was applied to mix the KCL solution with intracellular fluids to create a continuum of conductive medium. The advantages of micropipettes:

1. Low cost
2. Easy fabrication

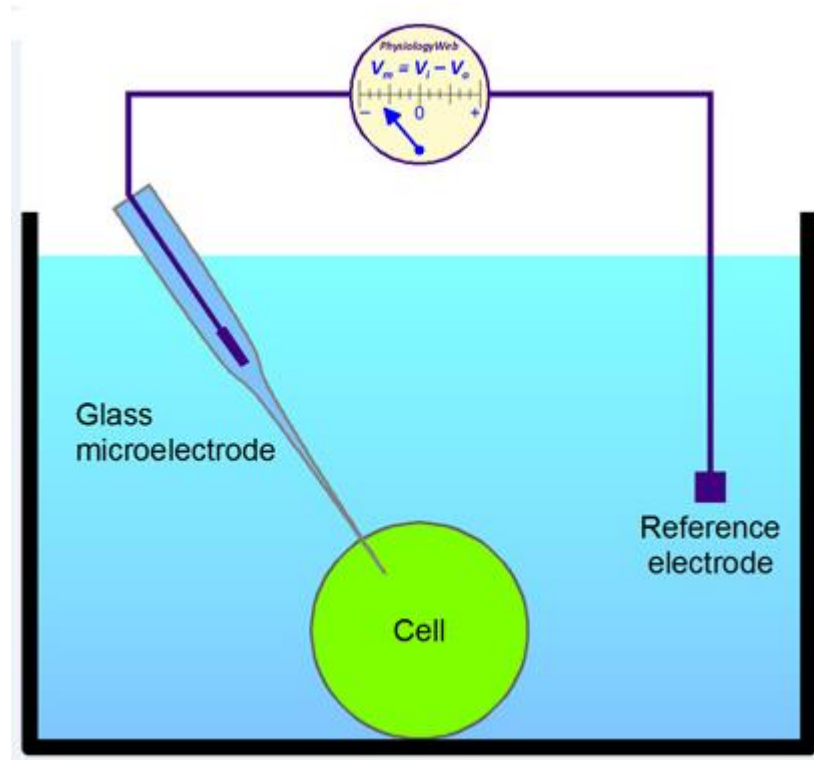


**Figure 2. 2 Glass Micropipette [32]**

The disadvantages:

1. The electrode is susceptible to breakage and blockage because it has brittle and narrow tip.
2. Limited recording bandwidth because of the low pass filter which formed from the high tip resistances ( $\sim 2$  to  $8M\Omega$ ) with the series glass wall capacitance.
3. Aggravated tissue trauma and damaged because of the brittle nature of micropipette electrodes when it was implemented in the brain.
4. Not suitable for chronic in vivo applications.
5. Only one recording site.

The glass micropipettes are used for intracellular recording. They are currently used in neuron stimulation experiments to record the evoked responses of brain tissue slices.

### **2.4.2. Multisite recording**

Multisite recording provide more benefit due to the ability of recording simultaneously more than one neuron to improve the study of neural interaction, functional relationships of neuron populations, and topographic organization. It is also used in neural augmentation systems and in implementing closed-loop neural prostheses. In contrast the single channel recording provides little information about the organization of neural circuits and systems and its function [33]. To record data through single site recording, successive recordings are required and repetitive stimulation. These cause a time consuming procedure and produce non correlated results.

### 2.4.2.1. Micro-wire

Micro-wire bundle electrodes replaced glass micropipettes in rodent and primate signal recording procedures. There are different types of micro-wire bundle electrodes:

1. Stereotrode provides pair of recording spots
2. Tetrotrodes provides four recording spots.
3. Niotrodes provides six recording spots.

One type of micro-wire electrode forms of Nickel-Chrome wires of ( $\Phi 25\mu\text{m}$ ) and coated with a  $3.5\mu\text{m}$  insulating layer (Teflon). A platinum/iridium wire ( $\Phi 38\mu\text{m}$  with a  $6.5\mu\text{m}$  insulation layer) is the core of the electrode then the Nickel-Chrome wires are spun on helical trace around the core. The electrode is fixed using epoxy resin (Epo-Tek 302-3M, Polytec PT, Germany). The bundle wires are cut and the tips are beveled at  $45^\circ$  to create recording sites by the exposed metal cores. The total diameter of the niotrode electrode array is  $<100\mu\text{m}$ . It provides 9 recording channels with channel impedance of  $300\text{k}\Omega$  at  $1\text{KHz}$  as illustrated in Figure 2. 3 left. The tissue displacement of single wire electrode was improved by a factor of 4.5 with niotrode. Hypothetically, several niotrodes can be integrated in 2-D matrix to increase the recording density as shown in Figure 2. 3. Right, but controlling the inter-electrode spacing precisely will be so difficult.

Other types of microwires are made from tungsten or stainless steel. Microwires were the first implantable electrodes to record chronically from the brain. This technique was used to focus on the individual neuron.

The drawbacks of this electrode are:

1. The electrode tip contacts with the most damaged cells so the recording is limited [15].
2. Low positional accuracy
3. Mechanical vulnerability structure.

Finally, glass micropipettes and micro-wire offer low cost and simple tool for single-site recording with low ratio of recording sites to displaced tissue.

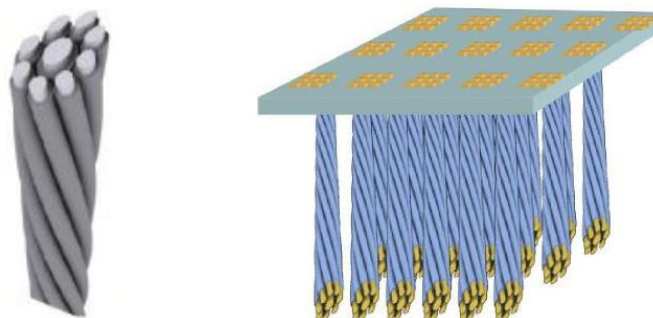


**Figure 2. 3 Micro-wire (Niotrode electrode array) [34]**

### 2.4.3. Thin film technology (Micromachined)

In thin-film technology, microfabrication and photolithography techniques are used to create high precision multisite recording electrodes which capture simultaneous sampling of multiple neurons. The technique depends on depositing and patterning conductive layers on dielectric substrate, this dielectric layer provides maintains

biocompatibility and electric insulation [35]. Thin film electrode technology introduced a remarkable leap in intra-cortical electrode technology.

#### 2.4.3.1. Single shaft electrode (Silicon based)

Microelectrode design benefited from the advancement of microfabrication technologies, and thin film electrodes were introduced with the potential to increase the number of recording spots. Single shaft electrodes with thin film technology have a planar structure, and carries several pads which are used as the interface channels with neurons. The electrodes are designed with multi recording site to increase the number of recording sites per displaced volume of tissue as well as increase the spatial resolution. To implement multisite microelectrodes with an array of recording pads, the silicon fabrication processes are used with electric connections which are formed from metal thin film deposition and patterning techniques. This silicon substrate forms the electrode. A 4 channel microprobe which is showed in Figure 2. 4, is fabricated on 15 $\mu\text{m}$  thick silicon shaft. This microprobe had a 3mm long shaft, and started with a width of 90 $\mu\text{m}$  at the base then narrowed to 20 $\mu\text{m}$  at the tip. The recording sites were deposited at different spacing from 30 to 200 $\mu\text{m}$  with gold material and for interconnections, polysilicon (or tantalum) was used. The last step was the insulated layer of silicon-oxide and silicon-nitride. The impedance of the recording sites ranged from 2M to 8M $\Omega$  at 1 kHz and the areas ranged between 100 to 400 $\mu\text{m}^2$ . This electrode failed under testing by rats and immersion in physiological saline after 12 days [36].

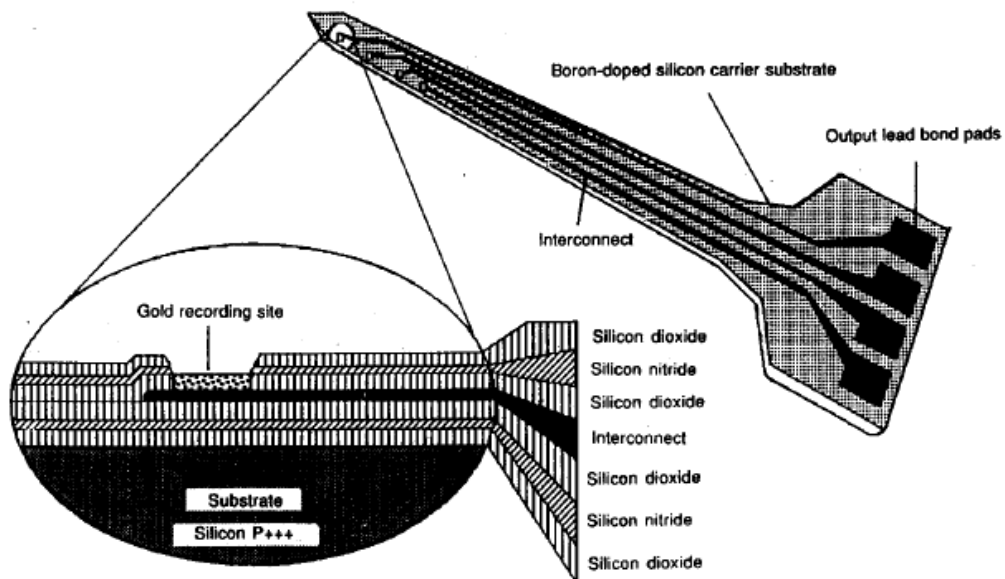
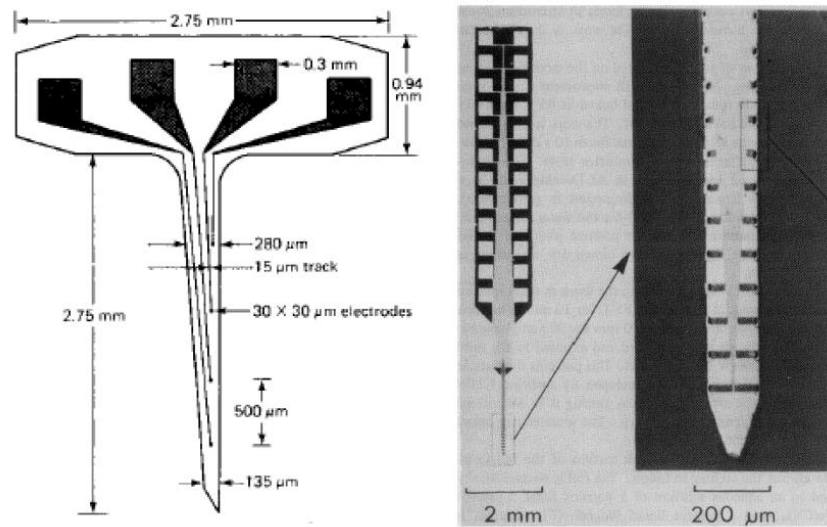


Figure 2. 4 Microprobe with 4 channels [39]

Another type of material (e.g Molybdenum) was used to make the shaft. This material supports two layers of polyimide with a gold metallization layer in between. Some windows in the upper polyimide layer were etched to expose the gold recording sites with area (30x30 $\mu\text{m}$ ) and separation distance between each one equaled 500 $\mu\text{m}$ . The electrode length was 3.75mm with width of the shaft was 135 $\mu\text{m}$  at the tip [37]. Another molybdenum electrode with 24 channels was designed which was arranged in 1x24 or 2x12 arrays by patterning gold. This design was on 17 $\mu\text{m}$  thick molybdenum substrate. Figure 2. 5 illustrates 2 types of molybdenum electrodes.



**Figure 2. 5 Two different types of Molybdenum single shaft electrodes [15]**

Figure 2. 6 exposed Ceramic electrode which was designed with Ceramic instead of Silicone. It had four recording sites ( $22 \times 80 \mu\text{m}$ ) which were separated by  $200 \mu\text{m}$  patterned on a ceramic shaft. Alumina was used to coat the electrode surface and when testing the electrode functionality in a saline solution, it was stable for 180 days [38].

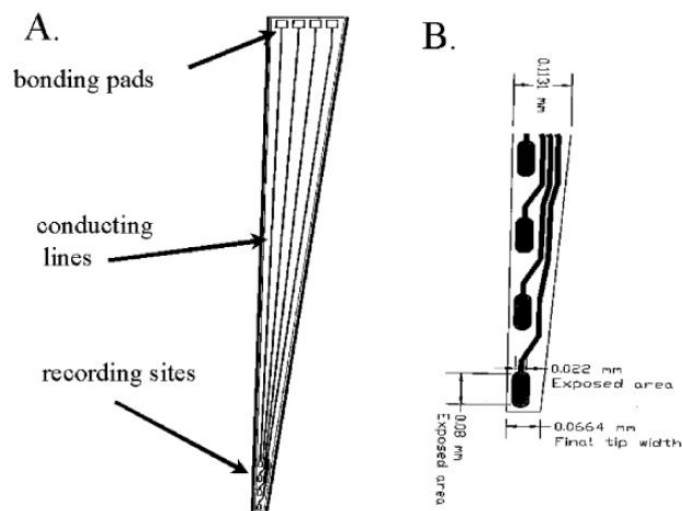


**Figure 2. 6 Ceramic electrode [15]**

#### 2.4.3.2. Needle arrays

Single shaft electrodes provide the ability to record the electrical activity of neural columns. There is a need to cover larger areas of neural interactions for a comprehensive perception and to achieve that the density of recording sites should be increased. 3-D microelectrode arrays were designed to provide simultaneous multisite recording for a large population of neurons. These electrodes are used to control neural prosthetics [39].

Needle arrays electrode forms of a matrix of micro-needles, each tip of needle has a recording channel. The needles with silicon based were used. Platinum (Pt), titanium nitride (TiN), soft conductive polymers such as Ppy and PEDOT, and sputtered iridium oxide film (SIROF) were used to coat the tip of the needles to reduce the impedance because the impedance of uncoated silicon tips was higher than coated materials and to facilitate charge transfer from the electrodes to neural tissue. There were some designs insulated the rest of the needle with biocompatible polymers such as polyimide or parylene-C. The needles could design into a sloped contour or patterned into the same length as Figure 2. 7 right. There are also a design with pyramid-shaped as Figure 2. 7 left [40]. One type of needle arrays was intra-cortical electrode which fabricated from on a silicon substrate. It contained of a 10x10 brittle needles matrix of 1mm length with a pitch of 400 $\mu$ m. Silicon-nitride was used to coat the platinum tips and silicon-oxide was used to isolate the needle rows. This electrode had on-chip circuitry for wireless transmission and amplification for flip-chip integration.

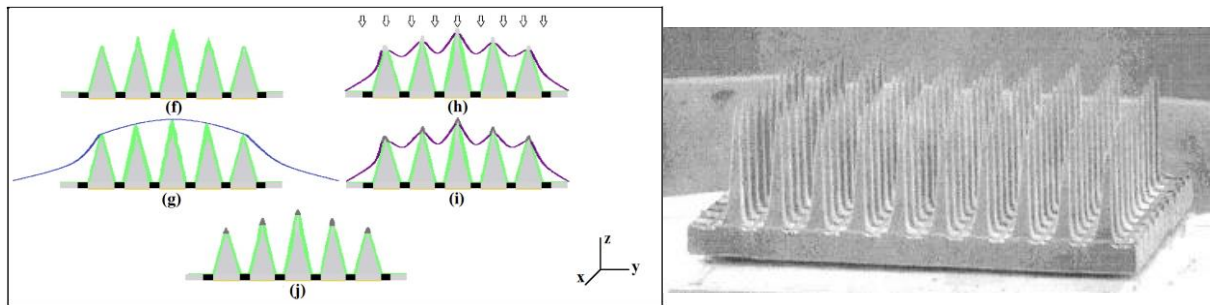


**Figure 2. 7 Left: 3D Pyramid array, Right: Same length of Needles [40]**

Electrical discharge machining (EDM) was an addition fabrication technique which allows to use several metals including titanium-aluminum -vanadium alloy (Ti90-Al6-V4), stainless steel, titanium, and tungsten-carbide, and then coating the needles with platinum to be biocompatible and tissue.

This technique was applied with high density electrode array which used in intra-cortical recording of brain activity [41]. The length of the needles of this electrode was 1mm with a pitch of 400 to 500 $\mu$ m. Figure 2. 8 exposed the fabricated electrodes. This technique was used also to produce needles with 5mm length with spacing of 250 $\mu$ m. The impedance of this electrode had a wide range because of poor soldering which was caused by adhesion problems of titanium alloys.

Some notes about some coated materials and some metals were used in needles:

- Tungsten is very noisy at low frequencies, and is not a good choice for recording these kinds of signals.
- Metal electrodes have less SNR because of lower impedance for the frequency range of spike signals. *(Our brains have about a hundred billion neurons that fire signals to communicate with each other all the time. These signals are electrochemical in nature, and travel from the cell body of a neuron through its transport stalk or the axon, to the next neuron – similar to passing the baton in a relay race. Every such firing signal is referred to as a spike, or an action potential. Spikes are produced in response to stimuli or spontaneously, and each spike typically lasts for 1 millisecond).*
- A platinum electrode plated with platinum black gives stable recordings, high SNR, and creates a porous low-impedance structure, but it is mechanically fragile.

- Iridium metal wire is extremely stiff, highly resistance to corrosion, and its surface is electrochemically activated, which causes it to increase the maximum charge density.
- CNTs on indium-tin oxide MEAs decreased the impedance at a frequency of 1 kHz, and increased charge transfer. CNT coatings can be applied to different materials and geometries. Tungsten and stainless steel wire electrodes were coated with CNTs.

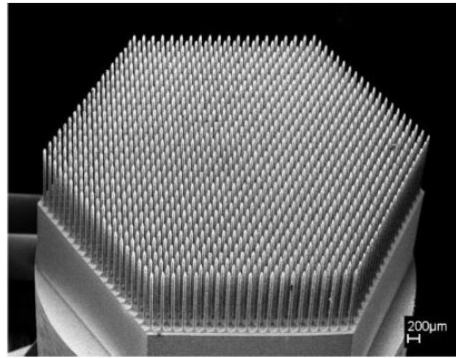


**Figure 2. 8 1141 pins of titanium electrode [43]**

Advances in silicon micromachining have brought forth new configurations of microelectrode structures such as the Utah Electrode Array (UEA) and Michigan Electrode Array (MEA). Both these devices offer advantages and disadvantages.

#### *2.4.3.2.1. Utah Electrode Array (UEA)*

UEA has been successful device but has only one active site per shaft. The active site is on the tip of the shaft. UEA was a part of DARPA-supported project which developed a bionic arm (Figure 2. 9 Left). UEA consisted of 100 silicon needles which was arranged in a 2D array, each needle represented only a recording site. An advantage compared to microwires was precisely spaced [42]. The needles had tip diameter of 50 $\mu$ m with 1mm length. The UEAs recording plane is parallel to the surface of cerebral cortex, thereby placing electrodes in the same cortical lamina.

#### *2.4.3.2.2. Microwire Microelectrode Array*

MEA is a device that contain multiple (tens to thousands) microelectrodes through which neural signals are obtained or delivered. Microwire MEAs are largely made of stainless steel or tungsten and they can be used to estimate the position of individual recorded neurons by triangulation. The ESIEE Neurocom group developed silicon needle array to provide 64, 256 or 1024 recording sites. The needles were fabricated using anisotropic and isotropic silicon etching to create 80 $\mu$ m needles with 50 $\mu$ m pitch. Figure 2. 9 right shows one design of extracellular 3D microelectrode array.

#### **2.4.3.3. Multi-shaft electrodes**

The drawback of needles array is the limiting recording to a planar field. Other types of the electrode can be contain several shafts, each shaft carries multiple recording spots. This structure allows to record more than neuron in the same column. High electrode density was designed to accommodate a large number of channels

distributed among several shafts. Several designs had shaft lengths ranging from 3 to 15mm and its shafts had tapered tips as shown in Figure 2. 10 [14].

The right part of Figure 2.10 also shows an electrode with 64 recording sites and had integrated 64:8 multiplexer and 8 channel amplifier which were used to access the recording sites. The recording sites were fabricated of iridium pads with dimensions  $10\mu\text{m} \times 10\mu\text{m}$  and spaced with  $200\mu\text{m}$ .

#### 2.4.3.3.1. Michigan Electrode Array (MEA)

The MEA has multiple active sites per shaft. MEA's plane is normal to the cortical surface, there by placing the electrodes in a line across the surface but a multiple lamina. During the 1970s one of the first silicon-based MEAs was made at Michigan University[35]. This kind of electrode can be combined with on-chip circuitry, wireless interfaces, and signal processing. Figure 2. 11 left shows recording or stimulation probe in the central nervous system which was considered the basic structure of a micromachined microelectrode probe. Figure 2. 11 right presents a 4 penetrating shank each shank had four uniformly recording sites. The description of this electrode was:

- silicon substrate
- Thickness of the shank is  $15\mu\text{m}$
- Length is 3 mm long
- Width is  $90\mu\text{m}$  at the base, decreasing to  $20\mu\text{m}$  at the tip.
- The surface area of the recording site ranging from  $100$  to  $400\mu\text{m}^2$ .

This type of high-density electrode is an intra-cortical electrode. It is inserted in the tissue to study the electrical activity of neurons by recording or stimulate neurons by inject electrical signals. The material of substrate (shank) should have some properties:

- Biocompatible
- Strong enough to be able to penetrate the pia arachnoid membrane over the brain.
- Small enough to prevent tissue trauma.

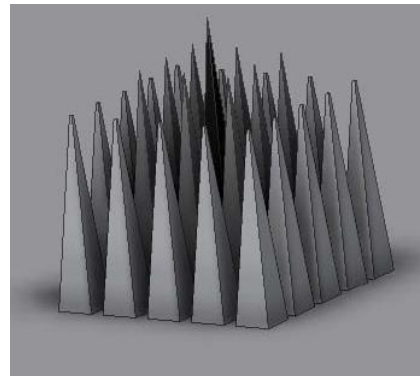
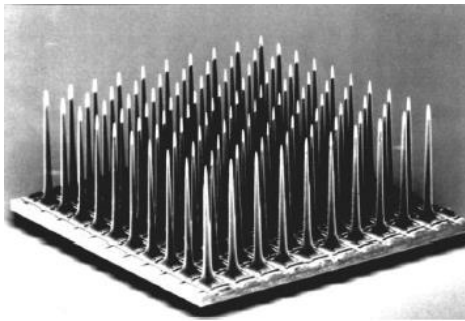


**Figure 2. 9 Left: Utah array, Right: 3D microelectrode array [45]**

Silicon is preferred because of it allows integrated electronics to be used directly in the probe substrate and is strong enough. A 3-D constellation of recording sites was implemented by stacking 2-D electrodes to simplify electrode integration and assembly of multi-shaft cortical. Figure 2. 11 is a formatting 96 channels by using 16 channel probes made the Microscale Implantable Neural Interface (MINI) which was considered an interface of the nerves system to simultaneously sample signals at many



points in the tissue, and provide insight into processes as memory formation, movement control, and perception [42]. Each probe had 4 recording spots, its area was  $1250\mu\text{m}^2$  with  $400\mu\text{m}$  pitch and the space between each probe was  $250\mu\text{m}$ . Each 3mm probes had  $20\times 60\mu\text{m}$  perforations to achieve tissue integration. After that, the probe was connected through flexible interconnects to form a module for signal acquisition [25].

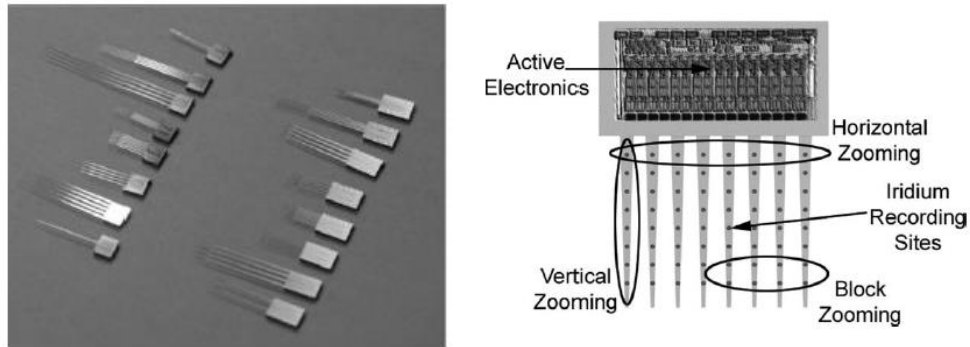


**Figure 2. 10 Multi-shaft recording electrode [45]**

#### 2.4.3.3.2. Double Side Penetrating Neural Electrode Array

In Caltech, a dual-side recording electrodes was developed by Laurent lab and Roukes group. Due to incapacity of simultaneously detecting the majority of single-unit spikes from both sides, a dual-side electrode array was fabricated by patterning recording sites on both sides of an implantable microstructure the front and back to provide higher spatial resolution measurements than single-side devices. This dual-side had the same footprint of the single-side electrode. Moreover that, to provide massively parallel recording in the brain, three principal recording directions were developed by using a multilayer array [43]. It provide 3D spike source within the enclosed measurement space. The designs of dual-side and multilayer arrays were illustrated in Figure 2. 13.

Another design of the double sided electrode was fabricated using glass material instead of Silicon to form the microelectrode. The glass is being a good insulator, which eliminates parasitic capacitance between the electrodes. This device increases the spatial resolution and active sites density (double), which help to map every neuron in the human brain. The length of shank is 0.5 cm and has multiple stimulation/recording sites (16 to 32 channel as proof of concept). Each neural recording/stimulation sites is fabricated at different depths of microelectrode array. The electrode array is made of glass and the metal pads are coated with 3  $\mu\text{m}$  of parylene-C [44].

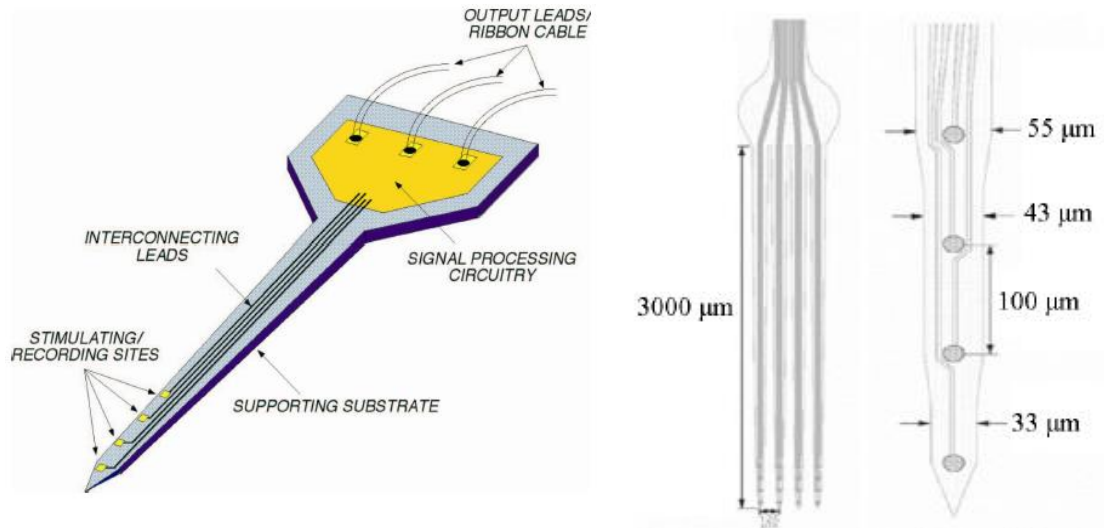


**Figure 2. 11 Left: Michigan probe: Basic structure of micromachined microelectrode, Right: four-shank electrodes (MEA) [15]**

#### 2.4.3.4. Flexible electrode

Several electrode designs were developed on ceramic and silicon substrates. The stiff electrodes might cause significant trauma when implanted this rigid electrodes in the brain tissue. Moreover, brittle shafts are subjected to fracture and might release debris in the brain. Therefore, to overcome these challenges of brittle electrodes, flexible substrates were introduced and designed in several forms to overcome the troubles of the fabrication, mechanical design, and tissue penetration [45].

Flexible arrays allow electrodes to penetrate the surface of the brain in a less invasive way to monitor and record. Because of flexible polyamide-based microelectrodes provides high mechanical flexibility, high resistance to solvents, good biocompatibility, and a strong addition to metal oxide, it is used for chronic neural recording [46]. Different polymers (e.g. parylene and polyimide) are used as a structural substrate. Parylene-based MEAs are considerably flexible, providing a stable electrical contact which leads to improving the SNR, and highly conformal coverage of the muscle surface [47]. It showed in Figure 2. 14. Then flexible CNT microelectrodes appeared and improved charge-transfer capacity, electrode impedance, and the adhesion between the recording sites and the substrate when the CNTs were grown directly on the polyimide substrate[48]. Another parylene-based multi-sided MEA which has sites at the back-side, top-side, and edge is presneted for neural recording and passive drug delivery. This creates a small footprint ( $85\mu m^2$ ). Figure 2. 15 exposes different designs of multi-sided microelectrode: (a) Front-side, back-side, and edge designs of electrodes with  $45\mu m$  spacing; (b) Open-channel design for passive drug delivery; (c) Hollow-channel neural probe for cell-based therapies.

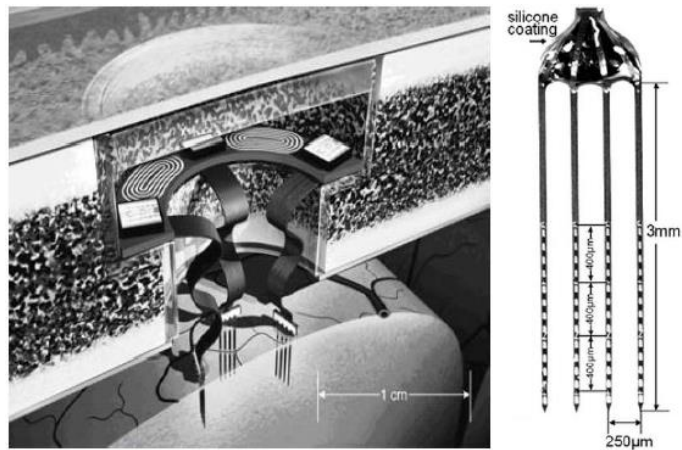


Figure 2. 12 Microscale Implantable Neural Interface with single probe [15]

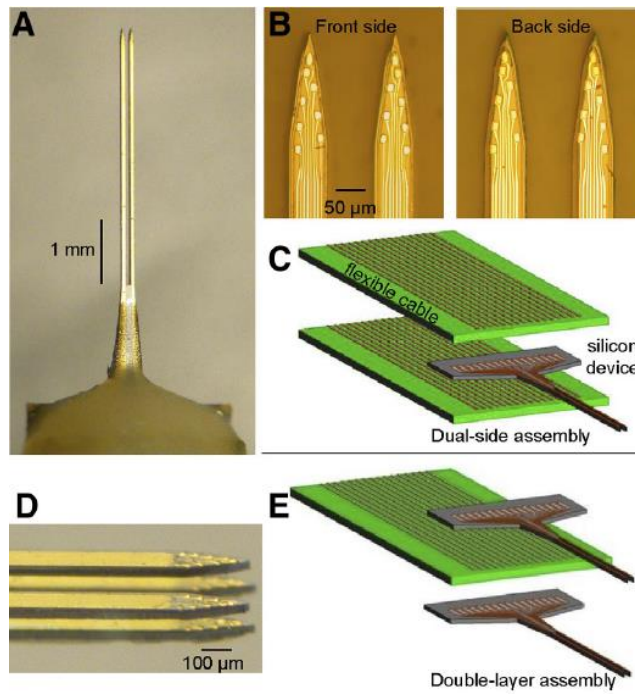


Figure 2. 13 Dual sided electrode and multilayer with Caltech [44]

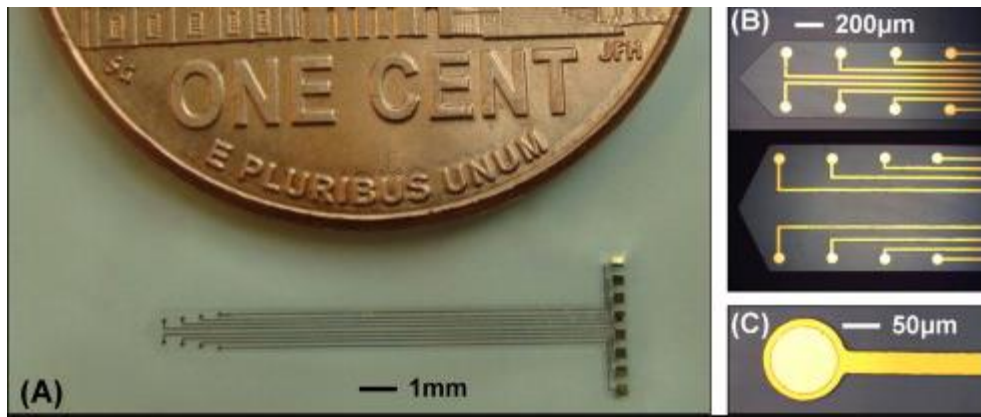


Figure 2. 14 Flexible parylene-based electrodes [32]

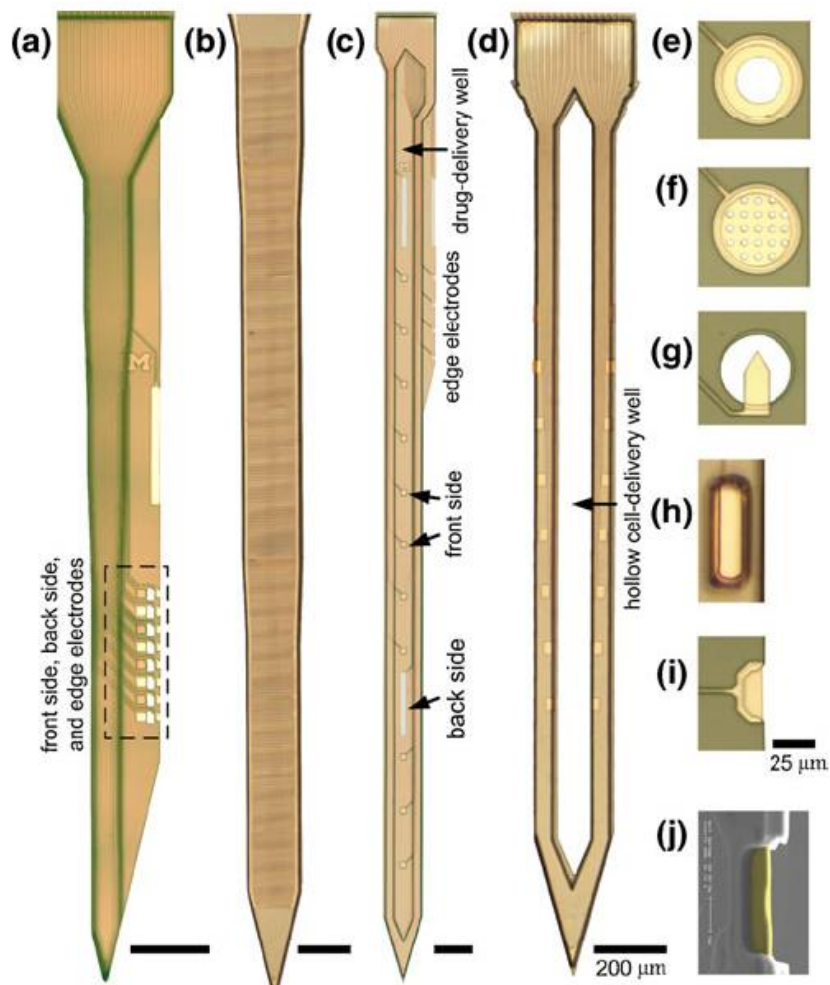


Figure 2. 15 parylene-based multi-sided MEA [34]

The Flexible electrodes have some advantages:

- Closer mechanical match with brain tissue.
- Polymer-based implantable electrodes improve long-term performance.
- high mechanical flexibility

- good biocompatibility
- high resistance to solvents
- a strong addition to metal oxides

And the disadvantage is due to the flexibility nature of these electrodes, involves some difficulties during insertion.

Nanomaterials have a significant important in improving electrode designs by increasing the selectivity and sensitivity, biocompatibility with the biological environment, and improving response time. CNTs are considered one of the best options of the electrode active sites due to their high aspect ratio, rich electronic properties, high mechanical strength, excellent chemical stability, and intrinsic large surface area [34]. Polymers are considered perfect materials which can be used to coat nerve electrodes because of its properties. They can modify with biomolecules to improve biocompatibility and to create also a biologically active electrode-tissue interface [49].

#### 2.4.3.5. Cuff Electrodes

Nerve cuff electrodes are conformed of medical grade silicone rubber which wrap around the nerve and then stimulate axons. The axons lead to all muscle fibers which are innervated by that nerve. This is an effective method to fully stimulate broad or pinnate muscles which are difficult to stimulate by muscle based electrodes. The advantage of nerve cuff electrodes that the current which are needed to activate the nerve is less than the current which are required to activate muscles because nerve cuff electrodes have a direct contact with the nerve. Moreover, they able to activate different functions or muscles individually and can stimulate different parts of the nerve potentially and selectively [50].

The embedded wiring and contacts of the cuff are made from platinum then the wires are insulated. Figure 2. 16 illustrates a design of the nerve cuff electrode

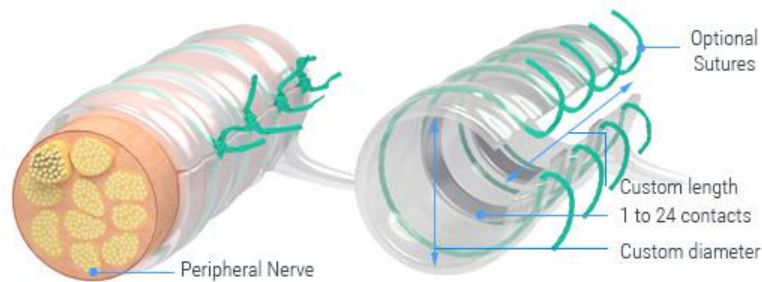


**Figure 2. 16 Nerve Cuff Electrode [53]**

#### 2.4.3.6. Optrode

The invention of optogenetics has given researchers the ability to move to a certain regions of brain as they choose. In contrast DBS, which uses electricity to change the activity of any neuron which is near the electrode, optogenetics uses light to affect specific neurons. Because the default of the neurons that they are not normally responsive to light, so in first, researchers should change the nature of the neurons to make them as light-sensitive. This is often accomplished by injecting a virus into the

target brain region. This virus can be designed to infect specific neurons and then provide these specific neurons with instructions to be coated with proteins which provide the ability to the researchers to control them with light. Bioengineers invented several types of these viruses to carry instructions for different types of light-sensitive proteins. Some of these viruses cause neurons to be more active, and others cause them to be less active [52]. Figure 2. 17 shows the difference between DBS and Optrode because in A the DBS affects all the neurons in its area, but in B the optrode affects the white neuron only. Figure 2. 18 illustrates the system of optrode which consists of a source light, fibers to transmit the light, and the electrode structure.

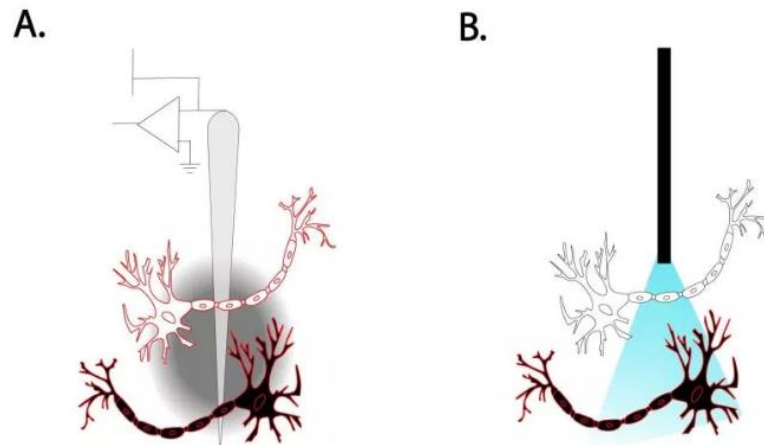


**Figure 2. 17 Effect of A. DBS, B. Optrode on neurons [52]**

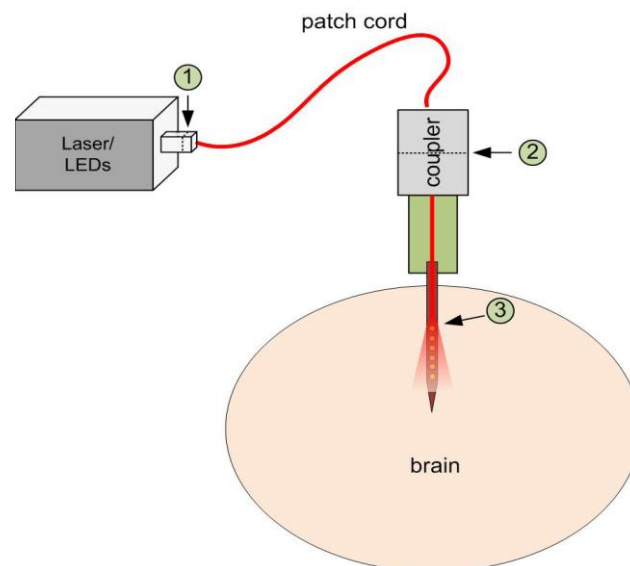


**Figure 2. 18 The Optrode system**

#### 2.4.3.7. Noninvasive Deep Brain Stimulation

Neurons have the ability to send signals to other neurons repetitively. When electrodes placed on the skull, it provide current at a certain frequency. The close neurons to the electrode sense the stimulation and transmit signals at the same



frequency. This electrodes cannot aim a specific region deep inside the brain because of much stronger stimulation affects the neurons near the skull. There is a new research in MIT University circumvents this problem by placing two pairs of electrodes on the skull. They utilize the phenomena of interacting or interfering between the electrical signals of the electrodes pair. The mean idea of this design is a creation of a new DBS electrode without needing to open-skull surgery to place the electrode into a specific regions. This design depends on 2 scientific insight:

1. The neurons do not be affected by the very high stimulation (more than 1 kHz).
2. The interference between the stimulation waves with each other.

When two waves meet, the interference occurs and combines a wave of decreased or increased strength. The frequency of the new wave depends on the relative locations and the properties of the two original waves. From this phenomena, when two waves meet and have slightly different frequencies, they will form an envelope wave. The new wave will have a frequency which will equal the difference of the two original waves' frequencies. Figure 2. 19 illustrates the idea of this design. This phenomena is called temporal interface. The frequencies of these two waves are 2 kHz and 2.01 kHz which are considered too fast for the neurons to follow, but the envelope wave will have a frequency of 10Hz which is the difference of the two original waves. The neurons in this region will be affected by the low frequency envelope [53].

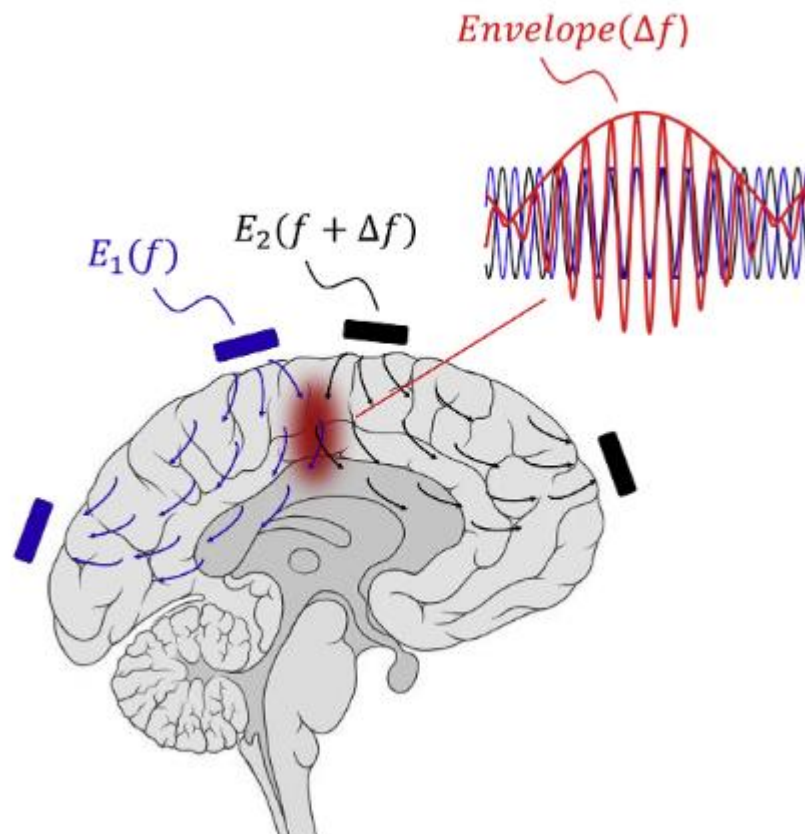


**Figure 2. 19 Noninvasive Deep Brain Stimulation Electrode [54]**

There are many challenges face this design, the first one is that the stimulation's accuracy is still lower than the level which is required by DBS treatment. The spatial precision of this deigns is still unknown. The second challenge comes from that the

volume of the human brain is almost 1,400 times larger than the volume of a mouse, so that the temporal interference technique is still unclear, and there is not any knowledge of is this design can target located deep regions inside the human brain. Third challenge is the difficulty of the validation of the stimulation in human brain because of the two methods which are used to check this work are both highly invasive and be used on human.

## **2.5. Consideration to check electrodes**

To proper electrode operation and failure, there are several practical that is taken in consideration. They involve physiological, electrical, mechanical, and chemical considerations. These topics are considered as guidelines and constraints which are used in the design process.

### **2.5.1. Tissue distortion**

The aim of the optimization process of the microprobes design is to be virtually invisible to the tissue to minimize tissue displacement and damage. The electrode destroys some neurons during insertion process and this area is called the kill zone. Therefore a principal factor affecting tissue displacement is the electrode geometry.

### **2.5.2. Pads structure**

Depending on the pads size and spacing, we can determine electrode dimensions and the channel density, it also influences the electrode functionality (e.g. number of channels) and biocompatibility as intensity of tissue trauma. So they are considered critical parameters of the design. Based on pad size, the impedance and charge capacity is controlled which in turn dictates the electrode application. Large pads are used for local field potential (LFP) recording and stimulation. They provide lower impedance ( $\sim 300\Omega$ ), while smaller pads which are used for spike recording and single neuron isolation has higher impedance ( $>2M\Omega$ ). According to surface area, the neural stimulation electrodes can be divided into two categories:

#### **1. Macroelectrodes:**

These electrodes are used for stimulation process. They have a large geometric surface area (GSA) greater than  $100,000\mu m^2$  and deliver the charge to the surface of the target tissue. They are characterized to achieve high-charge-per-phase and low charge density. However, the low charge densities avoid stimulation-induced electrode degradation and inhibit corrosion, the high-charge-per-phase may induce tissue damage.

#### **2. Microelectrodes**

These electrodes are used for stimulation process also. They have a small (GSA) less than  $10,000\mu m^2$  and penetrate the target tissue. They have low-charge-per-phase and high charge density. They have high selectivity in stimulating small volumes of tissue. The high charge densities lead to tissue damage and electrode degradation so to prevent electrode and tissue damage, keep charge density and charge-per-phase to be low.



### **2.5.3. Mechanical Failure**

During insertion and operation, there are some forces affect the electrode which must be capable of handling these mechanical forces. Flexible shafts provide conform to the surrounding tissue and strain relief. However, flexible shafts improve the electrode biocompatibility, they may collapse and are prone to buckling failure during insertion. In contrast, brittle and stiff electrodes would deal with insertion forces without failing, but due to electrode micromotion and dislocation, it may cause more post-operative tissue damage. Moreover, if a brittle electrode fails mechanically, it will fracture and dispense debris in the brain. A chronic electrode in vivo interfacing should have a ductile structure to be able to survive axial loading during implantation and to maintain the design biocompatibility.

The mechanical and electrical simulations have more than one simulation program such as Ansys and Comsol multiphysics. Comsol is the best choice because of the ability to definition of any type of physics problems and it is very open for any user to input new functions. So, all simulations are made using Comsol Multiphysics [55].

### **2.5.4. Comsol Multiphysics software program**

Simulation programs have become a main part of engineering and science. Digital analysis of components is important when optimizing designs or developing new products. Today a wide spectrum of choices for simulation is available; researchers need all things from basic programming languages to several implementing advanced methods. The environment of computer simulation is simply a translation of real-world physical laws to similar virtual form of the real-world. When the simplification of the translation process increase, the accuracy of the resulting model increases. Comsol is a computer simulator. It has a simulation environment which included the ability to add any physical effect to the model. It is a flexible platform which grants users to model all pertinent physical sides of their designs. COMSOL gives you the ability to build the model with real-world accuracy. Comsol has the ability to combine many types of simulation [56]. For example electricity is always escorted by some thermal effect. It also provides the ability to add another physics effect to the model. COMSOL is a complete problem-solving tool. COMSOL Multiphysics uses the finite element method (FEM). The software runs the FE analysis together with conformed meshing and error control using a diversity of numerical solvers. Comsol Multiphysics can be used in many application areas [57][58][59][60], as:

- Chemical reactions
- Diffusion
- Fuel cells and electrochemistry
- Fluid dynamics
- Fluid dynamics
- Electromagnetics
- MEMS
- Optics
- Porous media flow
- Radio-frequency components
- Structural mechanics
- Wave propagation
- Heat transfer

- Bioscience
- Acoustics
- Geophysics
- Microwave engineering
- Photonics
- Quantum mechanics
- Semiconductor devices
- Transport phenomena

COMSOL supplies its own scripting language. It provides the ability to access the model as a data structure or a Model M-file.

COMSOL Multiphysics gives a simple interface to MATLAB. This provides the freedom to combine simulation, PDE-based modeling, and analysis with other modeling techniques. It also offers the ability to create a model then exports it to Simulink to be a part of a control-system design.

COMSOL Multiphysics provides modeling and analysis for many application areas. It has several modules of the key application areas. It simplifies creating and analyzing models by using application-specific modules for specific solution methods to the particular discipline. The COMSOL has the following modules:

1. AC/DC
2. Acoustics
3. Chemical Species Transport
4. Electrochemistry
5. Fluid Flow
6. Heat Transfer
7. Optics
8. Plasma
9. Radio Frequency
10. Semiconductor
11. Structural Mechanics
12. Mathematics

Each module has specific application areas. Such as AC/DC, it offer a specific area which is called Electric Currents and this gives the ability to compute electric field, current and potential distributions in conducting media under conditions where inductive effects are negligible. Each specific area disciplines standard terminology and materials libraries, interfaces, specialized solvers, visualization, and elements tools. Figure 2. 20 illustrates the application areas in one module such as AC/DC.

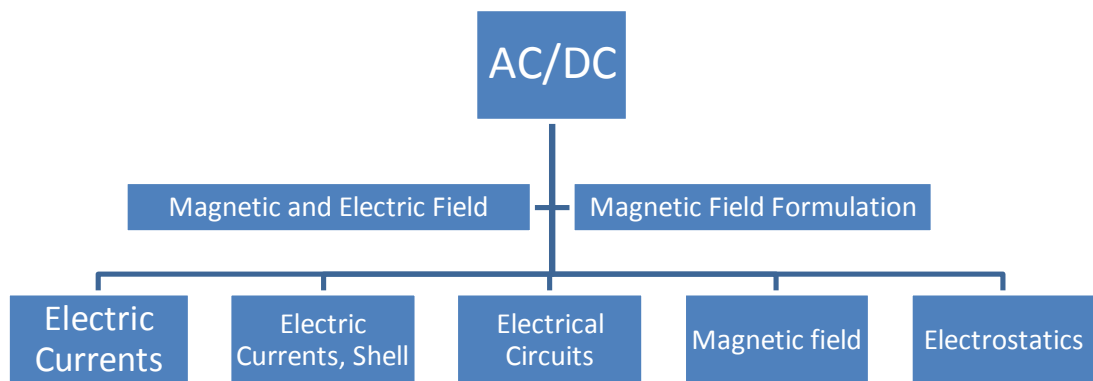


**Figure 2. 20 AC/DC Module**

The AC/DC Module offers a unique milieu for simulation of AC/DC electromagnetics in 3D or 2D. This Module is a sturdy tool for comprehensive analysis of capacitors, coils, and electrical machinery. This module offers running time-harmonic, transient, static, and quasi-static simulations and has an easy graphical user interface.

The Acoustics Module offers an environment for acoustics modeling in solids and fluids. The module provides transient, static, eigenfrequency, and frequency-response analyses for structures as well as time-harmonic, modal, and transient analyses for fluid pressure. Some application areas for the Acoustics Module are aeroacoustics, modeling of loudspeakers and microphones, automotive applications as mufflers and car interiors, and underwater acoustics [61].

The Heat Transfer Module provides all fundamental mechanisms of heat transfer. Such as general heat transfer with convection, conduction, and surface-to-surface radiation, Nonisothermal flow application mode, Bioheat equation to simulate heat transfer in biomedical systems, heat transfer for highly conductive layer in thin structures.

The Structural Mechanics Module helps in solving problems in solid mechanics and structural. Engineers use it to study the performance of new structures and devices. This module provides static and dynamic analyses in 3D coordinate systems for solids 2D axisymmetry, 2D, shells (3D), trusses (2D, 3D), plates (2D), beams (2D, 3D), and membranes (2D axisymmetry, 3D). The material models have linear descriptions, like linear elastic and viscoelastic material models. Beside thermal stress, large deformations (geometrical nonlinearities), and structural contact.

Any model in Comsol has the same steps to be built. The following steps illustrate the simulation workflow:

1. set up model environment
2. create geometric objects
3. specify materials properties
4. define physics boundary conditions
5. create the mesh
6. run simulation
7. postprocess results

More details will be considered in Appendix D.

### **2.5.5. Materials of electrode**

Implanting foreign bodies in a living system caused changes in the homeostatic mechanisms which affect the stabilization of the internal body equilibrium. When biocompatible materials come in contact with tissue, they cause minimal biological response and do not produce injurious, toxic, or immunological response. Materials biological performance is evaluated by the material and host responses. The host response is a systemic or local reaction of living systems to the foreign material. Inert electrodes do not force irreversible chemical changes on the surrounding environment [62]. There are several factors that affect the choice of electrode materials:

1. Biocompatibility
2. Mechanical strength
3. Impedance
4. Allergic responses
5. Radiographic visibility

After these simulations and depending on the results, the design of the DBS electrode is decided and then fabricated with micro-electro-mechanical system (MEMS) technology. Next section introduces a brief history of MEMS technology and its medical applications.

## **2.6. MEMS**

In the middle of the last century there was a breakthrough in electronic inventions starting from the innovation of the transistor in 1947 at the Bell Telephone Laboratories, and then the appearance of the integrated circuit (IC) in 1959.

The first IC appearance was at Texas Instruments as a hybrid IC and then at Fairchild Semiconductor as a fully monolithic IC in the same year. As a result, the world has seen what can be considered as a revolution in communication and information processing. The rapid development of microelectronics has led to the emergence of portable music players, laptops, computers, the internet, mobile phones, and digital video disc players. All of these applications are a few examples of this development. It had a significant effect on everyday life such as electronic mail, mobile phones, and different web-based services. This development of microelectronics relies heavily on rapid advances in semiconductor manufacturing technologies. This development helps in minimizing a lot of systems like sensors, actuators, and various mechanical and electrical components which are collected together to form what is famed with a MEMS or a microsystem.

The application range of microchips was expanded by the MEMS technology. It can be used in sense of acceleration, light, angular acceleration, pressure, or angular velocity. The microsystem can handle fluids and perform various biomedical or biochemical analyses, and it can control the light reflection to form a picture on a screen. Briefly, the MEMS technology extends the capability of expanding the microelectronic revolution specially, in the areas which need an interface between the real world and its various physical phenomena.

The history of MEMS devices already extends back for well over four decades. Nathanson et al. published the resonant gate transistor in 1965. It is considered the first reported MEMS device [26]. Then, the pressure sensors which are considered the early commercial MEMS technology were created by National Semiconductor in 1973 [27]. In early of 1979, Vaisala in Finland started its technology development. In 1984, it

produced the micromechanical silicon capacitive pressure sensors as a product. In 1991, the newly-established company Vaisala Technologies Inc. appeared and all the technology was transferred from Vaisala to it, then in 2002, it became VTI Technologies [28]. In 1989, Prof. Roger Howe of the University of California, Berkeley introduced the term MEMS itself at the Micro Tele-Operated Robotics Workshop held at Salt Lake City, UT, USA [29]. In 1992, O. Solgaard introduced the deformable grating light modulator (GLM). It is considered as a Micro-opto-electromechanical System (MOEMS). Since it was produced, it has been evolved to be used in several applications such as in graphic printing, display technology, optical communications and lithography.

In 1993, a foundry was created by Microelectronics Center of North Carolina (MCNC). The aim of this foundry was to let microsystems to have an effective cost for a huge number of different users and to have high processing with more accessible. It enhanced a process called MUMPs (Multi User MEMS Processes). It contained a 3 layers poly-silicon surface micromachining process. Since its beginning, to increase the versatility and flexibility of the process for the environment with multi-user, several modifications and enhancements have been made. After 5 years in 1998, another foundry of surface micromachining started. It was began at Sandia National Laboratories and the process was called SUMMiT IV. This procedure later developed into the SUMMiT V which has a five-layer polycrystalline silicon surface micromachining process. SUMMiT is an acronym for “Sandia Ultra-planar, Multi-level MEMS Technology.”

In 1999, the first MEMS optical network switch was developed by Lucent Technologies. Optical switches are considered optoelectric devices. It consists of a light source with a detector which used to produce a switched output. In a data communications network, the optical switches provide a switching function. These MEMS optical switches use micromirrors to reflect or switch a signal or optical channel from one location to another. This property is determined by the relative angle of the micromirror. This area of technology grow with high rate processing with different design configuration. New methods for merging MEMS actuators and sensors with bio-MEMS technology were discovered and scientists have been improving them. For example, applications include neural probe arrays, DNA arrays, insulin pumps, drug delivery systems, lab-on-a-chip (LOC), glucometers, Neural Electrodes, and microfluidics. There are a lot of trials by scientists to develop and enhance the micro-electro-mechanical systems, since the invention of the transistor [30]. Nowadays, Micro-optoelectromechanical systems (MOEMS) with MEMS constitute the specific technology branches using miniaturized integrations of electronics, optics, and mechanics.

Finally, in so many commercial products, MEMS devices have been used. Every day, many of applications and technologies are discovered. The earliest generation of MEMS devices were used in measuring objects as cars’ motion and engines’ pressure. Then, MEMS components control the communications networks and reduce Injuries by cars’ air bags.

Today, they are implanted in the human body to observe the act of blood pressure in addition to controlling drugs doses accurately. Microsystems sizes continue to decrease; this can be seen in the nano-electro-mechanical systems (NEMS). The evolution of MEMS, NEMS, and MOEMS applications continue endlessly and they breached many aspects of lives.

## 2.7. Conclusion

Recording electrodes have a high density of pads than the stimulation electrodes. Due to degradation of signal transmission through tissue-electrode interface, implanted electrodes have a short effective lifetime. Optimum electrodes should cover two important characteristics

1. long-term tissue compatibility
2. Fast response to signals.

Till date there is no ideal device available. One of the critical requirements of the neural interface is to have higher electrode density to map neurons from large volume of brain but not at the expense of increasing the device footprint.

High spatial precision is one of the important requirement of DBS. It is mean the accuracy of targeting a specific region because of the stimulation process of some brain regions which are unrelated to the disease will cause undesired side effects and reduce the effectiveness of treatment.

One of the main challenges in fabricating MEAs is finding appropriate coating materials which will be biocompatible and improve neural recordings.

The electrodes were classified according to various design features. Since there is a lot of differences between brains nature for rats and humans, different electrodes design are considered. Chapter 3 reviews the design procedure for rat electrodes with shaft length 3mm. Chapter 4 reviews the design procedure for human electrodes with another shaft length of 10mm to be compatible with human brain. Chapter 5 illustrates another type of DBS electrode which is called optrode. It is appeared to eliminate some drawbacks of electrical electrode.

## Chapter 3 : Rats Electrodes

There are several parameters that influence the electrode mechanical performance. These parameters include the electrode layout, architecture, material, and electrical simulation. It is required to improve the structure of the electrode with a rigid material to be capable of penetrating through the tissue without the needing of insertion assistive device and to minimize tissue trauma. Moreover, its structure has to be flexible to match with the ambient tissue stiffness in order to minimize post implantation tissue trauma. These mechanical properties have to be provided through a small footprint design to improve the electrode biocompatibility. Achieving rigidity and flexibility introduces design challenges. Finite element mechanical modeling and analysis using Comsol is employed in the design process. Several layouts are modeled and analyzed in Figure 3. 2 to identify the best designs capable of satisfying the mechanical requirements.

The electrode is subjected to insertion force which is estimated from literature and mechanical failure modes. These mechanical failures are identified for ductile and brittle materials. The electrode would subject to linear buckling failure and static failure due to axial loading and shear forces. Safety factor of 5 is assumed and several proposed layouts are modeled to analyze the failure loads and to estimate the minimum electrode thickness. The shaft thickness is the main degree of freedom, and the recommended thicknesses for the different materials and layouts are calculated. Finally, a comparison between these designs is introduced to improve the electrode mechanical performance and to enhance its biocompatibility then the electrode DC resistance is calculated or estimated by finite element modeling.

### 3.1. Electrode forces and failure models (Mechanical Analysis)

#### 3.1.1. Forces acting on the electrode

During insertion, there are three mechanical forces acting on the electrode, these forces are outlined on the free body diagram in Figure 3. 1 [63]. The tip force is the axial reaction acting on the electrode tip during penetration. The clamping force is the force normal to the electrode surface. During insertion, the normal force acting on the surface and the coefficient of friction produce friction force along the electrode surface. The total axial reaction force acting on the electrode is calculated from these forces. The applied insertion force should be greater than the total reaction force to achieve successful penetration without any of mechanical failures.

A wide range of penetration forces are defined from the mechanical perspective of various types of tissues and estimated to be from 1mN to 10mN [15]. This is lower than the penetration force of epidermal tissue by 2 to 3 orders of magnitude. This epidermal tissue penetration force is estimated to be 1N [51].

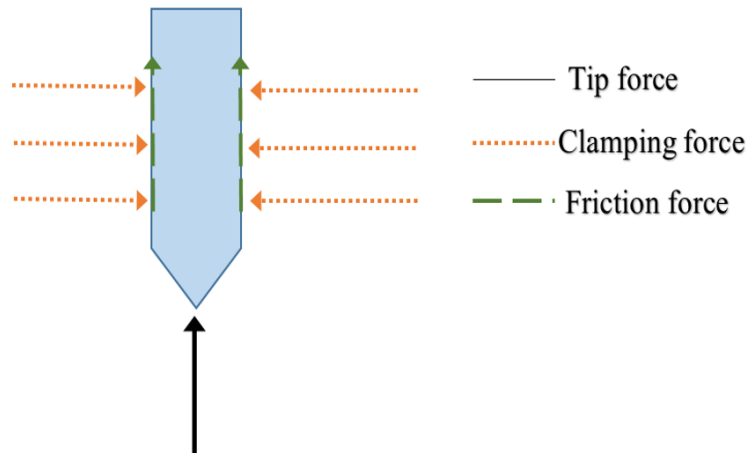


**Figure 3. 1 Forces affecting the electrode. There are three mechanical forces acting on the electrode, these forces are outlined on this free body diagram**

### 3.1.2. Modes of mechanical failure

During insertion, the electrode is subjected to two mechanical failure modes: buckling and fracture [64]. The electrode structural layer is tested with several materials, and different geometries. Each material has different failure modes depending on the material mechanical properties.

Two types of materials are used in the implementation of the electrodes: Brittle materials (e.g. Silicon) and ductile materials (e.g. metals and flexible polymers).

Metals as Copper and Nickel are implemented as a substrate and coated with thin layer of gold to be biocompatible with tissues. Under uniaxial stresses testing, the Brittle materials suffer from elastic deformation until the stress level exceeds the yield strength then, they show negligible plastic deformation followed by fracture. Therefore, the maximum loading limit for brittle structures is considered as the design parameter ultimate tensile strength (UTS). On the other side, when applying uniaxial stress on the ductile materials, they suffer from elastic deformation until reaching the yield point, followed by plastic deformation and finally cracking leading to fracture. When the maximum shear stress exceeds the maximum shear yield strength of the material, ductile materials fail [31]. Some of properties of the used materials are illustrated in Appendix A.

## 3.2. Electrode prototypes and mechanical analysis

### 3.2.1. Electrode prototypes

Several electrode layouts are introduced and their mechanical properties are tested in the pursuit of a design that accommodates a large number of stimulation channels. The proposed layouts are presented in Figure 3. 2. In general, the bases are designed with big size to facilitate treatment and provide large interconnect pads for easy connections, while the length of the prototypes shanks is enough to reside within 3mm inside the tissue and carry the interface pads.

The interconnect pads on prototypes C, E, F, H and I are arranged transversely, while those in A, B, D and G are longitudinal. The simulations of the electrode models



are analyzed to explore their mechanical performance as well as the effect of the electrode material and dimensions on the critical load. In addition, parametric modeling and sensitivity analysis are employed. The previous prototypes were drawn by Comsol and the steps is illustrated in Appendix D.

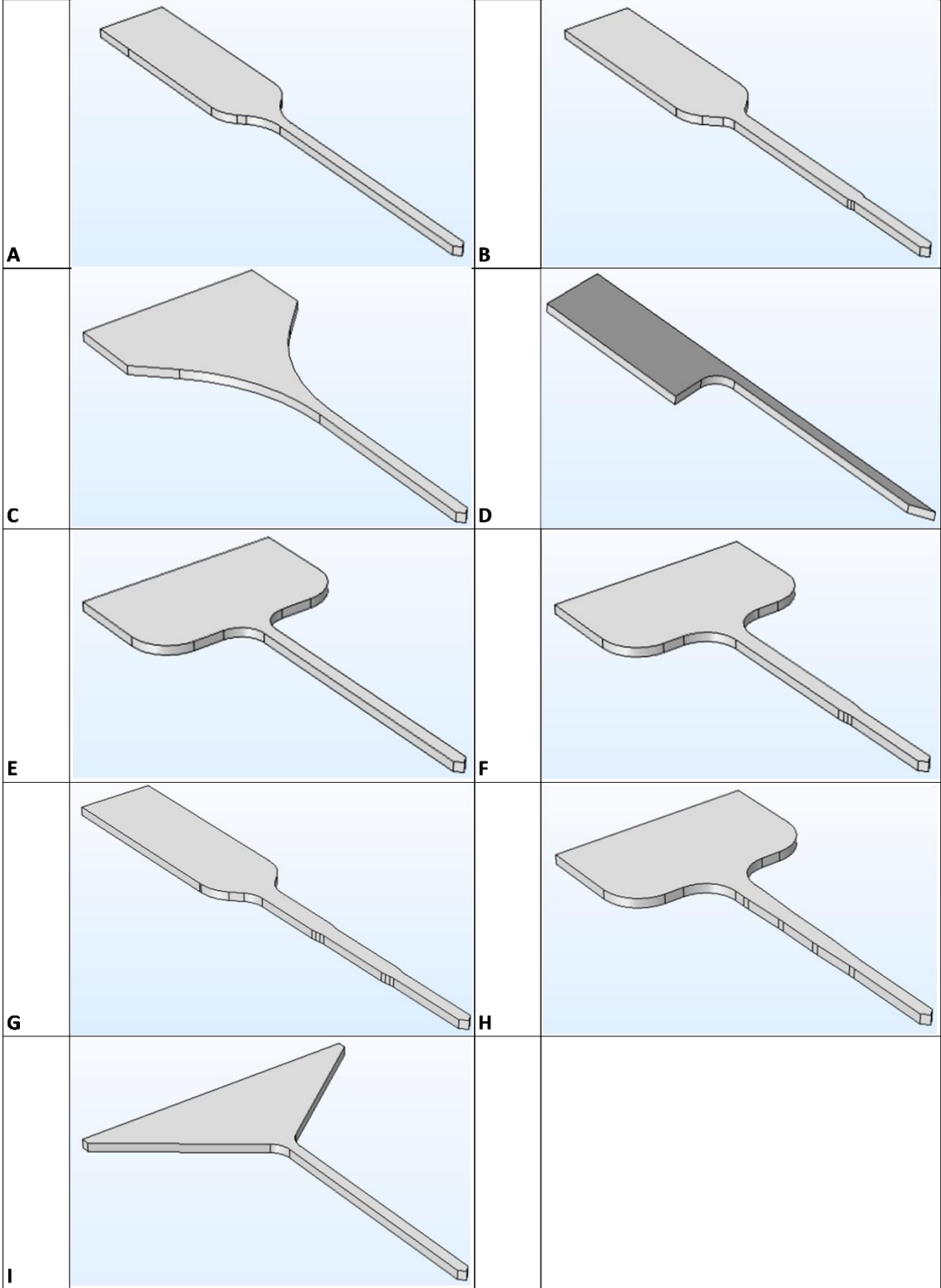


**Figure 3. 2: Several layout designs of the electrodes labeled as Prototype a, b, c, d, e, f, g, h and i**

## 3.2.2. Electrode mechanical analysis

### 3.2.2.1. Buckling analysis

Buckling is a failure mode that appears in thin structures when the axial force applied on the shank exceeds the critical load; which is known as the threshold value, and disturbs its structural equilibrium. This leads the shaft into an unstable state and the electrode shank geometry falls into buckling modes [65].

During electrode insertion, the instance just before tissue penetration is the most critical, where the electrode effective length and the axial load are at their maximum values [66]. The value of the critical load depends on the material, the electrode geometry and the end supports configuration.

Buckling resistance decreases with the presence of geometrical asymmetry, material defects, and eccentric loading which introduces bending moments and promotes curvature. The electrode should be designed to have a critical load higher than the force required for tissue penetration; to avoid buckling failure, otherwise, an insertion support tool is required. The electrode is modeled for linear buckling analysis and the different layouts are also modeled and analyzed. The critical loads are estimated to represent the forces that excite the buckling failure. While the tip is constrained in all directions to create fixed-free loading condition, unity axial force is applied to the electrode base. Eventually the buckling mode is extracted and the critical load is estimated [9], and then safety factor is calculated according to eq 3.1.

$$\text{Safety Factor} = \frac{\text{Failure Load}}{\text{Design Load}} \quad 3.1$$

Where: the Failure load is the Critical load

Design load: Penetration force estimated to be 1mN [67].

To investigate the effect of different electrode parameters on its mechanical performance, a shank with uniform rectangular cross-section is modeled. The thickness is varied from 20  $\mu\text{m}$  to 200  $\mu\text{m}$  while the shank width is fixed at 130  $\mu\text{m}$ . A 3mm Silicon or Nickel shank with thickness of 30  $\mu\text{m}$  has a critical load of 5mN, which dropped to 0.1mN for Polyimide shank. Polyimide sheet, Copper, Silicon, and Nickel photo-resist are modeled as the structural material. To survive a critical load of 10mN with Polyimide rectangular shank, a thickness varying from 120  $\mu\text{m}$  to 180  $\mu\text{m}$  is required depending on the electrode geometry.

### 3.2.2.2. Fracture

The electrode is subjected to lateral forces normal to the shank surface, during implantation and operation. These forces induce shear stresses [68]. Two sets of analysis are executed and fixed free support conditions are assumed. For ductile materials, the maximum von mises stress is assumed to quantify the electrode failure. The electrode model is configured for stationary analysis and the loading force value is set to the value of insertion force. The von mises stress is the result of the stationary analysis, illustrates the magnitude of stress levels and identifies high stress regions. For the analysis of brittle materials, the maximum principal stress theory (Rankine

criterion) is adopted. It states that failure occurs when the maximum principal stress, determined from uniaxial loading, reaches the ultimate tensile strength (UTS), and similarly for compressive stress. The three principal stresses at any point ( $\sigma_1$ ;  $\sigma_2$ ;  $\sigma_3$ ) might include tensile and compressive components.

The smallest negative value represents the maximum compressive stress, while the largest positive value represents the maximum tensile stress. This is due to the fact that brittle materials fail by fracture upon reaching the ultimate tensile stress, but do not yield nor endure plastic deformation [69].

COMSOL stationary analysis tool is utilized for calculating the fracture safety factor using suitable criteria with respect to material properties. The minimum safety is considered a safety factor of 5 [65]. In general, brittle materials fail in shear, while ductile materials fail in axial. For ductile materials, compression strength and tension are roughly equal, however, compression strength is much greater than tensile strength in brittle materials. The safety factor for axial loading is calculated by comparing the yield strength and von mises stress using Eq. 3.2 [56]. The accepted value is greater than or equal to 5. Finally, safety factor for shear force is calculated as the ratio between the maximum shear strength and the maximum shear stress of the design as illustrated in Eq. 3.3. The maximum shear stress of the design depends on the maximum principle stress ( $\sigma_1, \sigma_3$ ) as illustrated in Eq. 3.4.

$$\text{Safety factor with axial load} = \frac{\text{yield stress}}{\text{von miss stress}} \quad (3.2)$$

$$\text{Safety factor with shear stress} = \frac{\text{max. shear strength}}{\text{max. shear stress in design}} \quad (3.3)$$

$$\text{max. shear stress} = \frac{\sigma_1 - \sigma_3}{2} \quad (3.4)$$

### 3.3. Analysis Results

#### 3.3.1. Linear buckling

Thin Silicon and Nickel structures satisfy the mechanical requirements and avoid buckling failure. They score a minimum safety factor of 23 for layout A with thickness of 50 $\mu\text{m}$ . On the other hand, the minimum thickness of a Polyimide electrode, to barely survive buckling, is 100 $\mu\text{m}$  with a minimum safety factor of 3.1.

Table 3. 1, illustrates the safety factor of each layout with different materials and different thicknesses. Demonstrated results show that layouts E, F and H are the most stable, while layout A is the most vulnerable to buckling failure because it has the longest base length.

Figure 3. 3 illustrates the values of critical loads with different designs and materials with fixed thickness of 100  $\mu\text{m}$ .

Layouts E, F and H have wider bases than A, B and G, but are narrower than C and I, which explains their high resistance to buckling as illustrated in Figure 3. 4. When the base becomes much wider, the critical load decreases because the shank width is so small compared with the base and produces an unstable design; this is proposed in Figure 3. 5.

**Table 3. 1: Safety factor for different layouts: fixed-free linear buckling analysis**

	Si			Cu			Ni			Polymide		
	20μm	100μm	200μm	20μm	100μm	200μm	20μm	100μm	200μm	20μm	100μm	200μm
A	1.48	185.38	652.47	0.96	120.4	423.67	1.76	219.57	772.76	0.0249	3.11	10.95
B	1.71	213.72	934.36	1.11	138.83	607.09	2.03	253.16	1106.95	0.0287	3.59	15.68
C	2	251.36	899.21	1.30	163.35	584.03	2.37	297.81	1065.1	0.0336	4.2199	15.09
D	1.75	216.84	761.38	1.23	153.1	538.01	2.25	279.37	981.32	0.0319	3.9551	13.9
E	1.66	274.96	943.87	1.56	194.39	667.03	2.84	354.46	1216.58	0.0402	5.022	17.23
F	2.37	296.06	1154.9	1.68	209.34	816.44	3.06	381.69	1488.8	0.0433	5.408	21.09
G	1.79	223.93	1010.3	1.16	145.48	656.38	2.12	265.27	1196.85	0.03	3.758	16.96
H	2.5	312.17	1274.7	1.77	220.76	901.25	3.22	402.48	1643.4	0.0456	5.703	23.28
I	2.04	256.13	876.49	1.44	181.13	619.4	2.63	330.24	1129.7	0.0373	4.68	16

The design with wide base is not suitable for the rats because their brains are very small with a surface area of  $6 \text{ cm}^2$  [70], however, it is suitable for human's brain. Silicon and Nickel electrodes exhibit superior performance in resisting buckling failure. Nickel electrode with thickness of  $30\mu\text{m}$  would survive the applied axial force. The modulus of elasticity for Silicon and Nickel are of close values ( $E_{\text{Silicon}} = 170 \text{ GPa}$ ,  $E_{\text{Nickel}} = 220 \text{ GPa}$ ), accordingly; the critical loads for both materials are nearly the same value. On the other hand, Polyimide structures have very low critical loads due to their mediocre module of elasticity, and  $30\mu\text{m}$  shanks would fail.

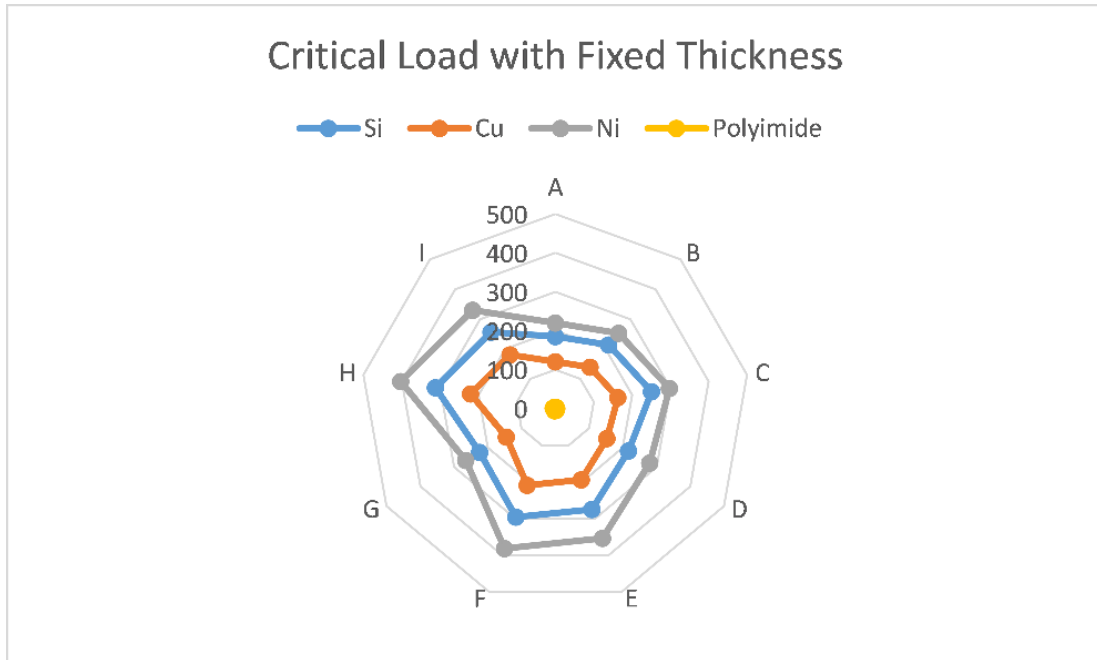


**Figure 3. 3: Illustrates the values of critical loads with different designs and materials with fixed thickness of  $100\mu\text{m}$**

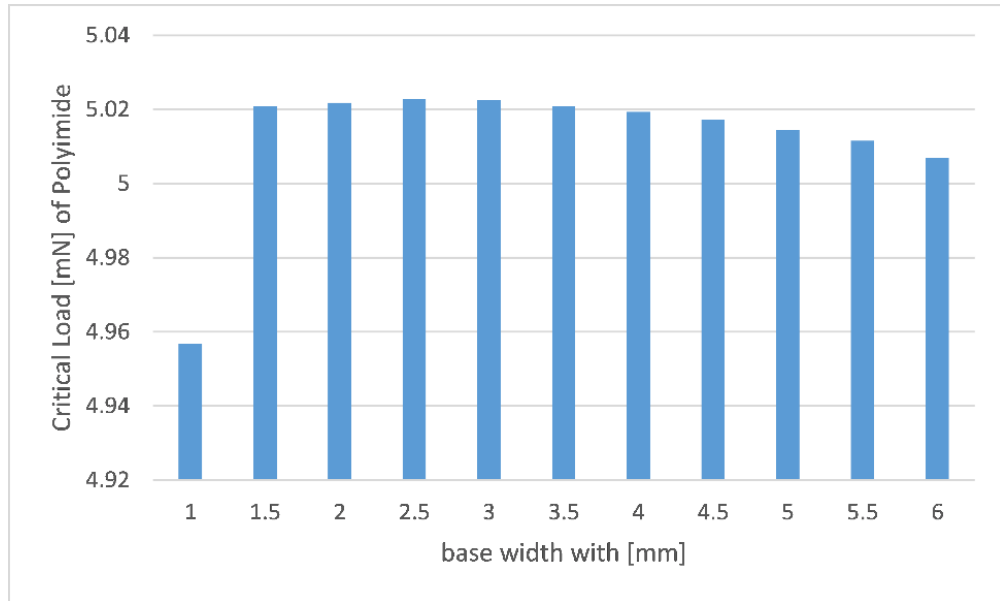


**Figure 3. 4: The effect of different base width on the critical load (design E with Polyimide material)**

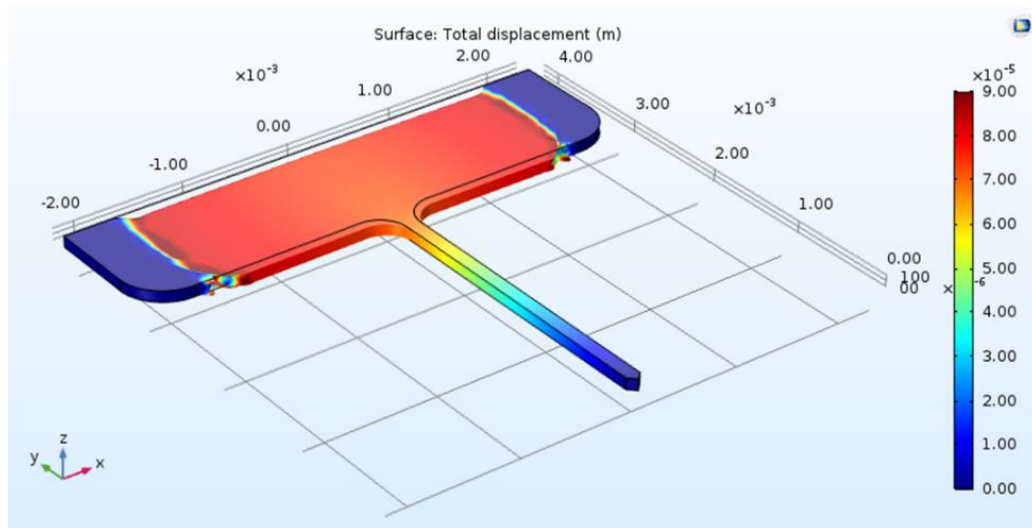


**Figure 3. 5: The distortion with very large base (design E with Polyimide material)**

### 3.3.2. Axial loading

The simulation results illustrate the superiority of Silicon electrodes in resisting axial loading. Silicon shanks with thickness of 50  $\mu\text{m}$  achieve an acceptable safety factor of 20 throughout the critical spots except for layout D. The asymmetry of layout D concentrates the tensile stresses along one of the sides, which cause the safety factor to drop below 5. The asymmetry and sharp edges of layout D have a huge effect on the static simulation when applying axial force to calculate the safety factor, but have no

effect on buckling failure. As for the 50  $\mu\text{m}$  Silicon electrodes, several designs show acceptable performance. Nickel electrodes come after the Silicon electrode in failure resistance. Most of the 70  $\mu\text{m}$  Nickel structures have a minimum safety factor of 5 which would survive axial compression and the minimum required thickness is 120  $\mu\text{m}$  to achieve the targeted safety factor of 10. On the other hand, Polyimide has bad mechanical properties compared to Silicon and Nickel, and the minimum thickness required for Polyimide to survive the mechanical loading exceed 200  $\mu\text{m}$  as shown in Figure 3. 6.

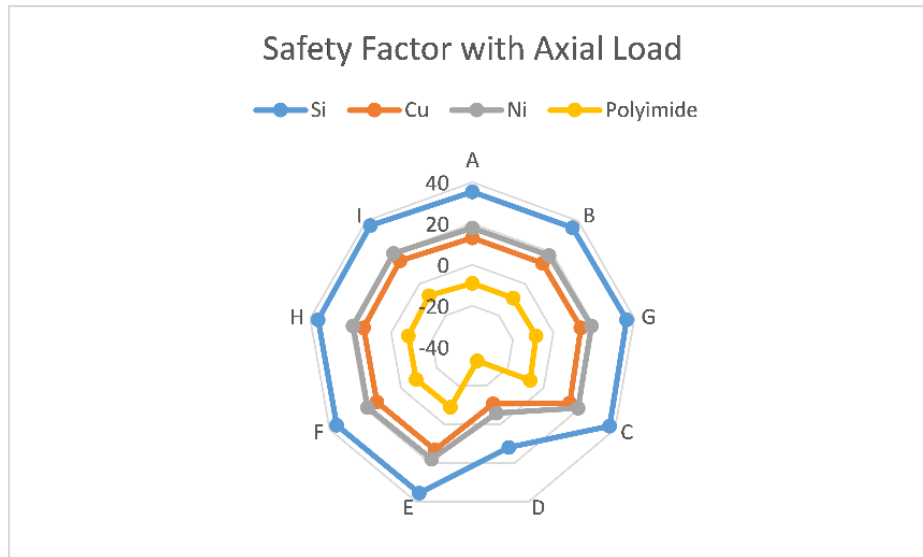


**Figure 3. 6: The log diagram for safety factor with axial load the different results of safety factors with axial load for different designs with different materials and fixed thickness**

Although Silicon achieves the mechanical performance required, for chronic electrode fabrication flexible substrates are preferred. Flexible substrates have the ability to restore its original shape after the force is eliminated, because it elastically responds to external stresses. Increasing the axial force beyond the yield point would cause permanent deformation without fracture till the ultimate strength is reached. In contrast, brittle (Silicon) electrodes would endure fracture right after crossing the yield point so these are not preferred for long term in vivo applications.

Furthermore, Polyimide is easy to process and is biocompatible; these properties make it eligible for electrode implementation.

### 3.3.3. Shear loading

During implantation and operation, lateral forces normal to the shank induce shear stresses, which affect the electrode and create off plane deformation. In this simulation, the electrode is subjected to 1 mN shear force equivalent to the value of the force required for electrode insertion [45]. Fixed-free support conditions are assumed.

The applied shear forces on the electrode shank produce compressive stresses on one side and tensile stresses along the other. Silicon electrodes analysis shows that the side undergoing compressive stresses does not endure failure, as the ultimate tensile

strength for the brittle material is lower than the compressive stress. In contrast, Nickel electrodes of different layouts and thicknesses show large safety factors along the compressed side. The results depend on materials to determine the minimum thickness of each layouts to prevent fracture during insertion assuming a single crystal defect free structure. However, layout D with Silicon showed vulnerable response to shear stress at 100  $\mu\text{m}$ .

The safety factor distribution contours for shear loaded with different materials and different layout electrodes are plotted in Figure 3. 7. Nickel shanks as thin as 40 $\mu\text{m}$  demonstrate acceptable performance with a minimum safety factor of 5. As for Polyimide, they are more vulnerable to shear stresses, and this is rectified by increasing the electrode thickness over 100 $\mu\text{m}$  to realize the required performance.

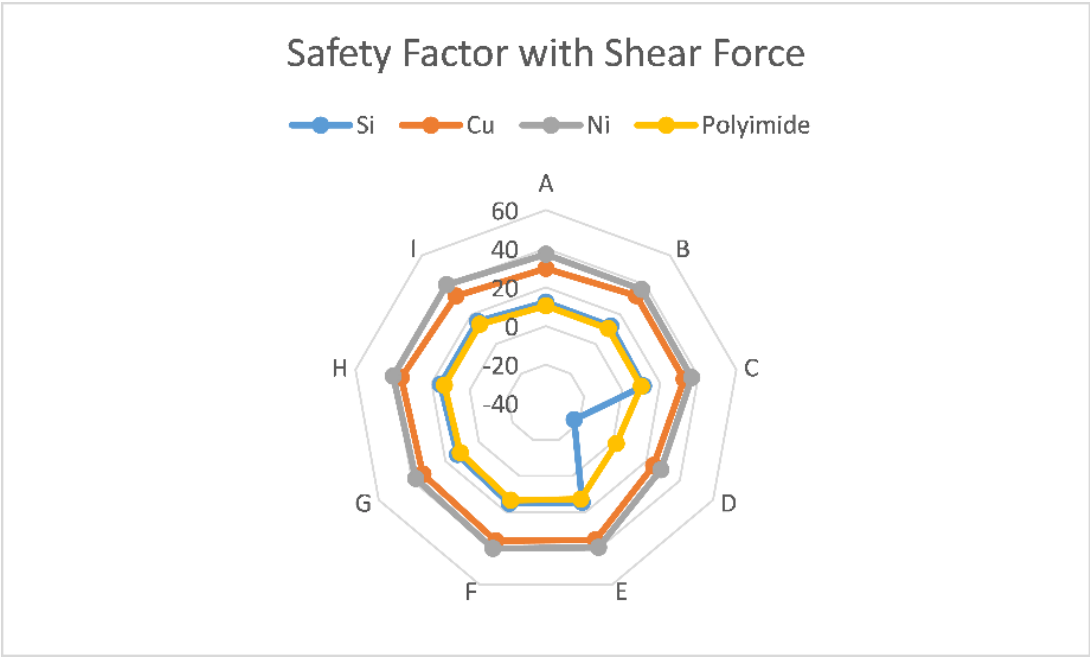


**Figure 3. 7: The log diagram for safety factor with shear load illustrates the different results of safety factors with shear load for different designs with different materials and fixed thickness**

### 3.3.4. FOM

FOM is calculated for each design, which is considered as a numerical quantity based on one or more characteristics of the design to represent a measure of efficiency. Low impedance, low noise, low fabrication cost, small cross section area, large number of channels, and high safety factor of mechanical analysis are the characteristics of FOM [71].

The previous results illustrate that Nickel exhibits superior resistance to buckling failure during implantation followed by Silicon. Besides that if fabrication costs are taken into account, the Polyimide material has the lowest cost which will cost almost \$900. Nickel and Copper come in the second rank with \$1800 and then applying the cost of a gold thin film. Using Si as the material costs around \$2100.

A comparative between all designs is carried out to indicate which design is better. The comparative depends on the values of FOM. The best design has the largest value



of FOM. The FOM depends on the different values of safety factor for each design that are calculated from mechanical analysis as well as the cross section area of the shaft and the fabrication cost of each material. All the other characteristics are constant for all designs such as impedance and noise because of the pads of all electrodes in these designs are constant.

Figure 3. 8 illustrates the results of FOM. It shows that the design C and I with Nickel material give the highest value of FOM but its bases are not compatible with rats because they are very large. Design H follows them so it is considered the best design. Design D with Polyimide material is considered the worst design because it gives the worst FOM.

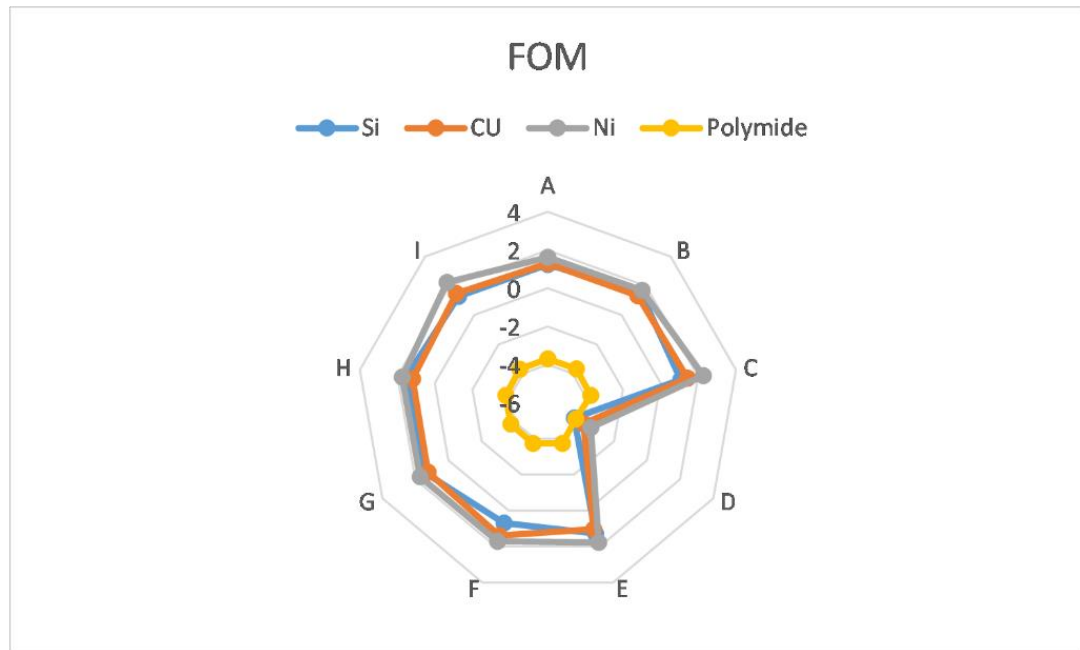


**Figure 3. 8: FOM for several designs with different materials**

### 3.3.5. Results of different stages

Several electrode layouts are presented and their mechanical properties are examined in the pursuit of a design that contains a large number of stimulation channels. The proposed layouts are showed in Figure 3.9. For easy connections between electrode and its circuit, the bases of the electrodes are designed with bigger size than the electrodes shank to provide large interconnect pads, in contrast all the prototypes shanks have the same length to reside within 3mm inside the tissue and carry the interface pads. Additionally, all electrodes have the same tip width which is enough to comprise the interface pads. The interconnect pads on prototypes B, C and D are arranged transversely, while those in A is longitudinal. The simulations of the electrode models are analyzed to explore their mechanical performance with different shanks shapes on the critical load.

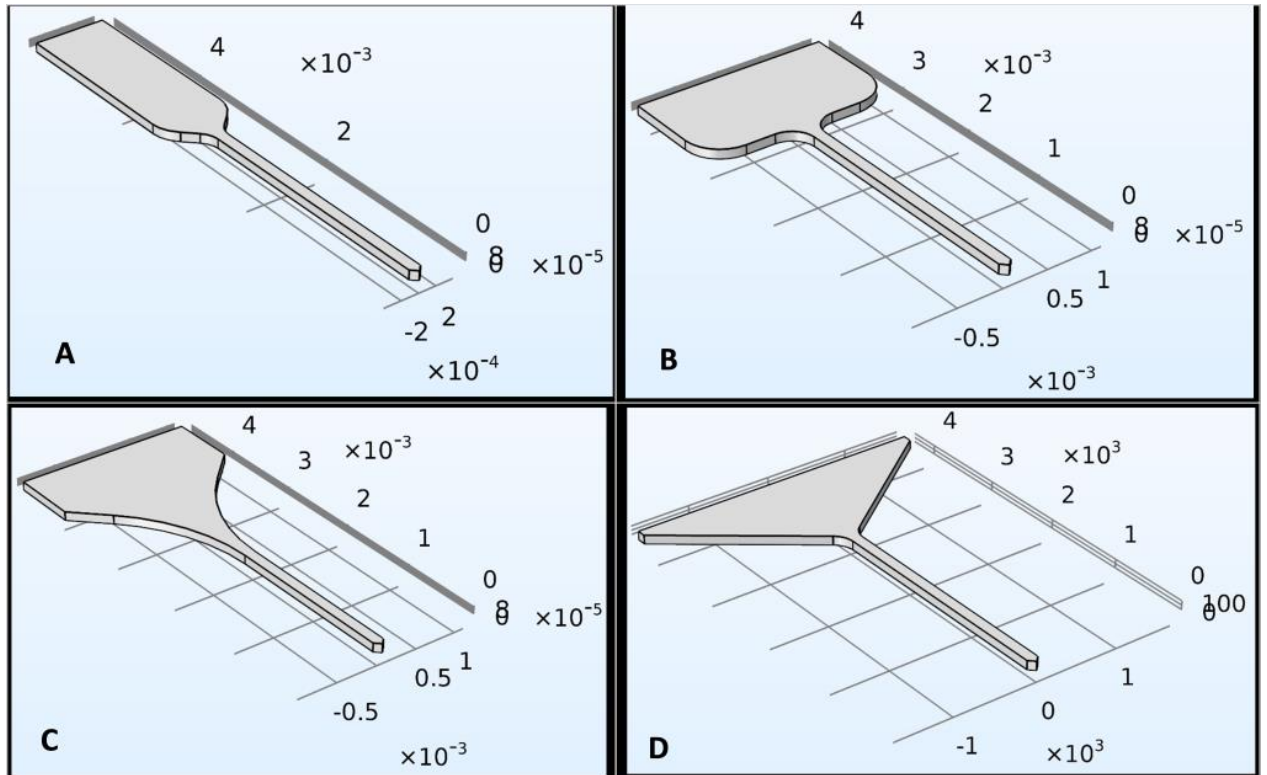


**Figure 3. 9: 4 different prototypes of electrodes**

The maximum von mises stress is assumed to quantify the electrode failure. The electrode model is configured for stationary analysis and the loading force value is set to uniaxial loading. The von mises stress is the result of the stationary analysis, illustrates the magnitude of stress levels and identifies high stress regions. It states that failure occurs when the maximum von mises stress, determined from uniaxial loading, reaches the ultimate tensile strength (UTS). This is due to the fact that brittle materials fail by fracture upon reaching the ultimate tensile stress, but do not yield nor endure plastic deformation [31]. COMSOL stationary analysis tool is utilized for calculating the fracture safety factor using suitable criteria with respect to material properties. The safety factors for each axial loading and shear force are calculated by comparing the (UTS) and von mises stress using equation 3.5.

$$\text{Safety Factor} = \frac{UTS}{\text{Von mises stress}} \quad (3.5)$$

Demonstrated results show that layout B with 4 stages are the most stable, while layout A without stage is the most vulnerable to buckling failure because it has the longest base length without degradation in shank width.

Figure 3.10 illustrates the values of safety factor with different designs. Layouts B, C and D have wider bases than A and when increase the stages, they give high resistance to buckling. The shapes of the design A with different stages are illustrated in Figure 3.11.

Design B without stages gives the best resistance to buckling than the other designs without stages, so when adding the stages it improves the resistance to buckling failure

and this resistance is directly proportional with the number of stages. Figure 3.12 exposes the degradation of safety factor of design A with number of stages.

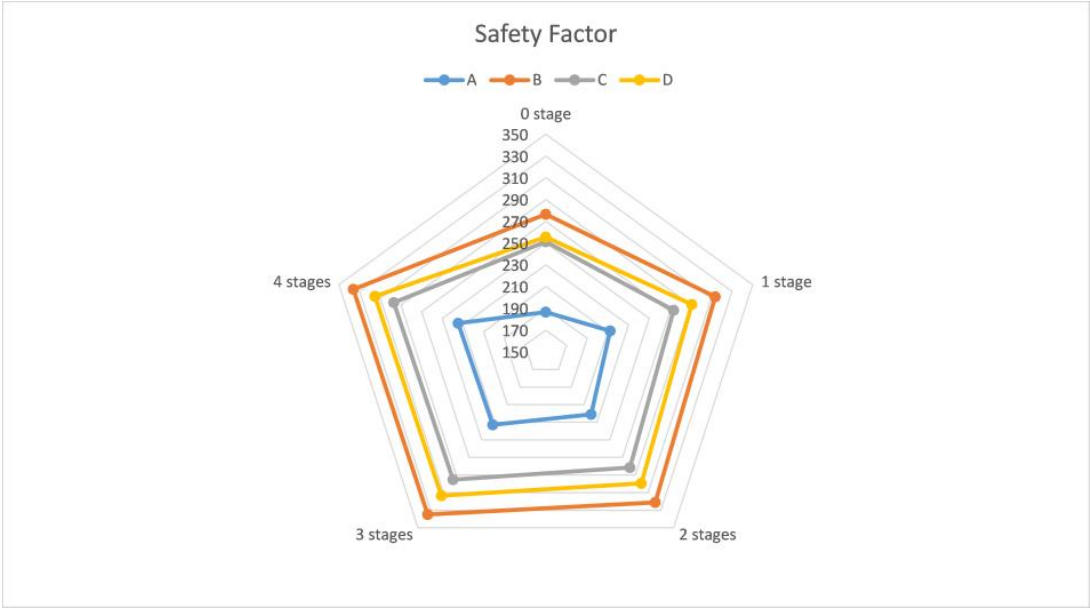


**Figure 3. 10: Safety Factor with Buckling Analysis**

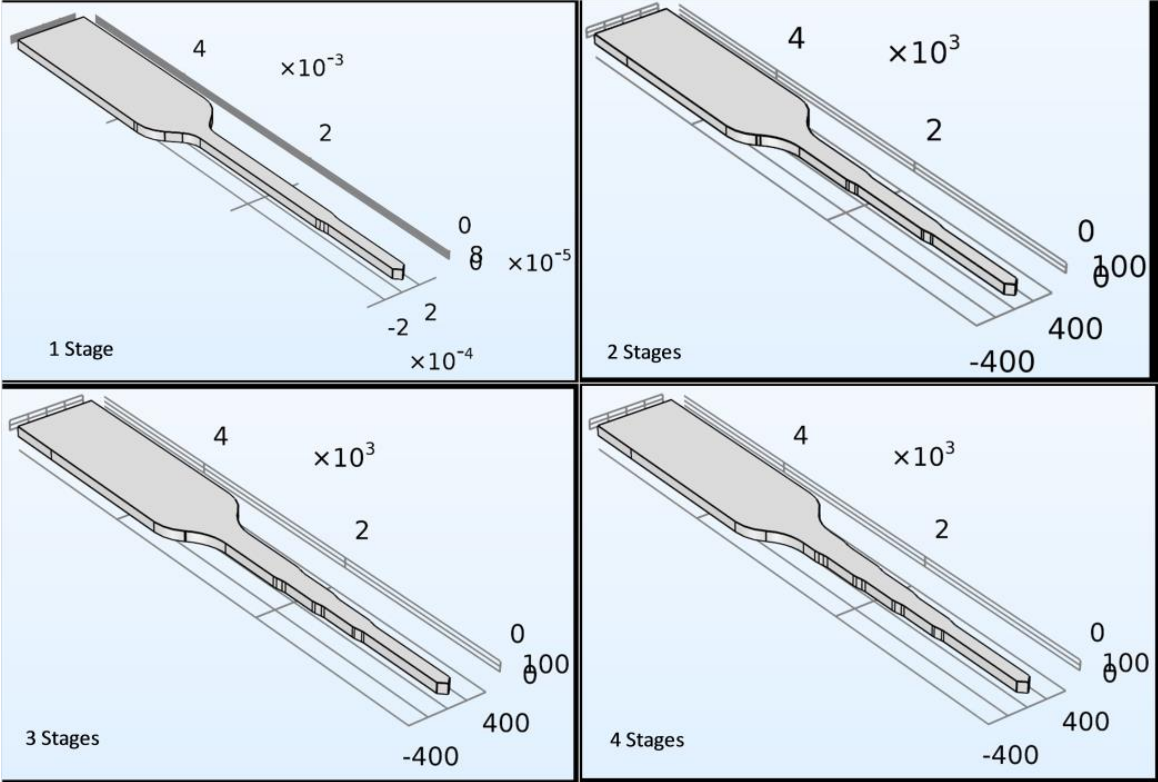


**Figure 3. 11: Design A with different number of stages**

The simulation results illustrate the superiority of electrode C without stages in resisting axial loading. It has the best smoothing link between base and shank so it gives the best safety factor without needing to increase the stages in the shank, but has no effect on buckling failure as design B shows better resistance buckling failure than design C. In case of design A, 2 stages exhibits superior performance in resisting axial failure as illustrated in Fig 3.13. Also, electrode design B with 2 stages exposes the higher performance than the other designs of B with higher stages or lower. Design A and B has the same shape of the link between the base and the shank of the electrode so the results of simulation illustrate that these 2 designs have the best resistance of axial load with 2 stages design. In otherwise design D has a different result which is that the shape with 1 stage has the best resistance to avoid axial failure. Design D has a different base shape as it is similar to a triangle. Design C has the most smoothing link between the base and the shank so it illustrate the highest safety factor without any stages. Finally Design C without stages exposes the best performance with axial load and design D with 1 Stage comes after it. The exhibition of all designs are illustrated in Figure 3.14.

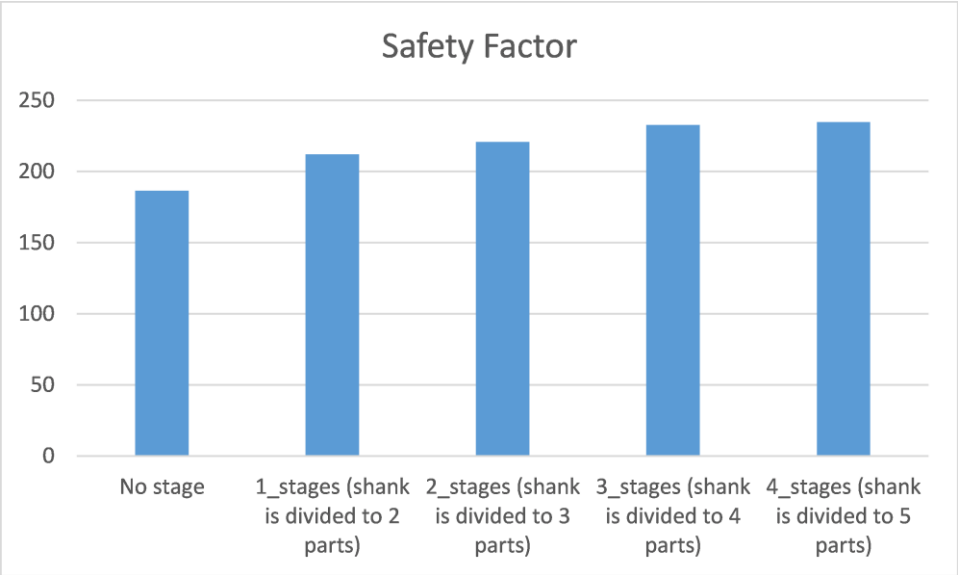


**Figure 3. 12:** Safety Factor with Buckling Analysis of design A

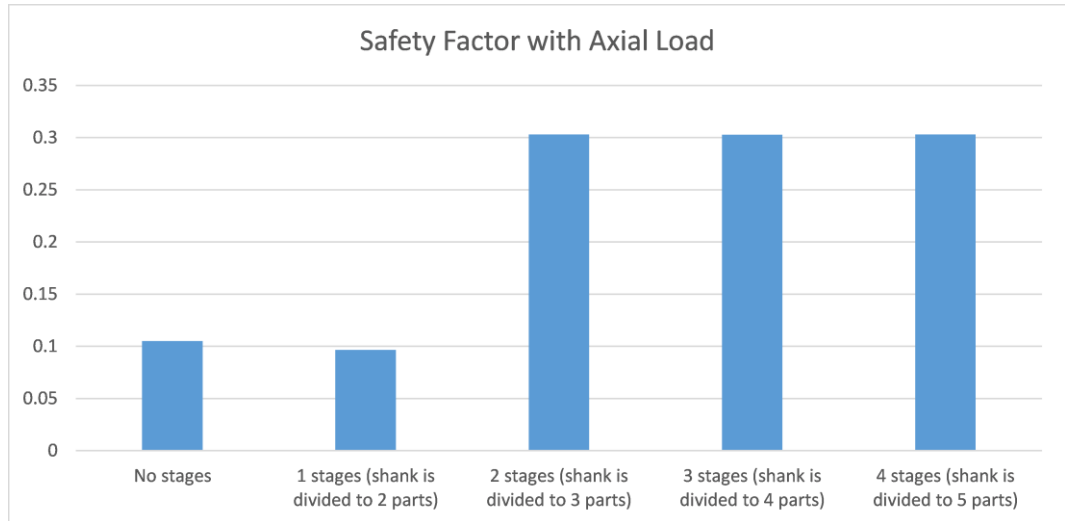


**Figure 3. 13:** Safety Factor with Axial Load of design A

During implantation and operation, shear stresses are induced by lateral forces which are normal to the shank. These shear stresses affect the electrode and produce plane deformation. The value of the required force for electrode insertion is 1mN [14]. In this simulation, applying shear force which is equivalent to the value of the force required for insertion process. Fixed-free support conditions are assumed.

The shear forces which are applied on the electrode shank induce compressive stresses on one side and tensile stresses along the other. As the ultimate tensile strength for the brittle material is lower than the compressive stress, so Silicon electrodes analysis illustrates that the side undergoing compressive stresses does not resist failure. Figure 3.15 presents the attitude of each design with different stages under the shear force.

The simulation results illustrate the superiority of electrode B with 2 stages in resisting shear loading. It has a similar result like buckling analysis, as in buckling analysis design B give the best results. When comparing with the number of stages in each design, the results will illustrate that the best performance with shear load is same as the best performance with axial load in designs A, B, and C. But design D with 2 stages gives the best performance in resisting failure with shear load.

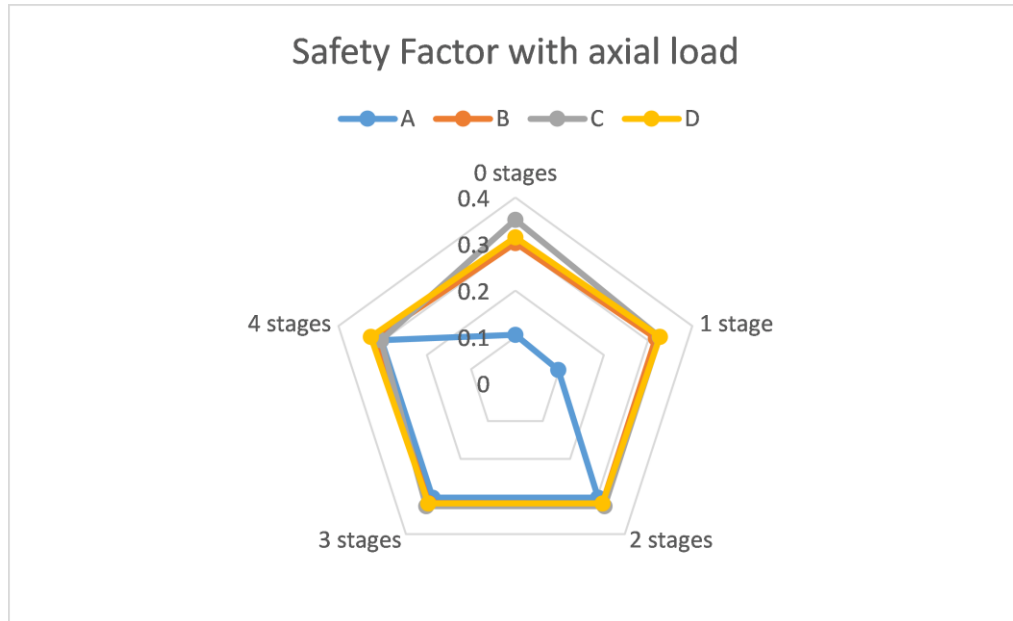


**Figure 3. 14: Safety Factor with Axial Load**

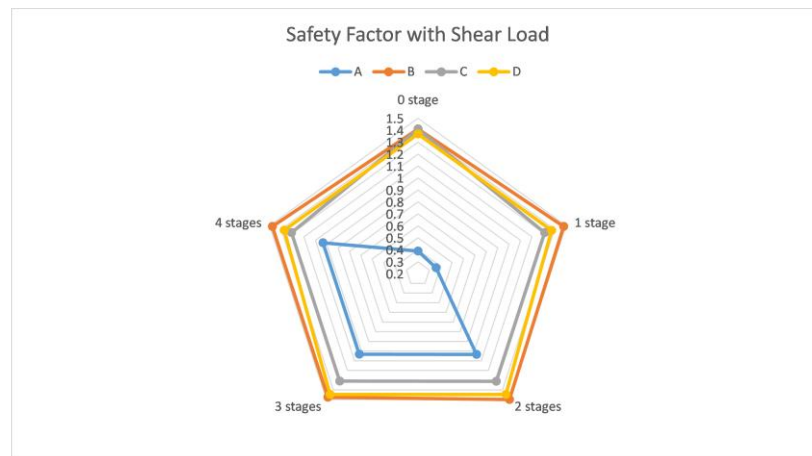


**Figure 3. 15: Safety Factor with Shear Force**

From the previous results, Design B with 4 stages exhibits superior resistance to buckling failure during implantation followed by design B with 3 stages then 2 stages. Design D with 4 stages comes in the fourth rank. In second case of failure, fraction failure with axial load, Design C without stages performs as the best design in resisting this failure, then followed by design D with 1 stage. In case of failure compared with shear load, design B with 2 stages has superior resistance.

A comparison between all designs is carried out to indicate the better number of stages in each design. The comparison depends on the values of critical load, safety factor with axial load, and safety factor with shear force.

- The best number of stages in design A is 2 stages.
- The best number of stages in design B is 2 stages.
- The best number of stages in design C is no stages.

- The best number of stages in design D is 1 stages.

Finally, by comparing these results, Design B with 2 stages is considered the best one followed by design C without stages then design D with 1 stage. Design A with 2 stages ranks the fourth.

### 3.4. Electrical simulation

The electrode DC resistance is estimated by finite element modeling.

The resistances of the design depend on the track thickness and length because a constant track width is used. Several materials are used and its DC resistances are compared, then if thermal properties are taken in consideration, the material which has the highest thermal conductivity is preferred.

There are 2 designs one for human and the other one is for rat's electrode. The simulation tests the effect of different design parameters on its value.

#### 3.4.1. Pads

The electrode metal structure consists of interconnect pads, routing tracks, vias, and stimulation pads. Components as vias, routing tracks, and stimulation pad, which have a narrow cross-sections, are expected to significantly contribute to the value of the resistance. Figure 3. 16 shows the metal structure model, and the components are illustrated with different colors. The interconnect pad has unity voltage and a Zero voltage is applied to the surface of the stimulation pad. Parametric model is simulated to study the effect of several variables including material types, dimensions, and temperature. Component dimensions are varied to cover a possible range of practical fabrication values, the design parameters values are listed in Table 3. 2. The results are executed and post processed to investigate the effect of different parameters on the resistance.

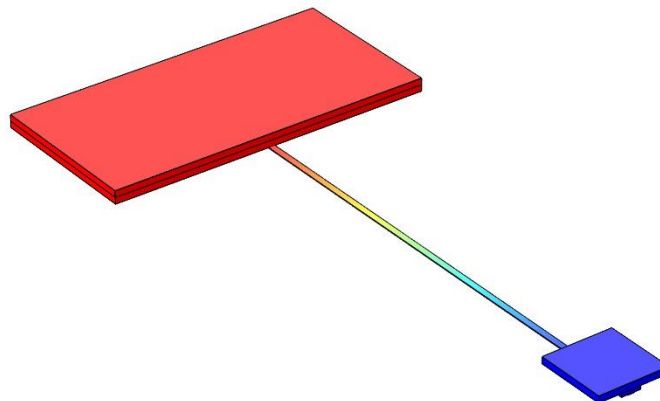


**Figure 3. 16: model for the electrode metal structure**



The first simulation is made is to calculate the DC resistance. Applying a voltage difference to a conductor creates a current flow and the intensity of the current is usually a function of the applied voltage difference. In the simplest (linear) case, the current flow and the voltage difference are proportional; the proportionality constant is the resistance of the device. So the physics type that is used is **AC/DC>Electric Currents (ec)**.

**Table 3. 2: Parameters**

Routing track length	From 1500 $\mu$ m to 5000 $\mu$ m
Routing track width	10 $\mu$ m
Routing track thickness	From 300nm to 1 $\mu$ m
Pad via width	30 $\mu$ m
Pad via length	100 $\mu$ m
Pad via thickness	10 $\mu$ m

Some simulations are made on several materials (Gold (Au), Platinum (Pt), Titanium (Ti), and Aluminum (Al)). These simulations include different track thickness as illustrated in the previous table. The results of its DC resistance are exposed in Table 3. 3. This table illustrates that gold has the lowest DC resistance but to get the lowest resistance and in the same time reduce the cost, form the tracks and the vias from Al, then stimulation pad and interconnected pad from Au.

Any foreign bodies are implemented in a living system, excite changes in the homeostatic mechanisms. These homeostatic mechanisms stabilize the internal body equilibrium. Biocompatible materials produce minimal biological response and do not create injurious, toxic, or immunological response when contact with tissue.

- Gold is biocompatible.
- Platinum is more tissue response than gold and stainless steel and No gliosis after 30 days but produces denser capsule.
- Aluminum is biocompatible.
- Titanium is biocompatible.

The simulation is repeated for another two biocompatible materials (Tantalum because it is a biocompatible, and Nichrome which is recommended for medical implants.)

**Table 3. 3: DC resistance for different materials**

Track Thickness [nm]	Au	Pt	Ti	Al
300	4.758 $\Omega$	24.379 $\Omega$	83.45 $\Omega$	6.112 $\Omega$
400	3.571 $\Omega$	18.297 $\Omega$	62.633 $\Omega$	4.587 $\Omega$
500	2.859 $\Omega$	14.646 $\Omega$	50.136 $\Omega$	3.672 $\Omega$
600	2.384 $\Omega$	12.212 $\Omega$	41.804 $\Omega$	3.062 $\Omega$
700	2.044 $\Omega$	10.473 $\Omega$	35.849 $\Omega$	2.626 $\Omega$
800	1.786 $\Omega$	9.168 $\Omega$	31.383 $\Omega$	2.298 $\Omega$
900	1.591 $\Omega$	8.153 $\Omega$	27.907 $\Omega$	2.044 $\Omega$
1000	1.433 $\Omega$	7.341 $\Omega$	25.128 $\Omega$	1.84 $\Omega$



Track Thickness [nm]	Nichrome	Tantalum
300	238.672 $\Omega$	28.653 $\Omega$
400	179.134 $\Omega$	21.505 $\Omega$
500	143.392 $\Omega$	17.214 $\Omega$
600	119.562 $\Omega$	14.354 $\Omega$
700	102.532 $\Omega$	12.309 $\Omega$
800	89.757 $\Omega$	10.775 $\Omega$
900	79.816 $\Omega$	9.582 $\Omega$
1000	71.869 $\Omega$	8.628 $\Omega$

The simulation is repeated with 2 different properties with changing the length of the track and with the thickness in the same time and the results is exposed in Table 3. 4.

If taking the temperature's effect on the Dc resistance, the simulation is repeated under physics (Joule Heating), and we will calculate the current distribution from the results and the change in temperature. Because of that the change in temperature does not exceed than 1°C, the DC resistance does not be affected. The initial Temperature that the simulation is made on it is room temp. 20°C or human temp. 37°C. The resistivity of Aluminum changes from (2.43e-8 @ 0°C, 2.67e-8 @ 20°C to 3.63e-8 @ 100°C) so the change from 20 to 37°C does not make a perceptible change in DC resistance.

Figure 3.17 illustrates the change in Dc resistance of Au material with different thickness and length.

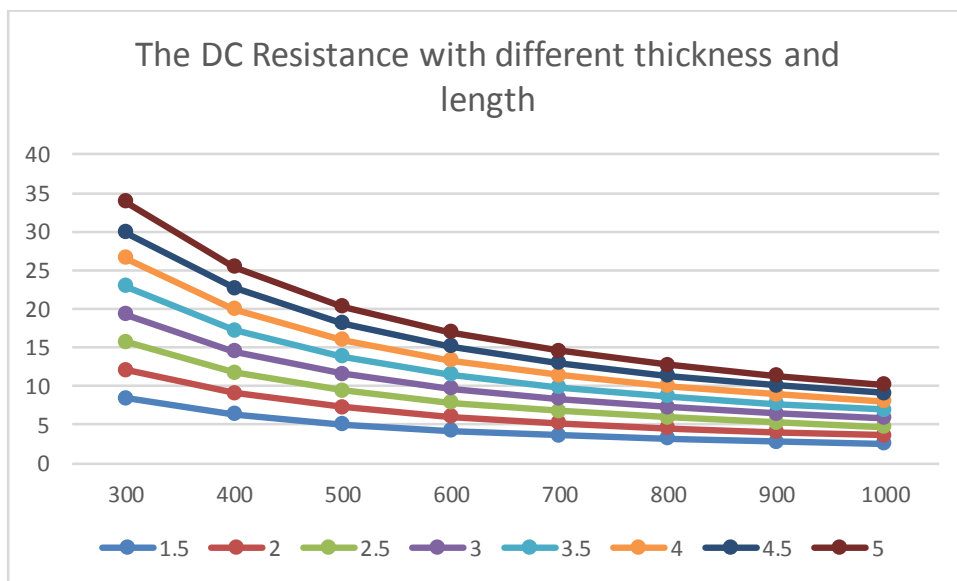


**Figure 3. 17 : illustrates the DC resistance of Au with variable thickness and length of track**

**Table 3. 4 Dc Resistance with Several Thickness and Length**

Thickness	Length	Tantalum	Nichrome	Al	Pt	Ti	Au
300	1.5	50.6	421.8	10.8	43.1	147.47	8.4
400	2	54.5	453.9	11.6	46.4	158.71	9.0
500	2.5	56.8	472.7	12.1	48.3	165.28	9.4
600	3	58.3	485.4	12.4	49.6	169.71	9.67
700	3.5	59.4	494.6	12.7	50.5	172.94	9.86
800	4	60.2	501.5	12.8	51.2	175.35	9.998
900	4.5	60.8	506.9	12.98	51.8	177.22	10.105
10000	5	61.4	511.3	13.09	52.2	178.76	10.192

### **3.5. Conclusion**

This chapter presented a review of several prototypes of the proposed electrodes, which were analyzed to satisfy the design requirements. Design H with Nickel material gives the best results which is suitable for rats. Design C and I with Nickel material have the highest FOM but are not compatible with rat brain.

On the other hand, the Polyimide electrodes do not undergo the axial loading which induces fractures and are vulnerable to failure. Shear analysis results are in favor of Nickel electrodes due to its ductile properties, and Polyimide designs with thick cross-sections can replace silicon.

It also introduced a review of several prototypes of the proposed electrodes with different stages, which were analyzed to compare between their mechanical performances. Design B with 2 stages gives the best results. On the other hand, Design A without stages is considered the worst design in resisting the failure. The best design with the smallest shank width is design C.

Some electrical simulations were done due to several materials with different thickness and different length of the tracks between pads. The gold material gives the best results in Dc resistance with different thickness and track lengths. It is considered a good material for biomedical devices because of its biocompatibility.

## Chapter 4 : Human Electrodes

In this chapter, several electrode layout designs with different materials are introduced and their mechanical analysis during insertion into the brain tissues is studied. From this analysis, a prediction of which design, with which material and which dimensions will overcome the mechanical failure and can be implemented without needing an insertion assistive device. Electrode mechanical analysis is presented with two mechanical failure modes the electrode is subjected to on insertion: buckling and fracture. Thus, linear buckling analysis and stationary analysis with axial and shear loading are illustrated for both brittle and ductile materials with the help of COMSOL Multiphysics. These electrode layouts are juxtaposed to estimate which design achieves the best critical load and safety factor due to the applied forces.

### 4.1. Electrode dimensions and prototype

Human brain is a very evolved networked-structure made up of billions of nerve cells, known as neurons. This brain could lose part of its functionality when many cells are lost as a result of developmental effects, strokes or tumor amputation. For example, these disorders can lead to deficiency in the motor system, which is known as Parkinson disease. It could also produce abnormal signals from the brain, causing bizarre sensations, behaviors, emotions and sometimes loss of consciousness. Such disease is known as Epilepsy.

Recently, deep brain stimulation (DBS) microelectrodes proved their efficiency in the therapy of neural disorders, where the electrodes are implanted in the malfunctional brain region, and by sending electrical signals, these disorders are resolved. So far, many developments have been introduced to deep brain stimulation electrodes, starting with glass micropipettes and followed by microwire bundle electrodes [51],[72].

Recently, some types of deep brain stimulation electrode have appeared such as foldable neural electrode [73]. This microfabricated electrode is a type of flexible DBS electrode of the cavity wall of thalamic lesions resulting from brain infarcts. It is allowing stimulation at different anatomical locations. It is fabricated from Polyimide and its length is 40 mm so it needs an insertion assistive device through penetration surgery and implantation, the electrode is introduced through a cannula. Another type is an implantable micromachined neural probe with multichannel electrode for both recording and electrical stimulation was designed [74]. This flexible, Polyimide-based microelectrode is composed of a long shank (14.9 mm in length) with small thickness  $5\mu\text{m}$ . So this electrode with this dimensions will need an insertion assistive device during implementation. The human DBS electrodes have a variable range of the shank length from 6mm to 40mm in some papers.

Several designs are proposed based on initial designs for rat electrodes [31]. All the design are illustrated in Figure 4.1. The shank length is increased to 10mm to be suitable for the human brain [15]. In order to compare the different designs, the thickness is made constant at  $100\mu\text{m}$  for all electrodes. The minimum width for the shank is also equal for all designs at  $130\mu\text{m}$ . The initial designs mostly differ in base design and dimensions.

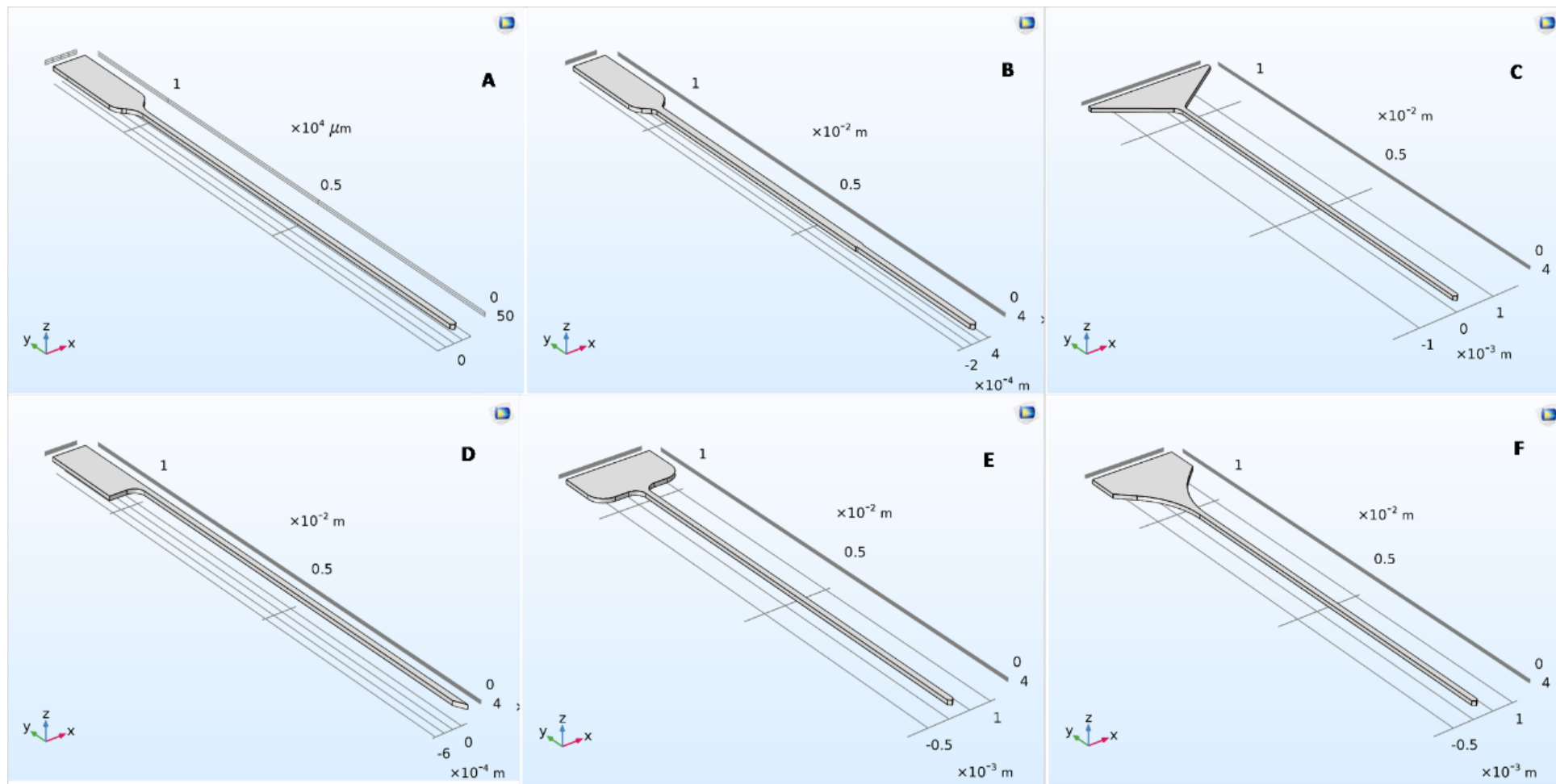


**Figure 4. 1:** The several layout designs of the electrode

The electrodes have different base designs except for design A and B. Both designs are similar except for the shank. Design B has a shank with two stages descending in width and length. The first stage of the shank which is the nearest part to the base is the widest stage and is nearly two thirds of the total length. The width of the shank increases total area but the tip width is still constant. On the other hand, the mechanical properties, specifically buckling resistance is expected to improve. The idea to divide the shank into several stages is expanded up to 5 stages for design B as can be seen in Figure 4.2.

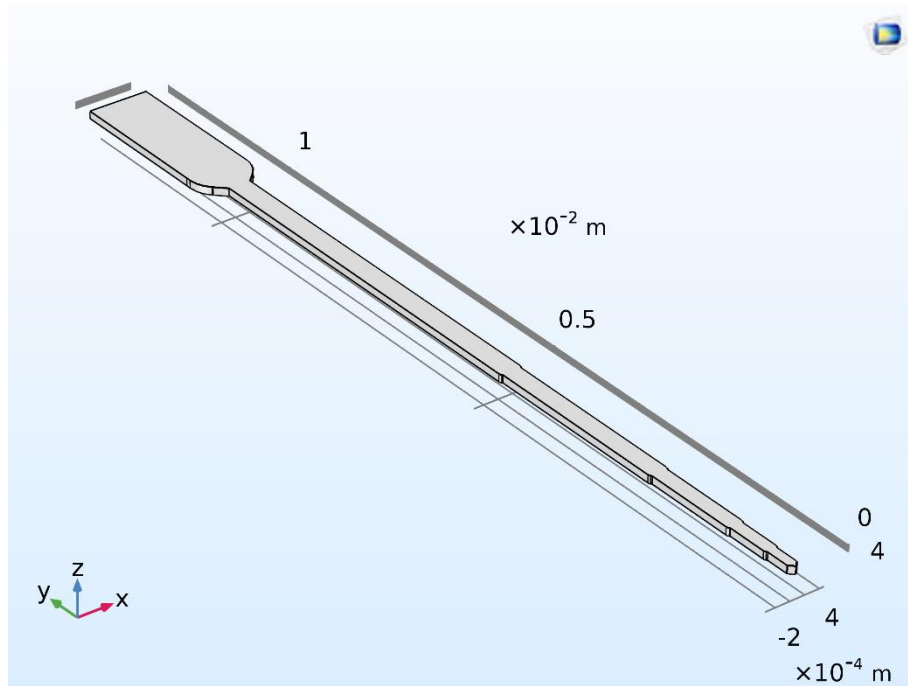


**Figure 4. 2:** Design B with five stages, each stage wider than the following stage by 40  $\mu\text{m}$  and is double its length.

The staged design is also applied to designs C, D, E and F. A comparative analysis between the different designs up to three stages is carried out with shank width of different stages ranging from 210  $\mu\text{m}$  to 130  $\mu\text{m}$ . All designs follow the same shank design to allow for a proper comparison between the different bases.

The region connecting the different stages is expected to develop high stress due to the abrupt change in width. Accordingly, sharp edges, which are illustrated in Figure 4.3:a are filleted to allow for a smoother transition. Another method that allowed for a smoother transition is developed using Bzier Polygons [56], as in Figure 4.3:b, to alleviate stress from the intermediate regions.

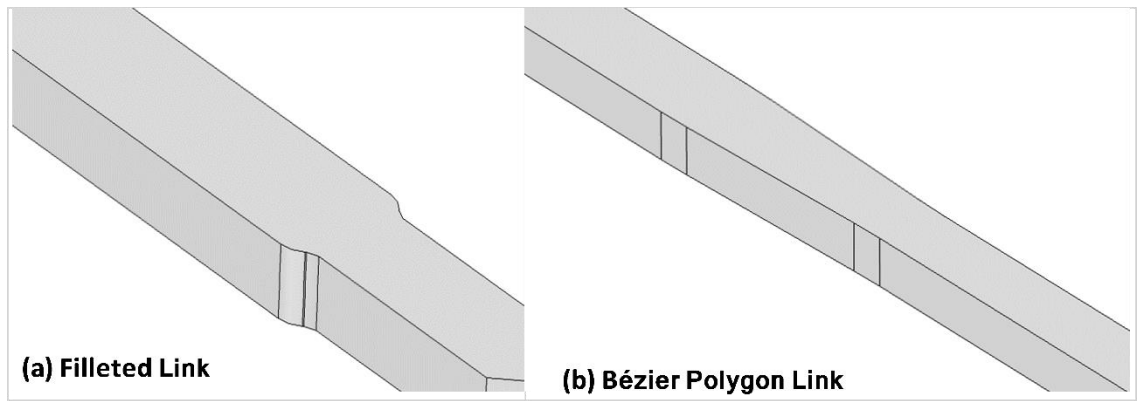


**Figure 4. 3:** Left: Filleted Link. Right: Bzier Polygon Link

It is important to note that the device total area should be kept minimum as long as its mechanical integrity is not sacrificed. Although the staged design increases shank area, it is intended to reconcile with better mechanical performance. Different design ideas are also applied to the staged design for the sake of providing a comparative insight between varying stage lengths. Three different ideas are further explored in this paper; equal stage lengths is illustrated in Figure 4.4: a , longest first stage is illustrated in Figure 4.4:b and longest final stage is illustrated in Figure 4.4:c.

There are two mechanical failure modes, the electrode is subjected to on insertion: buckling and fracture. Accordingly, the Mechanical Analysis includes the studying of linear buckling, and stationary analysis with axial and shear loading. The conducted tests are done with different designs and several materials, each having its own failure mode bases on its mechanical properties. The safety factor is calculated for each one of these tests for both ductile and brittle materials. Ductile materials such as Polyimide and metals (Copper and Nickel) and brittle materials such as Silicon are used as materials for the implemented electrodes.

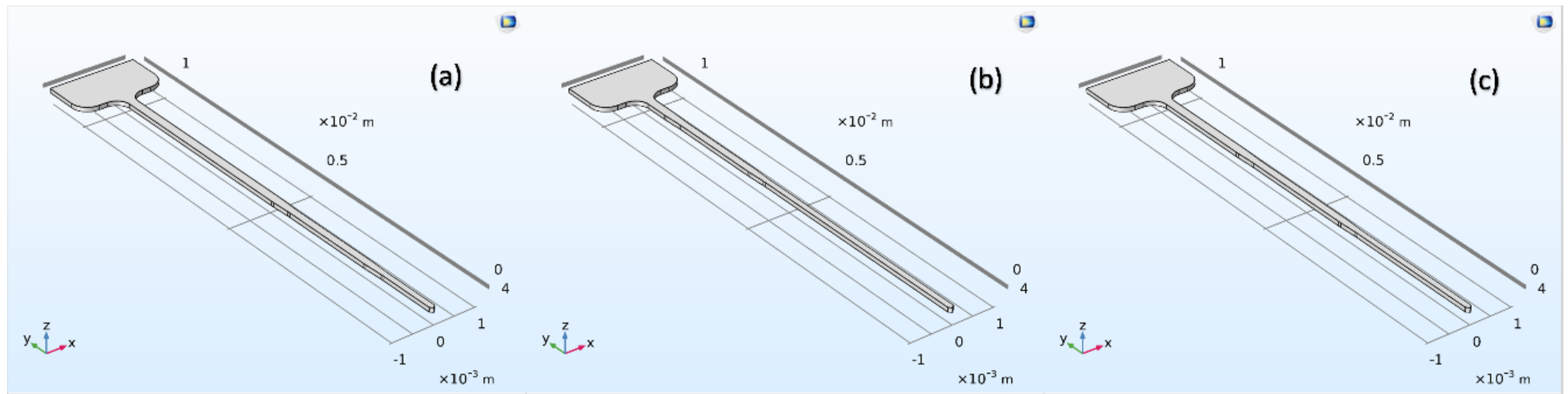


**Figure 4. 4:** Design E with 3 different stage lengths: a) longest first stage. b) Longest final stage. c) Equal stage lengths.

## 4.2. Linear Buckling Analysis

Buckling is a failure mode that takes place when the applied axial force exceeds the critical load [66]. The critical load value varies depending on the implemented electrode design and the used material. Thus, in order to avoid buckling failure, the electrode should be designed to have critical load higher than the required tissue penetration force. At the same time, to have high resistance to buckling failure, the electrode structure should be symmetric since buckling resistance diminishes with the existence of geometrical asymmetry, material defects, and eccentric loading [65].

Linear Buckling Analysis is applied on the electrode structures with different materials, while constraining the motion of the tip in all directions, thus creating fixed-free loading condition. A uniaxial unity force is applied to the electrode base. Buckling safety factor is calculated based on equation 3.1.

The simulation runs and sweeps for all materials for linear buckling analysis. The critical load factor outputs are used in safety factor calculations as in equation 3.1. The results are presented in Table 4.1.

The buckling analysis results clearly favor designs E and C. The shorter base width in design A, B and D leads to its disadvantage. While, the circular junction design of F does not help it either. The simple designs with wide bases clearly triumph with design E coming on top.

Material wise, all designs satisfy the requirements of safety factor of 5 minimum except Polyimide. Nickel is the top material of choice for buckling resistance. On the other hand, Polyimide has very weak mechanical properties that makes it unsuitable at this thickness. Increasing the thickness for Polyimide electrodes will make the device thicker than allowed for neural electrodes usage.

As predicted, increasing the number of stages of the shank improves its buckling resistance. From single stage to two stages, nearly all electrodes gain around 10%-12% increase in safety factor. Another 14-16% increase is also noted on adding a third stage. This result is expected as a thicker shank means more buckling resistance.

## 4.3. Fracture Analysis

Stationary Analysis is applied to the electrode structure. Axial force is applied one time during axial stress and buckling failure analysis, while shear force is applied during shear stress analysis. The tip was fixed in its position using fixed constraint (fixed-free loading condition). A magnitude of 1N for axial force and 1mN for shear force was applied to the electrode base.

For analyzing axial stress acting on the electrode, the maximum stresses are calculated and compared with the yield and ultimate tensile strengths according to the material type (ductile or brittle) [64]. For brittle materials, UTS is used because it has a smaller value than yield strength and it will give the lowest safety factor which is considered more accurate. For ductile materials, yielding deformation comes as a response to axial stresses, followed by plastic deformation, necking and finally hardening and cracking. Ultimate tensile strength is larger than the yield strength and tensile (or compressive) yield strength is approximately double of the shear yield strength. So that ductile materials fail through shear loading rather than tension or compression and using the yield strength to calculate the safety factor. Comsol tool is used for calculating the fracture safety factor utilizing the appropriate criteria according to the material properties. The minimum safety factor is considered to be 5. The von



mises stress measured by COMSOL demonstrates the magnitude of stress levels. The von mises stress measured by COMSOL demonstrates the magnitude of stress levels. Von Mises stress or Equivalent tensile stress ( $\sigma_v$ ) is a scalar form of von Mises yield criterion, calculated from the Cauchy stress tensor. It is used to predict the materials yielding when their maximum stress equals the maximum deformation stress that can be achieved experimentally in a tension test at yielding. The regions with maximum applied stress are used in safety factor calculations. These maximum stress points represent the regions where electrode failure starts.

**Table 4. 1: Linear Buckling Safety Factor Results**

Design	Material	Design A,B	Design C	Design D	Design E	Design F
Single Stage	Silicon	30.55	35.7	32.93	36.7	33.4
	Copper	21.04	25.24	23.24	25.9	23.6
	Nickel	41.9	46.04	42.42	47.3	43
	Polyimide	0.59	0.65	0.6	0.67	0.61
Two Stages	Silicon	33.5	40.1	37.24	40.9	37.5
	Copper	21.7	28.31	26.29	28.9	26.5
	Nickel	43.2	51.63	47.98	52.7	48.3
	Polyimide	0.61	0.73	0.68	0.75	0.68
Three stages	Silicon	38.7	46	43.1	47.1	43.1
	Copper	25.1	32.49	30.44	33.2	30.4
	Nickel	49.8	59.27	55.55	60.6	55.5
	Polyimide	0.71	0.84	0.79	0.86	0.79

Equation 4.1 is used for calculating the safety factor for axial stress or shear stress in case of ductile material:

$$\text{Safety Factor} = \frac{\text{Yield Strength } (S_y)}{\text{Von Mises Stress}} \quad (4.1)$$

Equation 3.5 is used to calculate safety factors in case of brittle material.

During implantation and operation, there are lateral forces normal to the shank inducing shear stresses affect the electrode and create of plane deformation, so that in the second static structural analysis, the electrode is loaded with 1mN. The maximum shear stress is calculated by Von Misses Stress or Tresca from COMSOL Multiphysics [15]. Tresca criterion states that yielding occurs when the difference between the maximum and minimum principal stresses is equivalent to twice the maximum shear stress that can be obtained experimentally in a tension test at yielding. Both methods acquire almost the same results.

#### 4.3.1. Axial Stress Analysis

Axial stress analysis runs under axial loading force of 1N. The results are analyzed and safety factor calculations are done as in Equation 4.1, 3.5. A minimum safety factor of 5 is required for a potential device as stated earlier.

The results are tabulated in Table 4.2.

**Table 4. 2: Axial Stress Safety Factor Results**

Design	Material	Design A,B	Design C	Design D	Design E	Design F
Single Stage	Silicon	0.358	0.384	0.021	0.339	0.36
	Copper	5.1	5.683	0.291	5.027	5.537
	Nickel	9.131	10.09	0.544	8.7	9.488
	Polyimide	0.4	0.44	0.02	0.41	0.46
Two Stages	Silicon	0.313	0.276	0.019	0.257	0.255
	Copper	4.59	4.007	0.291	3.789	3.643
	Nickel	8.044	7.088	0.506	6.619	6.525
	Polyimide	0.36	0.32	0.02	0.3	0.28
Three stages	Silicon	0.315	0.264	0.019	0.284	0.265
	Copper	4.59	3.861	0.291	4.153	3.861
	Nickel	8.081	6.788	0.488	7.313	6.825
	Polyimide	0.36	0.3	0.02	0.33	0.31

Design D has significantly low values, this means that asymmetrical designs are poor choice and are susceptible to break easily. Design C is the best at single stage design but deteriorates faster at high stage counts. Significant changes in safety factor can be observed between single stages and two stages.

The introduction of fillets between stages allows for the development of high stress values which can be blamed for this drop. Material wise, Nickel has the best performance against axial stress loading and is the only material to satisfy the minimum condition of 5 safety in all results. Silicon, Polyimide and Copper perform very poorly in this analysis.

Design E has the best results in linear buckling analysis. In axial stress analysis, although it comes only second to last in single stage design, the three stages design is able to compete better. A workaround for the issue causes with the introduction of fillets will improve these results. The designs using fillets versus Bezier polygons are compared next. Using design E for comparison, a stress plot in Figure 4.5: Left shows that the sharp stages causing a large stress and Figure 4.5: Right illustrates that the smoothing stages have a small stress.

Table 4.3 shows the results for buckling and axial stress analysis for design E with some modifications. As expected, axial stress safety is almost restored to the initial value of the single stage design. The results also compare modification of stage lengths. Axial stress safety does not suffer significant changes, but on the other hand, buckling safety changes more considerably.

The changes to buckling safety are expected, since decreasing the length of the wider stage means a thinner device overall which is more prone to buckling. These results show the tradeoffs between buckling resistance and total area. Both stage numbers and stage lengths can be tuned to achieve suitable design parameters.

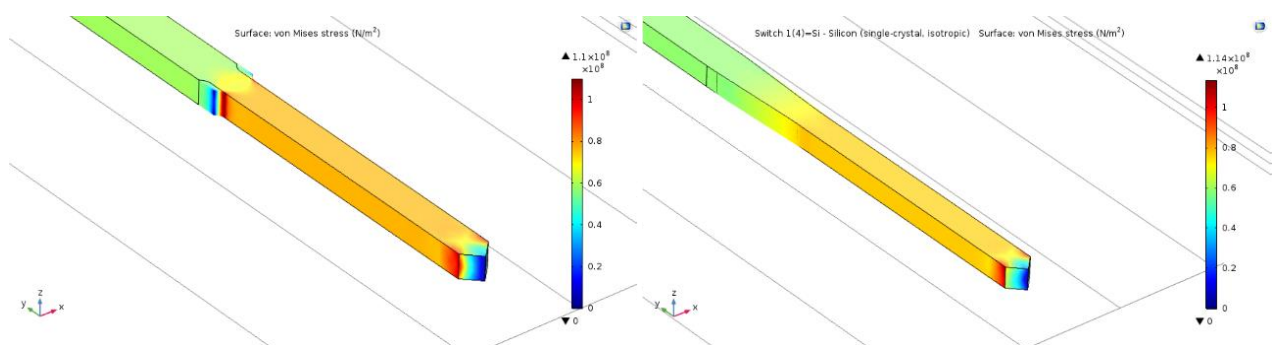


**Figure 4. 5:** the max stress in different designs: (Left) Design E with fillet, (Right) Design E with Bezier polygon

### 4.3.2. Shear Stress Analysis

Shear loading analysis runs under a tangential boundary force of 1 mN. The results are computed and the maximum stress values are used in safety factor calculations in accordance with equations 4.1, 3.5.

Table 4.4 summarizes the results for shear stress safety factors. Asymmetry has failed design D in this test as well. Variations with number of stages does not follow a pattern. Design E and F have very small variations while design A, B and D have more significant drops. Design C has the best results among two stages designs, while designs A, B, D, E and F are better in single stage designs. The shear stress results for modified E designs are included in Table 4.4. Material wise, Nickel is by far the best. It

is the only material that approximately satisfies the minimum requirements of 5 safety factor.

**Table 4. 3** DESIGN E WITH BEZIER POLYGONS

Design E 3 stages	Material	Buckling Safety Factor	Axial Stress Safety	Shear Stress Safety
Equal lengths	Silicon	41.22	0.33	0.56
	Copper	29.12	5.03	4.45
	Nickel	53.11	8.7	7.54
	Polyimide	0.75	0.41	0.5
Long Last Stage	Silicon	38.09	0.33	0.53
	Copper	26.9	5.03	4.45
	Nickel	49.08	8.72	7.54
	Polyimide	0.7	0.41	0.5
Long First Stage	Silicon	46.34	0.31	0.55
	Copper	32.73	4.66	4.17
	Nickel	59.72	8.08	7.2
	Polyimide	0.85	0.38	0.47

### 4.3.3. Figure of Merit

In this part, a comparison between all designs is carried out to indicate which design is better. The comparison depends on the values of FOM. The best design has the largest value of FOM [6]. The FOM depends on the different values of safety factor for each design that are calculated from mechanical analysis as well as the fabrication cost of each material and take the shank width in concentration. All the other characteristics are constant for all designs such as impedance, noise, number of channels, and cross section area of the electrodes tip because of the pads of all electrodes in these designs are constant.

Figure 4.6 illustrates the results of FOM. It shows that the design C with single stage with Nickel material gives the highest value of FOM, so it is considered the best design. Then it is followed by design E with 3 stages which ranks second. Design D with single stage and Polyimide material is considered the worst design because it gives the worst FOM.

**Table 4. 4: Shear stress safety factor results**

Design	Material	Design A,B	Design C	Design D	Design E	Design F
Single Stage	Silicon	0.65	0.64	0.34	0.56	0.58
	Copper	4.73	4.7	2.6	4.45	4.4
	Nickel	8.26	8.22	4.5	7.53	7.64
	Polyimide	0.37	0.36	0.2	0.36	0.36
Two Stages	Silicon	0.59	0.66	0.31	0.56	0.59
	Copper	4.34	4.75	2.34	4.45	4.31
	Nickel	7.62	8.45	4.08	7.49	7.58
	Polyimide	0.34	0.36	0.18	0.36	0.34
Three stages	Silicon	0.51	0.5	0.34	0.55	0.47
	Copper	2.39	3.66	2.6	4.38	3.48
	Nickel	6.61	6.45	4.5	7.42	6.12
	Polyimide	0.3	0.29	0.2	0.34	0.28

#### 4.3.4. Electrode design insights

It is clear that Nickel possesses the highest buckling resistance during insertion followed by Silicon, and it has the best performance against axial and shear stresses loading. However, Polyimide performs very poorly in these analyses. Polyimide has very weak mechanical properties that makes it unsuitable at this thickness and at the same time using thicker Polyimide electrodes would make the device inapplicable for neural electrodes usage. Asymmetrical designs are prone to breakage easily during axial stresses.

Also, increasing the number of stages has an eminent effect on linear buckling resistance. Design C with single stage using Nickel displays capable mechanical performance and its FOM is the highest one. So depending on FOM values the best design is design C with single stage with Nickel material and is followed by design E with 3 stages with Nickel. The worst one is design D with single stage and Polyimide material.

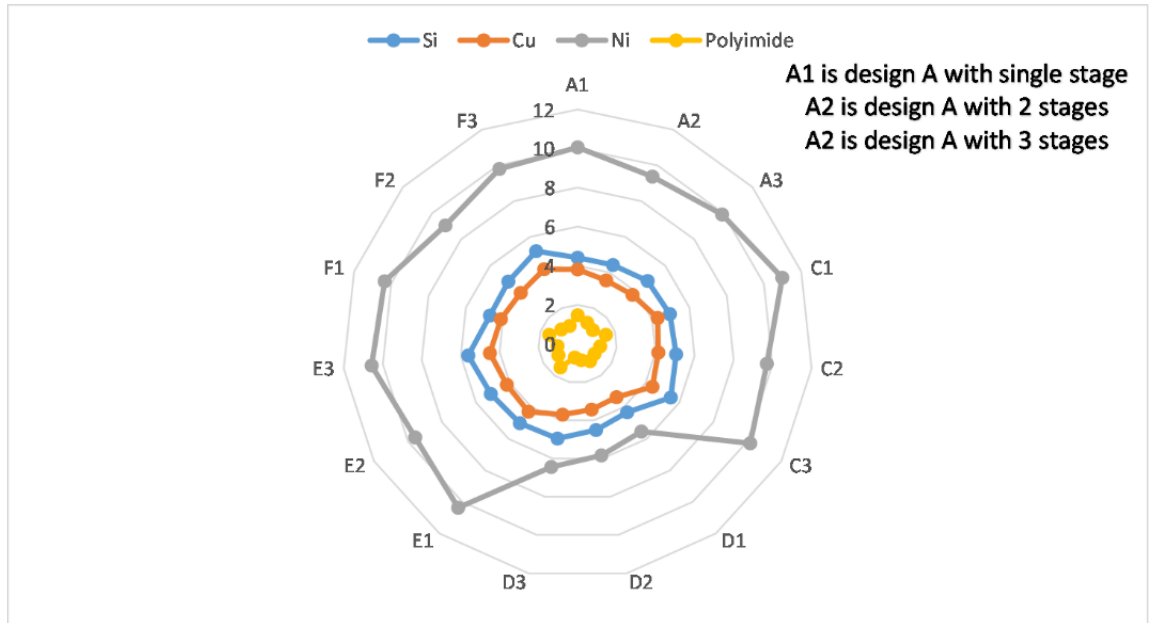


**Figure 4. 6:** The FOM for several designs with different materials

## 4.4. Electrical simulation

The electrode DC resistance is calculated or estimated by finite element modeling.

The resistances of the design depend on the track thickness and length because we use a constant track width. A several materials are used to compare its resistance. There are 2 designs for human electrode, one consists of one metal layer and the other consists of 2 metal layers. Low impedance is the target of the design because in stimulation process, current sources is used and we need to reduce the power consumption so low electrode impedance helps in that. Low power consumption leads to:

- Extend the battery life of implanted systems
- Reduce power dissipation
- Reduce joule heating
- Reduce noise generation

Depositing a rough gold layer will increase the surface area which yielding lower capacitance and decreasing the interface impedance.

### 4.4.1. One Metal Layer

Depending on our fabrication and to simplify the process of fabrication and the steps of it, the design is made of one metal layer with the parameters that are illustrated in table 4.5. Figure 4. 7 shows the design of the pads and track between them.

**Table 4. 5 Parameters**

Routing track length	From 9000 $\mu\text{m}$ to 12000 $\mu\text{m}$
Routing track width	30 $\mu\text{m}$
Routing track thickness	From 300nm to 1 $\mu\text{m}$
Shaft width	500 $\mu\text{m}$

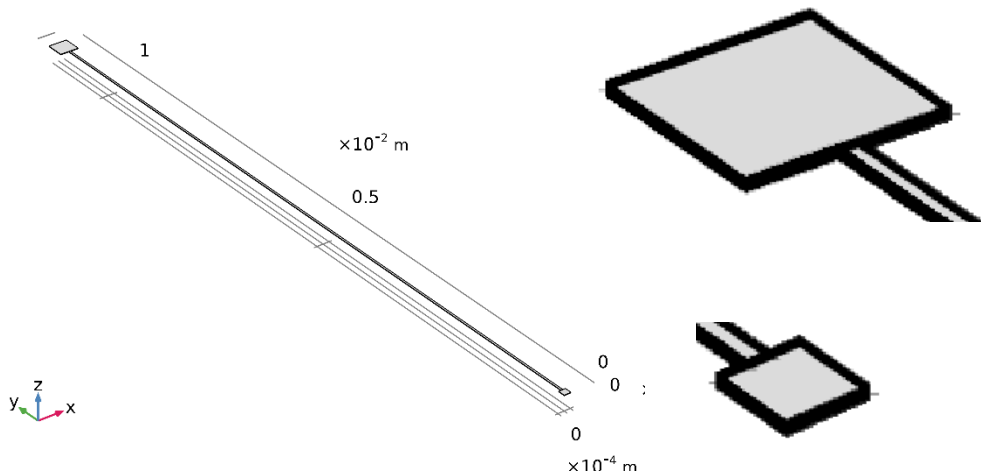


**Figure 4. 7 Interconnection pad, Stimulation pad, and track**

The results of the DC resistance of the Au material with different thickness of the layer are illustrated in table 4.6.

**Table 4. 6 DC resistance of Au**

Thickness [nm]	R [ $\Omega$ ]
300	26.54
400	19.92
500	15.93
600	13.28
700	11.38
800	9.96
900	8.85
1000	7.97

If calculating the DC resistance for Ti, Pt, and Al for constant thickness at 500[nm], the results will be:

Ti gives R = 279.45 $\Omega$

Pt gives R = 81.64 $\Omega$

Al gives R = 20.47 $\Omega$



#### 4.4.2. Two Metal Layer

The design of the 2 metal layers is as the rat design but with the track length changes from 9[mm] to 11[mm] because the shaft length is 10[mm]. The details of the design was illustrated in the previous chapter in Figure 3. 16. Table 4. 7 illustrates the results of the simulation of DC resistance for different thickness and several materials.

**Table 4. 7 DC resistance in  $\Omega$  for different thickness**

Thickness[nm]	Au	Ti	Pt	DC R “Al”
300	77.13	1352.7	395.18	99.07
400	57.85	1014.6	296.40	74.31
500	46.28	811.68	237.12	59.45
600	38.57	676.43	197.61	49.54
700	33.06	579.81	169.38	42.47
800	28.93	507.35	148.22	37.16
900	25.72	450.99	131.75	33.03
1000	23.14	405.91	118.58	29.73

#### 4.5. Conclusion

Several electrode structures were introduced and analyzed to meet the design requirements using different materials.

The mechanical analysis results and fabrication cost estimation provide guidelines for the electrode design and material choice. The different designs ideas introduced several degrees of freedom in electrode design. Number of stages, stage length, stage width as well as device material can all be tuned to achieve different mechanical performance.

Some electrical simulations were done due to several materials with different thickness, different length of the tracks between pads and different number of metal layers. The gold material gives the best results in Dc resistance with different thickness and track lengths. It is considered a good material for biomedical devices because of its biocompatibility.

# Chapter 5 : Optrode

This chapter illustrates some information about optrode, its simulation, and the reasons of investigation of this design.

## 5.1. Optrodes

Optrode is the scientific name of the optical electrode device. Its idea comes from the idea of designing a dual modality device which has the capability of delivering optical stimulus and record intracellular neural signal simultaneously. In the beginning of 1980, the optrode was developed as an optical-chemical sensor and used to detect changes in PH or chemicals and the amount of samples were small [75]. The first design consisted of an optical fiber and phosphors which were located on the tip of the fiber and then the detected signals were considered the dynamic changing or quenching of luminescence from the phosphors. Optical methods were established in the fields of medical imaging, neuroscience, and diagnostic. Optogenetics is a new neuromodulation technique which helps in modulation the nature of the neurons to be sensitive of incident light with a specific light wavelength to active or silence neurons [76]. Since its discovery in 2005, optogenetics has provided a revolutionary method to understand the relations between brain functions and brain circuits, so that, neurons are genetically encoded to produce and express light-sensitive proteins which called opsins. Optogenetics is achieved by the use of light-sensitive control tools which may be targeted by gene delivery. Light-gated ion channels in the microbial opsin family are the main control tool. microbial opsins include:

1. channelrhodopsin-2 (ChR2), responsive to blue light for neuronal excitation.
2. halorhodopsin (NpHR), responsive to yellow light for inhibition.
3. channelrhodopsin from *Volvox carteri* (VChR), activated by green light, and ChR2 chimeras.

The process of injection with the opsins and the change in the nature of the neuron is illustrated in Figure 5.1. Once these proteins are modulated, neural activity can be treated by exposing the cells to appropriate light with the suitable wavelength. By optogenetics, neural function can be controlled by multi-modal, and it provides genetic targeting of specific cell types, moreover it reduces the electrical stimulation artifacts when recording electrical activity. These multilateral features are combined to create a powerful tool set that provide the ability of studying the neural circuitry and to be used with treating with psychiatric and neurological disorders such as depression, social dysfunction, epilepsy and Parkinson's disease. Some developments of new technologies followed the appearance of the optogenetics, which provided the distribution of light inside the brain. These technologies also combine optogenetics with other modalities which include electrophysiology. But till now, most current optical devices require complicated, bulky setups and have limited capabilities [77].

The essential problems in the current devices are:

1. Increasing tissue temperature.
2. Excessive power consumption
3. Impractical connections to external light sources
4. Limited or no spatial addressability due to the use of single fibers.

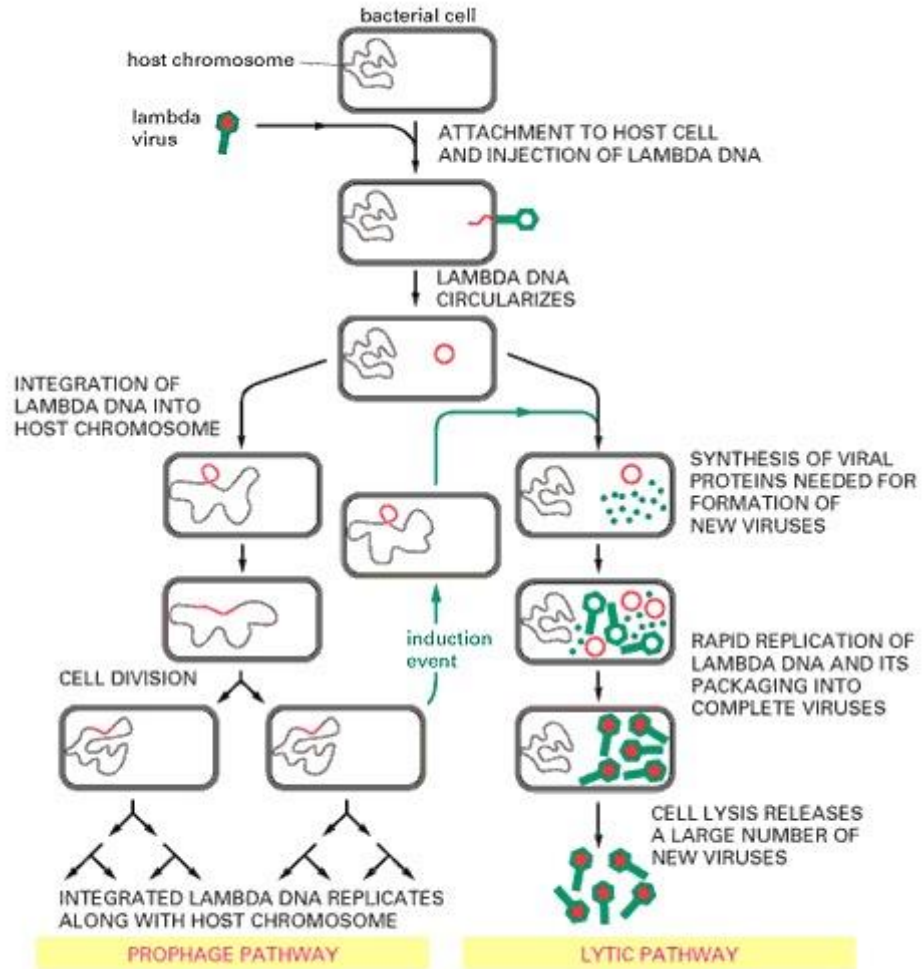


**Figure 5.1: Illustration of injection process**

## 5.2. Different types of optrode

Optrode can be divided as illustrated in Figure 5. 2. It has different types; one has an external light source and uses optical fibers to transfer the light from the external source to the shaft. Figure 5. 3 illustrates an optrode with an optical fiber, but fibers have drawbacks in its large cross section area and when needing to insert a bundle of fibers, the optrode will have a huge area and all fibers will give the same light with the same wave length [78]. Figure 5. 4 shows different shapes of fibers and when it was located on the tip of the shaft, it gives a high spatial resolution [79]. To overcome these drawbacks, the designs of optrode is developed and appeared as a fiber-less optrode which uses the waveguide to transfer the light to the shaft. Figure 5. 5 introduces the first design of optrode without fibers. It has a monolithically integrated optical waveguide mixer which provides a transmission of a multicolor light at a common waveguide port. As a result, the same neuronal population has multicolor modulation. The implementation of this device has a gradient-index (GRIN) lens which provides an efficient coupling between a dielectric optical waveguide mixer and a side-emitting injection laser diode (ILD) [80]. Fiber-less has some disadvantage like its large dimensions and limited wavelengths of the light source. Other types use an internal

light source as  $\mu$ LED. When concentrating on only one type of these, we will take the source light such as  $\mu$ LED because it has some advantages:

- Simplicity
- Low cost of system implementation
- Low power than Laser system
- Has the potential to be integrated with wireless

The ways to deliver the light from LED to target cell

- Coupling to microfiber or waveguide
- Mounted on the tip of the probe (the advantage of this type is )
  - highly compact device size, which enables high spatial resolution
  - Reduced tissue damage during surgical insertion

Disadvantage:

- Undesirable heating of nerve tissue during operation
- Remains a major challenge for stimulating either surface and deep targets
- Thermal effect may bias the outcomes of optogenetic experiments, especially when tissue near micro\_LED receive continuous light illumination as opsin\_negative controls

$\mu$ LED can also be used as external or internal light source. A small comparison between some developed optrodes which consist of internal  $\mu$ LED on its shafts. There are two types of the  $\mu$ LED, one is fabricated external and then adhered with the shaft and this type has a large area, so it increases the area of the shaft. Another type is integrated on the shaft through the fabrication process and in this case it has a smaller area than previous type.

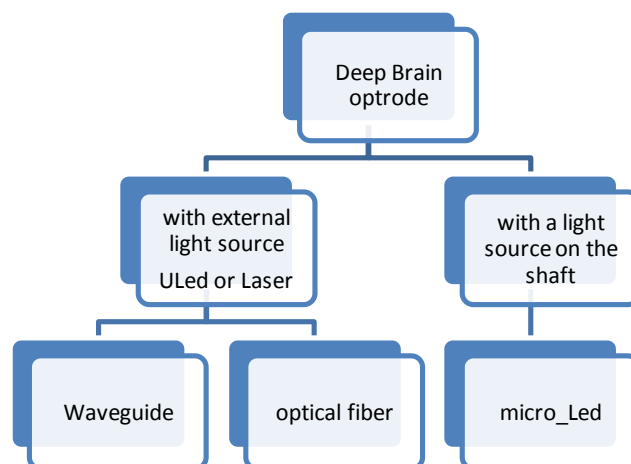


**Figure 5. 2 Partitions of optrode**

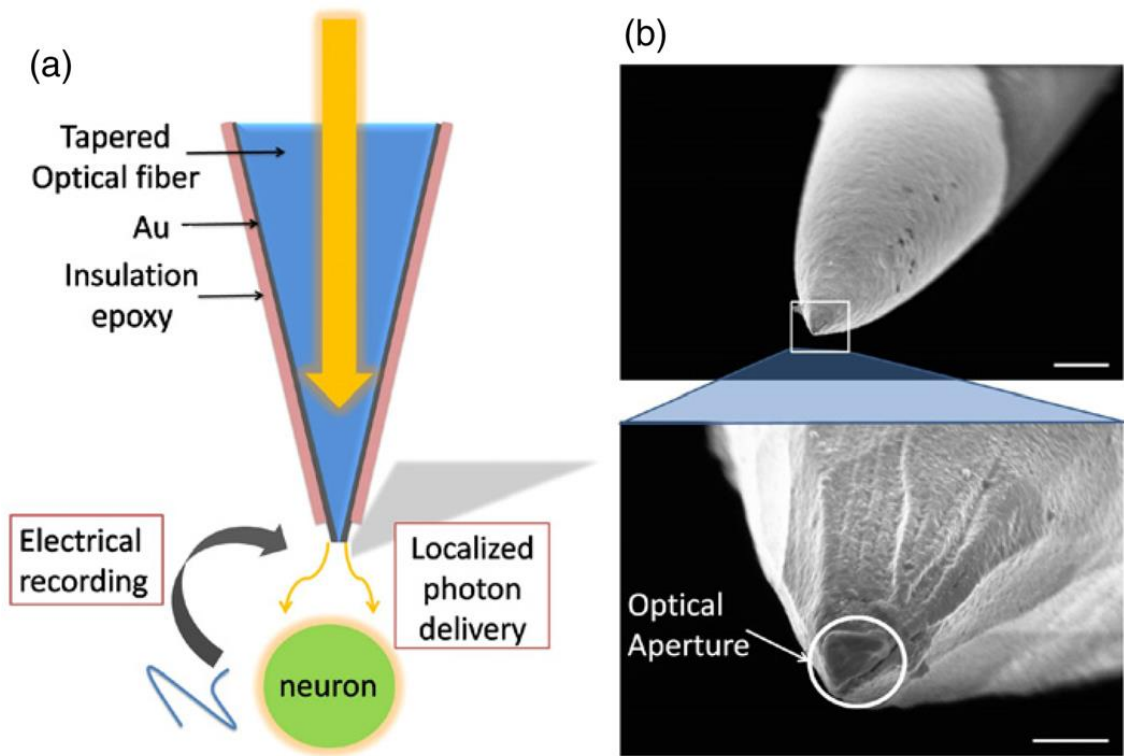


Figure 5. 3 Optrode with optical fiber [56]

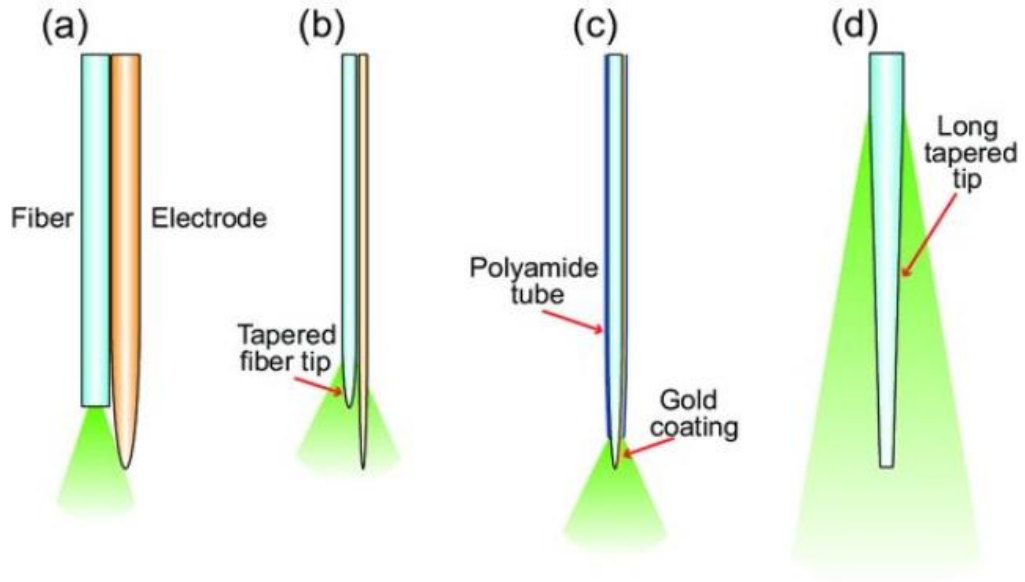
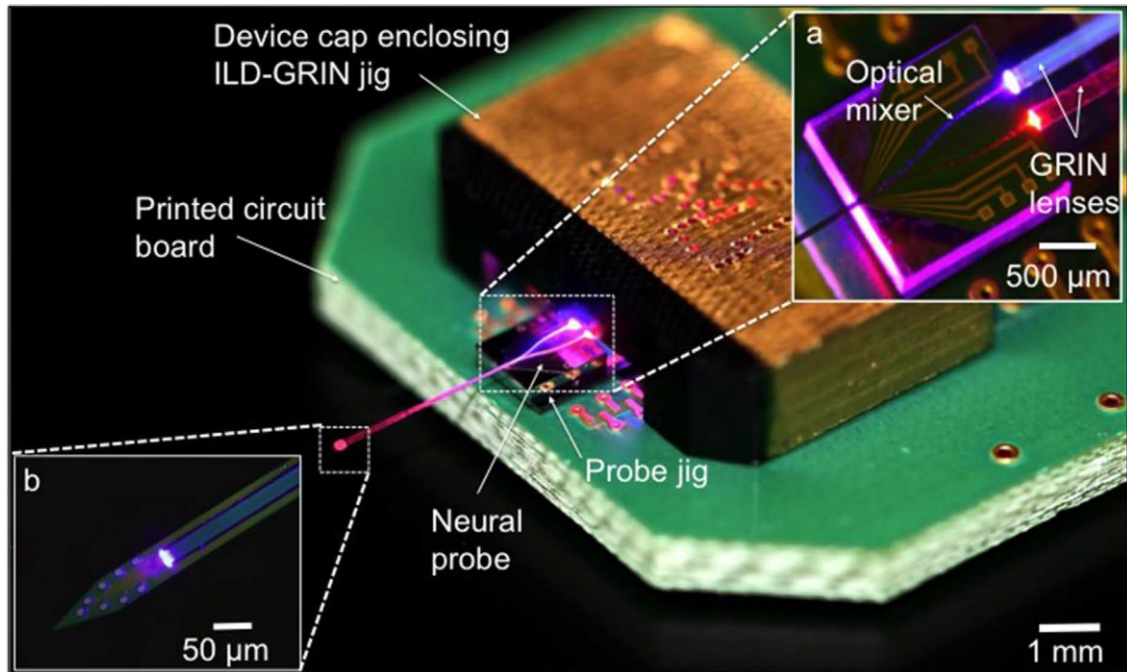


Figure 5. 4 Different shapes of fibers [57]



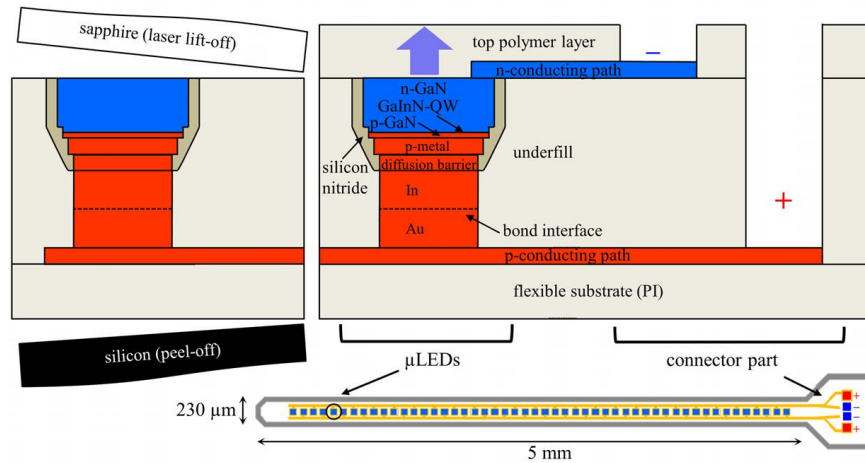
**Figure 5. 5 Fiber-less optrode [80]**

### 5.2.1. $\mu$ LED

The existence of micro-sized light-emitting diodes ( $\mu$ LEDs) on the shaft of the electrode allows increasing the number of distinguishable wavelength of light because it provides the ability of using different  $\mu$ LEDs with different colors (etc. blue, green, yellow). Some developments of the optrode with  $\mu$ LEDs are achieved like:

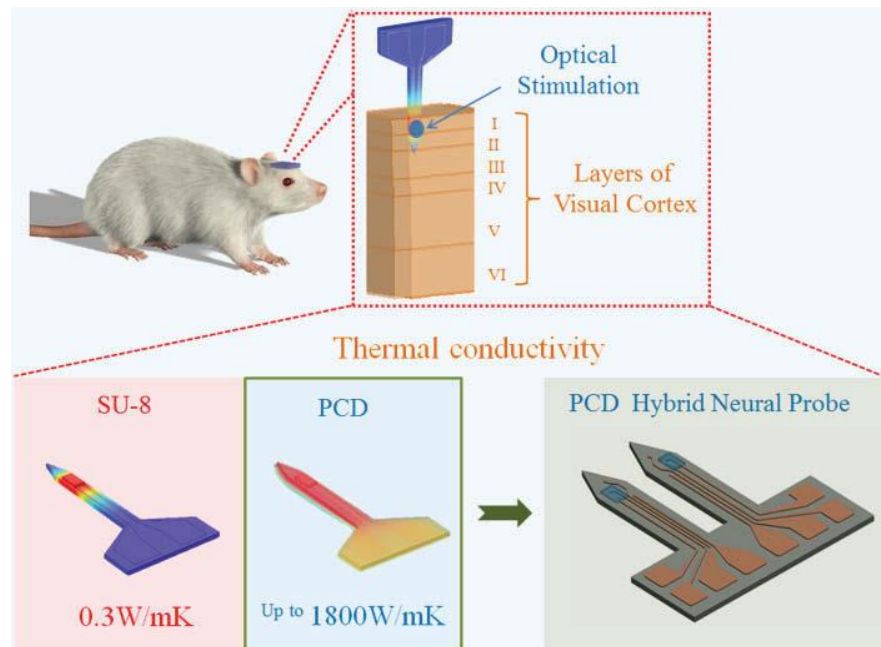
1. Use flexible substrate
2. Use more than  $\mu$ LED with different frequencies
3. Use substrate materials have good behaviors in biomedical applications.
4. Implementing the  $\mu$ LED with smaller dimensions.
5. Decrease the power and the temperature.
6. Decrease the effect of the electric field of the  $\mu$ LEDs on the other recording sites to decrease the noise.

Figure 5. 6 showed a type of optrode that use GaN-based  $\mu$ LED array. It has a flexible substrate and was fabricated of  $15\mu\text{m}$  thin. A laser-based layer transfer process enables highly flexible devices; it is used for transferring GaN-LEDs from sapphire to a polyimide-on-silicon carrier wafer. The fabricated optrode has 50 LEDs with cross section area of  $50 \times 50\mu\text{m}^2$ . All of LEDs are contacted via conducting paths on both pand n-sides of the LEDs. The probe consists of a linear array of the  $\mu$ LEDs which are bonded to the flexible polyimide substrate. They are peeled off the carrier wafer and then attached to flexible printed circuit boards. The probe has a width of  $230\mu\text{m}$  and the LEDs have a radiant emittance of  $6\text{mW}/\text{mm}^2$ , corresponding to emitting  $60\mu\text{W}$  at  $1\text{mA}$  after peel-off [81].



**Figure 5. 6 μLED array on a flexible substrate [59]**

Figure 5. 7 exposes a hybrid optrode combining microelectrodes on a (PCD) polycrystalline diamond substrate and LEDs. It was used for electrical recording and optogenetic stimulation of neural activity. PCD is a material which has a very high thermally conductive which reaches up to 1800W/mK, so that PCD has the ability to dissipate the Joule heat to surrounding areas, and as a result, the risk of thermal is reduced and that decreases damaging in nerve tissues. The maximum temperature rise of was less than 1.3°C, during repetitive optical stimulation. This optrode has only one stimulation site (LED) and has three recording sites with separation 0.5mm. Its shaft dimensions is 0.9 mm × 5 mm with base dimensions of 2.38 mm × 6.5 mm [82].



**Figure 5. 7 Optrode with a polycrystalline diamond (PCD) substrate [60]**

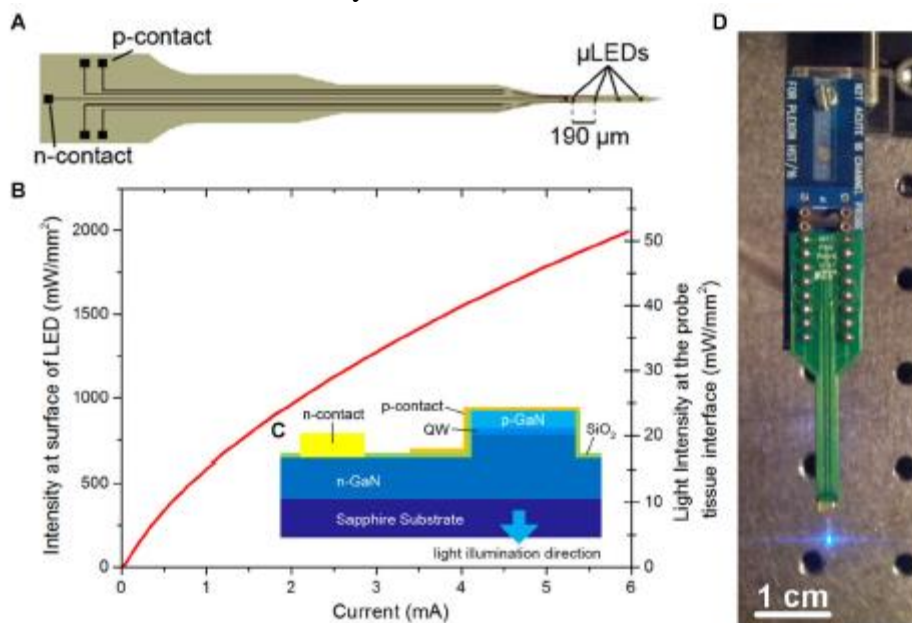


Figure 5. 8 illustrates implantable wireless optrode which is developed to be the smallest version with  $20\text{ mg}$  and  $10\text{ mm}^3$  as its size. Its implant produces sufficient light power of  $20\text{ mW}/\text{mm}^2$  and stimulation with minimal tissue heating  $<1\text{ }^\circ\text{C}$  [83].



**Figure 5. 8 Wireless optrode [83]**

The probe in Figure 5.9 contains independently controllable multiple micro-LEDs, which emit light at  $450\text{ nm}$  wavelength with an irradiance power of  $2\text{ W}/\text{mm}^2$ . Monte-Carlo simulations estimated that optical stimulation using a  $\mu\text{LED}$  can modulate neural activity within a localized region. To validate this prediction; when a comparison between the stimulation with  $\mu\text{LED}$  and the stimulation with an optical fiber, the results illustrate that the  $\mu\text{LED}$  probe excited strong responses in deep neurons. There is an ability to integrate some of optical stimulation sites onto a probe, so the optrode with  $\mu\text{LEDs}$  can control neurons locally [84].



**Figure 5.9 Sapphire based  $\mu\text{LED}$  probe [62]**

Another optrode is fabricated using SU-8, which is considered an effectively material because it increases light coupling efficiency, reduces fabrication complexity,



and has excellent mechanical stiffness. Also, SU-8 is considered more biocompatible and flexible, and can reduce brain damage. Figure 5. 10 shows the SU-8 based optrode. For chronic implantation, Parylene-C is used in coating the probe because this encapsulation can potentially improve reliability of the device and the long-term biocompatibility. This coated material decreases the attenuation of light transmission and provides clearly light-induced neural activity [85].

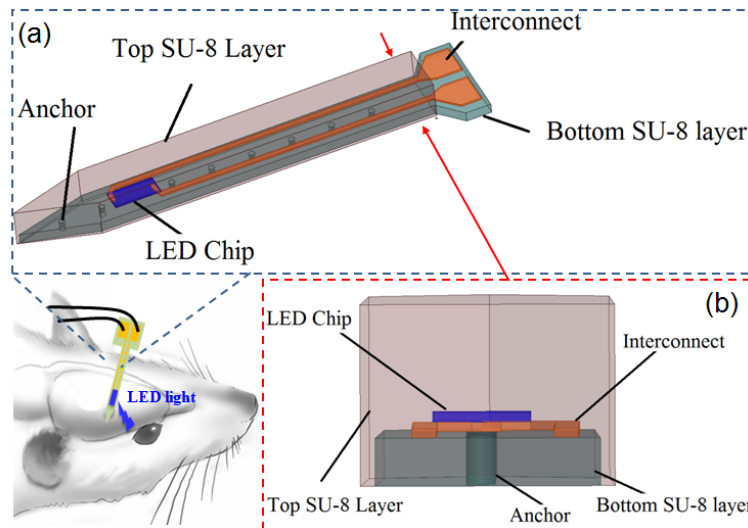


**Figure 5. 10 Miniaturized SU-8 Optical Probe [63]**

Figure 5.11 illustrates a design which combine  $\mu$ LED and recording sites onto silicon substrate. Each shaft has 8 recording sites and 3  $\mu$ LED stimulations. The monolithic probe provides high scalability and spatiotemporal resolution and also high precision for cellular-level circuit analysis in deep structures of intact.

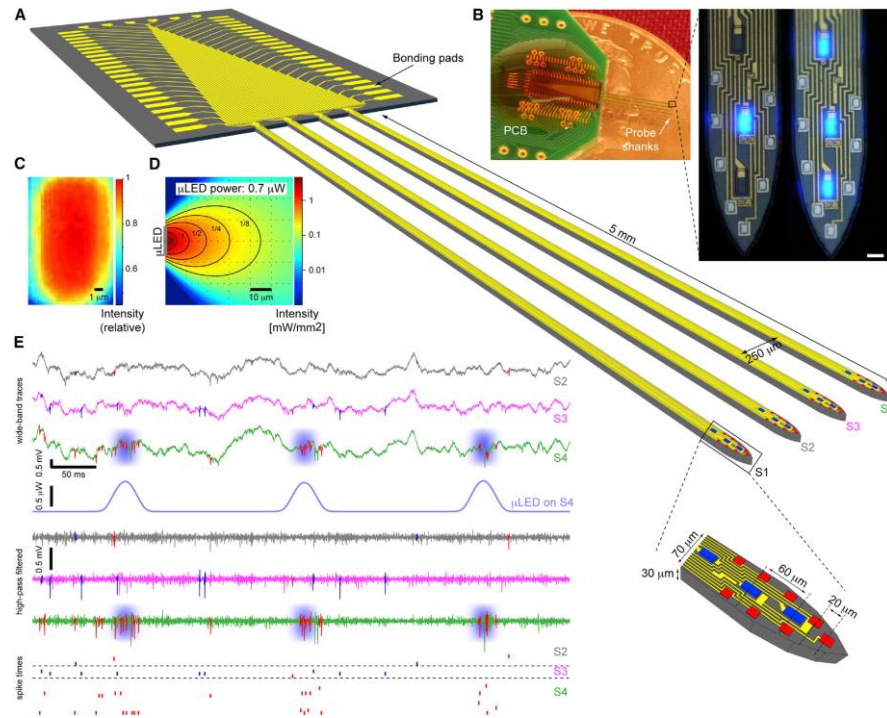


**Figure 5.11 Monolithically Integrated on Silicon probe [86]**

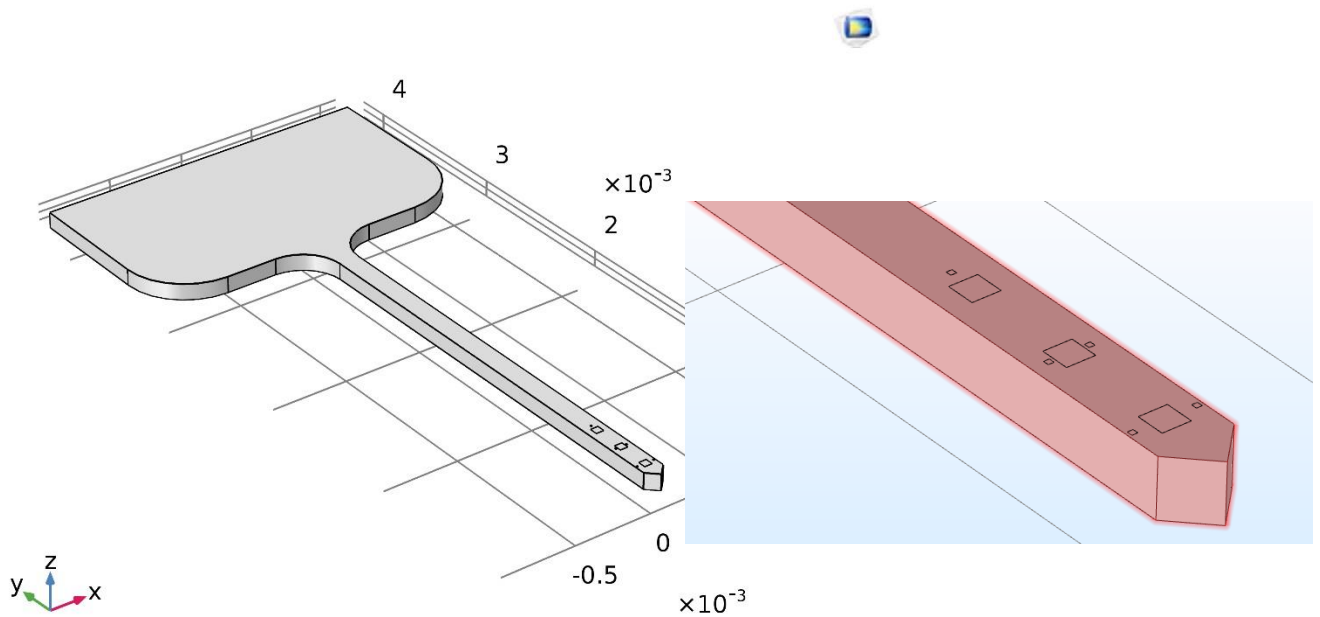
In this design, GaN and InGaN multi-quantum well epitaxial layer on Si substrate are used to implement the  $\mu$ LED. And also to reduce the effect of the  $\mu$ LED on the recording electrodes and their long interconnection lines, a double metal layer topology are used [86]. Table 5.1 exposed some of the dimensions of the design.

Number of Recording sites	8
Cross section area of recording sites	13 x 11 $\mu$ m
Number of stimulation sites	3
Cross section area of stimulation sites	15 x 10 $\mu$ m
Shank dimensions	L= 5mm x W=70 x t=30 $\mu$ m
Base dimensions	L=2.3 x W=5.2mm
The optical power density	1 $\text{mW}/\text{mm}^2$ @ V=3.2v and I=13.8 $\mu$ A

**Table 5.1 Properties of the monolithic probe**

### 5.3. Simulations

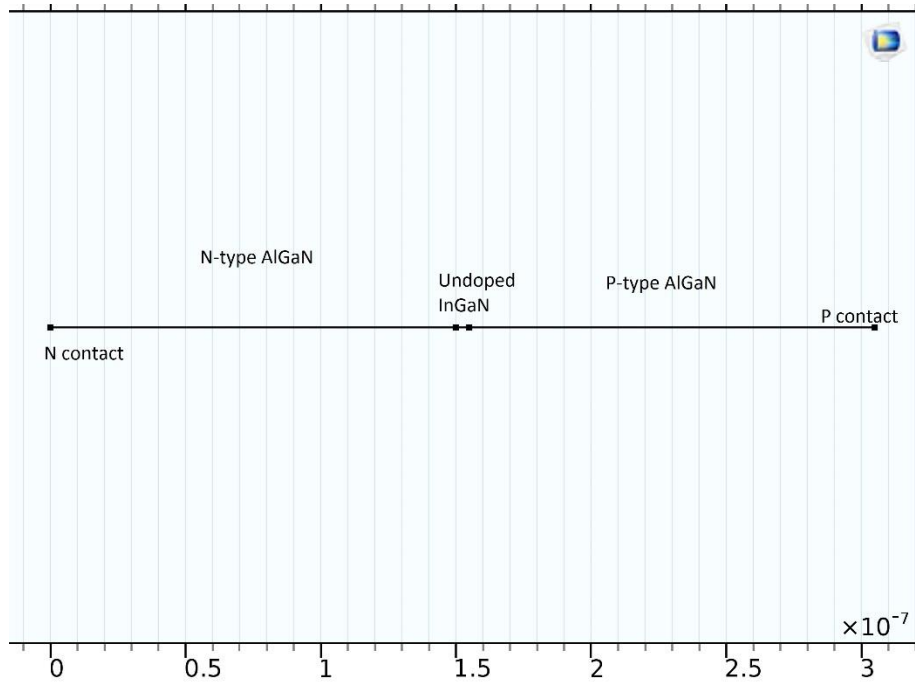
There is an estimated design on the same shape of design E electrode with 3  $\mu$ LED and 5 recording pads as illustrated in Figure 5. 12. There are some simulations are done on the  $\mu$ LED as a separated device and with its substrate.



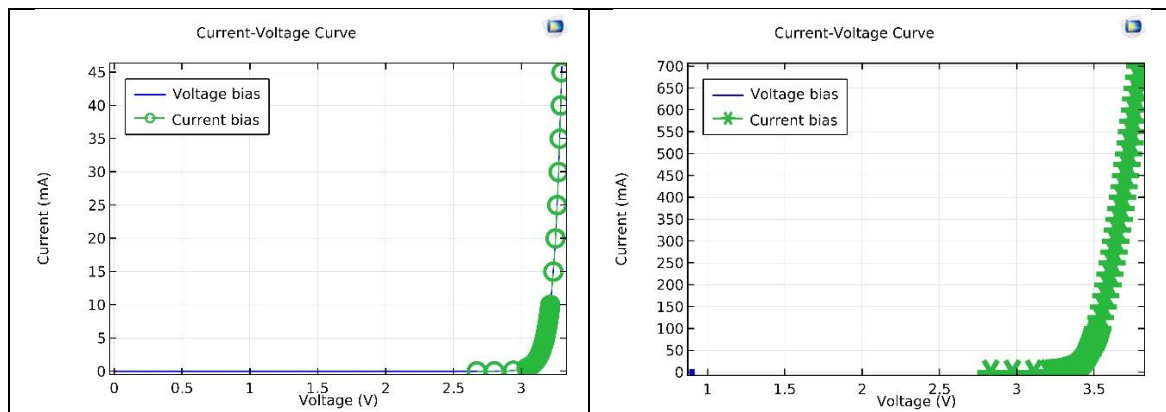
**Figure 5. 12 Optrode**

### 5.3.1. $\mu$ LED simulations

If trying to model the  $\mu$ LED in 3D, there are many obstacles because of its too small dimensions so that there is a trails to simplify the model with 1D and make some simulations to calculate the changes of the current with the voltage and to predict its intensity and the power [87]. From Comsol, there is a similar model but with different area so this model is used with some editing in area and then there are different results. The model was simulated with cross section area equaled  $200\mu\text{m} \times 200\mu\text{m}$  and our model has a cross section area  $50\mu\text{m} \times 50\mu\text{m}$ . The  $\mu$ LED consists of N-type material (N-type AlGaIn) then undoped material (InGaIn) then P-type material (P-type AlGaIn). Figure 5. 13 shows the 1D model of the  $\mu$ LED and these lengths represent the thickness of each material. The first needed results are the relation between the voltages with the current. From the results, the current will increase than  $1\mu\text{A}$  after voltage reach to 2.6V. The applied voltage in simulation changes from 0 to 3.3V. Figure 5. 14 illustrates the effect of decreasing the cross section area on the current with the same applied voltage. In large area current reached to 700mA but with small area it decreased to be with maximum value equals 45mA. Table 5. 2 has the values of voltage with current and from this table, we decide that the current will be over  $1\mu\text{A}$  after 2.6V. To get the power and the intensity of the  $\mu$ LED, the simulation will be done on the current from  $1\mu$  to its maximum value and take the voltage with 2.6V. Figure 5.15 exposes the intensity of the  $\mu$ LED, this intensity depends on the undoped area and the cross section area of the device because when decrease the cross section area the number of carriers decrease. Figure 5.15 presents the emission rate throughout the device for several values of the current biases. The InGaIn layer is the only region of the device which has a high concentration of both electrons and holes, so in all cases the emission from the InGaIn layer is significantly larger than in the cladding material. When the current bias increases, the rate of emission also increase due to the increasing in carrier injection rate.



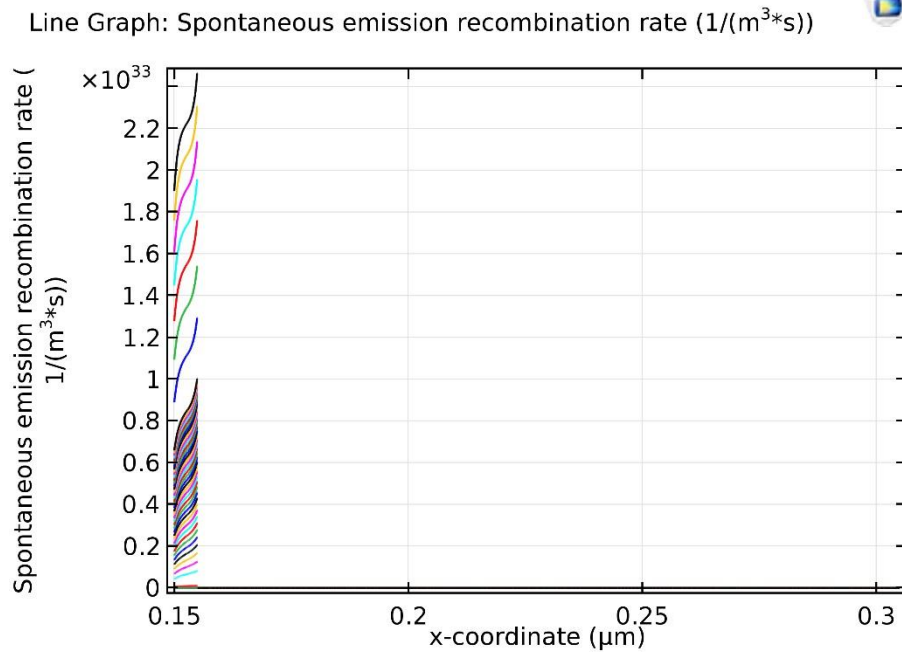
**Figure 5. 13  $\mu$ Led 1D model**



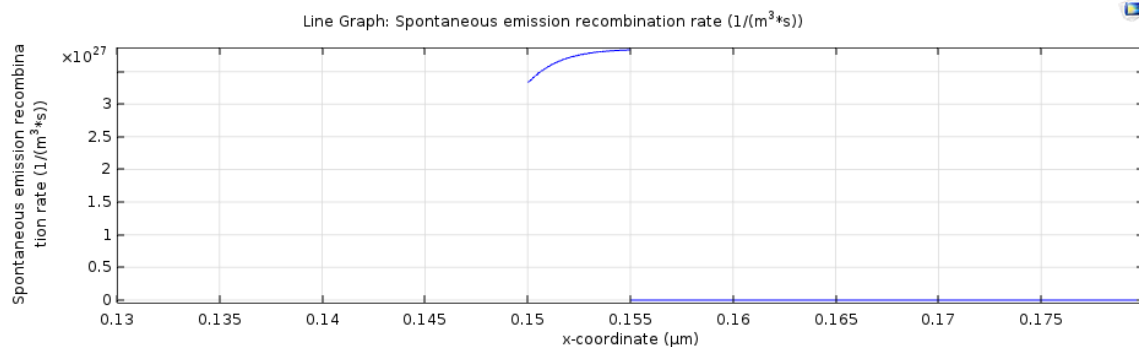
**Figure 5. 14 Left: Current vs. voltage @ $50 \times 50$ . Right:  $200 \times 200$  (area)**

**Table 5. 2 Voltage vs. Current**

Applied Voltage (V)	Current ( $\mu\text{A}$ )
0	-2.9E-5
0.1	-7.4E-6
0.2	8.3E-5
0.3	-8.1E-5
0.4	1.1E-5
0.5	3.2E-5
0.6	-9.8E-6
0.7	6E-5
0.8	8.1E-5
0.9	5.6E-5
1	-4.9E-6
1.1	6.5E-5
1.2	-6.2E-5
1.3	-4.9E-5
1.4	-6.1E-5
1.5	7.3E-5
1.6	2.3E-5
1.7	-4.3E-5
1.8	4.3E-5
1.9	-4.9E-5
2	1.3E-5
2.1	6.7E-5
2.2	5.4E-5
2.3	6.8E-4
2.4	4.3E-3
2.5	0.03
2.6	0.3
2.7	1.6
2.8	9.5
2.9	50.9
3	258.8
3.025	390
3.05	590
3.075	897
3.1	1369
3.125	2100
3.150	3235
3.175	5002
3.2	7760
3.225	12074
3.250	18824
3.275	29390
3.3	45901



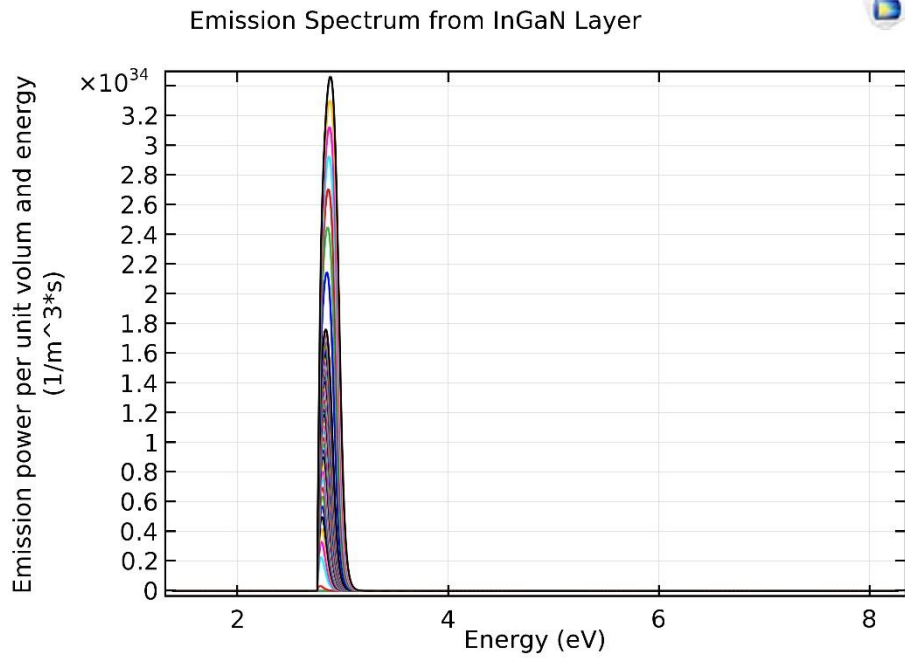
**Figure 5.15 Emission Rate of the  $\mu$ LED**



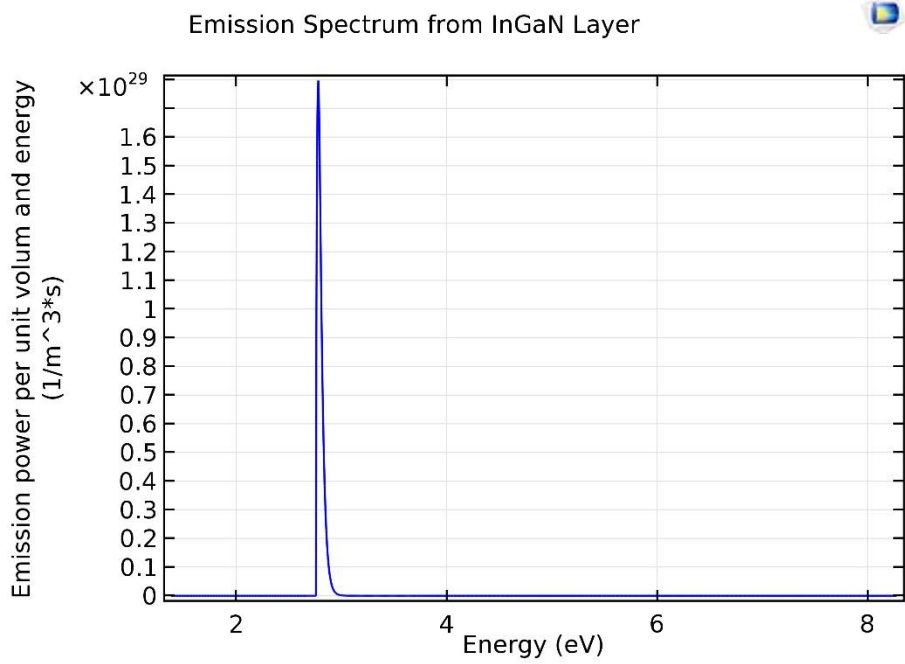
**Figure 5. 16 The emission rate due to 1 $\mu$ A**

Figure 5. 16 shows the emission rate of the InGaN material of the  $\mu$ LED due to only one applied value of current bias which equals 1 $\mu$ A.

Figure 5. 17 shows the emission spectrum of the InGaN layer. The peak emission happens around photon energies of 2.8-2.9 eV, which matches the wavelength range of ~430-445 nm. This corresponds the blue range of the spectrum. From the figure, the total emission intensity increases with the increasing of the current bias. The InGaN is the material which are used to generate the blue light and if needing to generate another wave length, another materials should be used [88]. Figure 5. 18 shows the power per volume for only applied value of the current bias.



**Figure 5. 17 Emission Spectrum (power per unit volum)**



**Figure 5. 18 Power per unit volume with 1μA**

Figure 5. 19 illustrates the emission power of the device per unit area as there is an ability to change the area of the μLED to be suitable with the shaft dimensions and to increase the ability to implement the maximum number of the μLED.

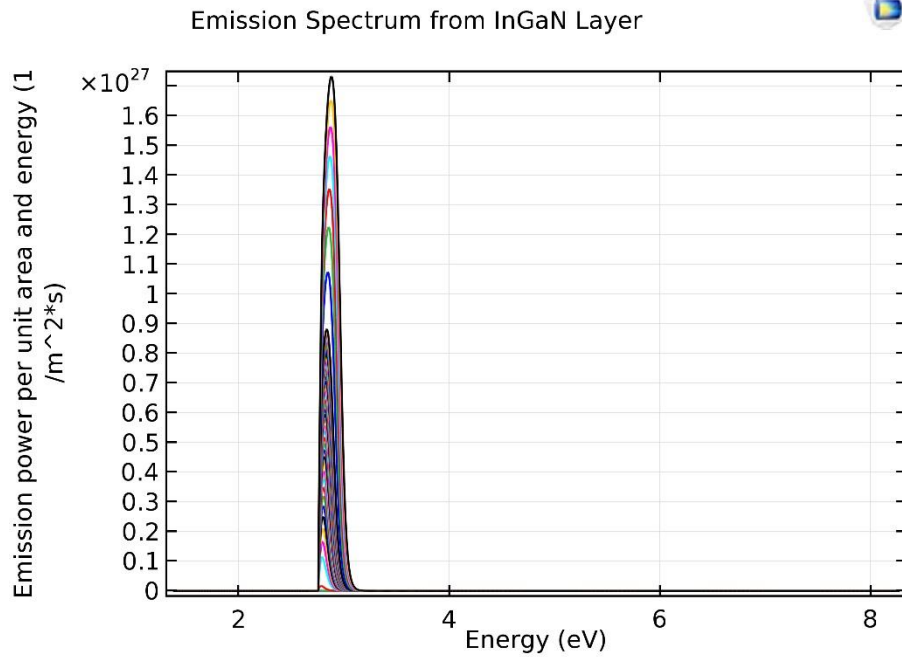
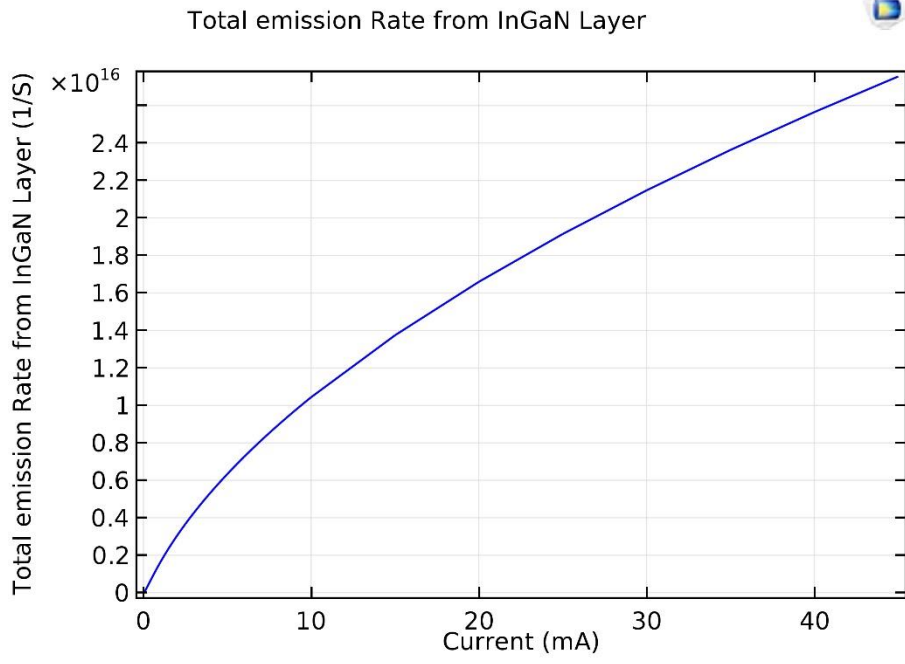


**Figure 5. 19 Emission Power per unit area**

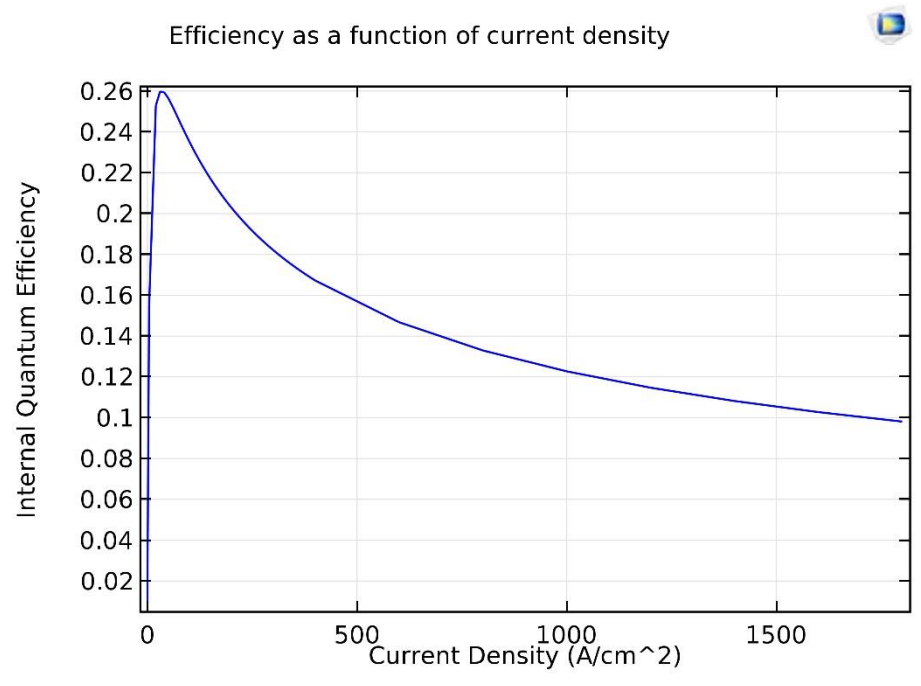
Although the total emitted light increases with current bias, it is not always favorable to use larger currents to increase the device brightness. Because when increasing the current density, the efficiency of the device decreases, and produces a sublinear increase in the total emission rate with current bias.

Figure 5. 20 exposes the total emission rate as a function of the current bias from the InGaN layer. This phenomenon is known as  $\mu$ LED droop “a mysterious drop in the light produced when a higher current is applied”. So that, the solid-state lighting community is considered as an advanced subject of the researchers to progress within. One metric of the efficiency which can be used to evaluate the  $\mu$ LED is the Internal Quantum Efficiency (IQE). This is the ratio of the number of photons emitted from the  $\mu$ LED to the number of electrons passing through the device - in other words, how efficiently the device converts electrons to photons and allows them to escape. Figure 5. 21 shows the IQE as a function of the current density. It has its peak around  $30A/cm^2$ . Figure 5. 22 shows the change of power density with current bias so if applying 2.6V, the power density will reach to the minimum required power density “ $1mW/mm^2$ ” at current bias 7.8mA.





**Figure 5. 20 Total Emission Rate**



**Figure 5. 21 Efficiency of the device**

Optical Power Density as a function of current bias

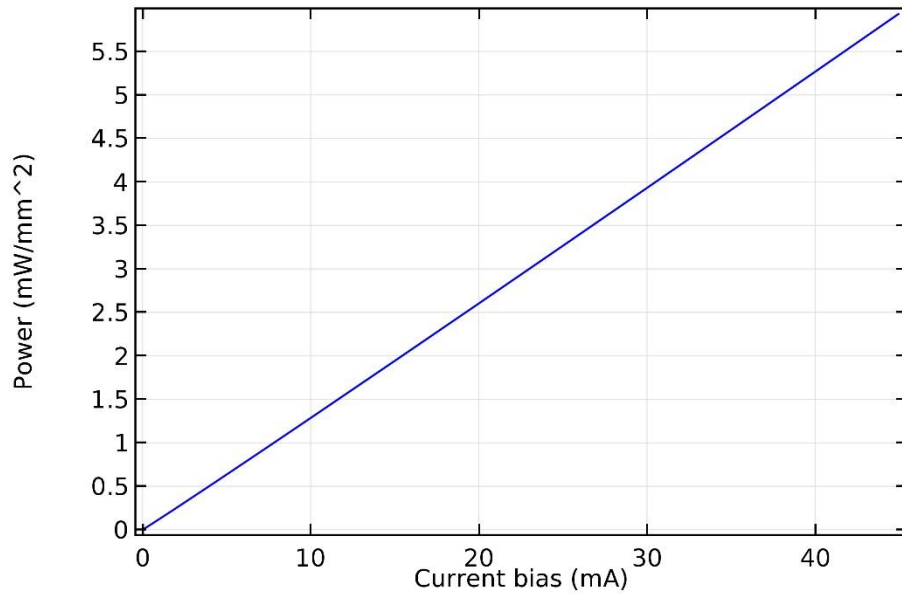


Figure 5. 22 Optical Power Density

## 5.4. Over all model simulation

### 5.4.1. Electric field

Electric field was generated from the difference between the voltage between cathode and anode of the  $\mu$ LED and its effects on the recording wires on the shaft so it can cause noise. To solve this problem or to reduce its effects, make 2 metal layers. Figure 5. 23 illustrates the effect of the electric field, the two smallest upper rectangles represent the recording wires.

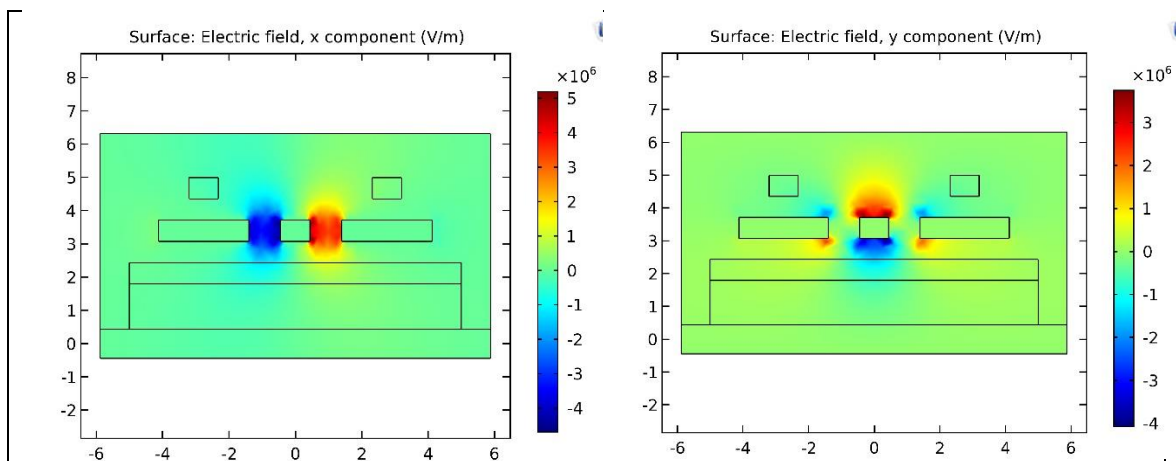


Figure 5. 23 Electric field in X and Y component

### 5.4.2. Thermal Analysis

Figure 5. 24 shows a 3D model of the shaft with 3  $\mu$ LEDs to check the change in temperature due to the  $\mu$ LED power. In this model, the surrounding area is considered as air. Figure 5. 25 has a model of the brain to have a simulations with the temperature changes in the brain

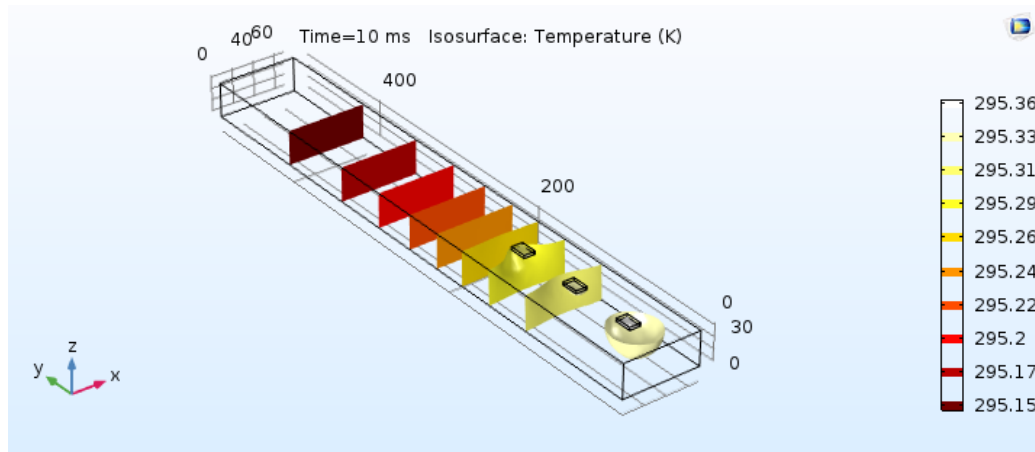


Figure 5. 24 Thermal analysis of  $\mu$ LED

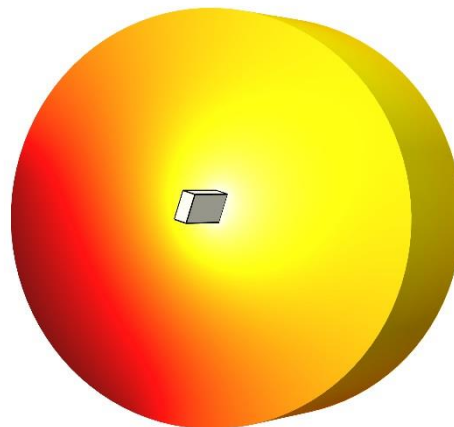


Figure 5. 25 Thermal analysis of  $\mu$ LED with brain model

## 5.5. Conclusion

This chapter presents another type of deep brain stimulation electrode which make stimulation by light and is known as Optrode. This type of electrodes has an advantage of high spatial precision because of the neuron is injected by certain material to be sensitive to a certain wavelength of light. So that only the neurons which have changes

in its proteins will be affected by the light and the other neurons will not be affected. Optode disposes of that the electrical signal affects all the neurons and this is considered a main drawback of the electrical DBS electrode. The simulation on optrode is done to check the effect of the electric field from the light source on the wires to reduce the noise in case of recording data. The second check is to test the increasing in the temperature which has a bad effect on the brain tissue. The results from simulation shows that the increasing in Temperature is less than 1°C and the effect of electric field is so small if fabricate the design with two metal layer. A model of  $\mu$ LED is simulated to check the effect of decreasing the cross-section area of it on the intensity and the power and to decide the suitable voltage with current to achieve minimum power more than  $1mW/mm^2$ .

## Chapter 6 : Electrode Fabrication

In this chapter several electrode designs are proposed to satisfy a range of design applications and requirements. The first step of fabrication is started with a simple structures comprising single metallization layer to determine the fabrication processes and equipment. The next step is to implement design with 2 metallization layers which is considered more complicated design. Although the target was to implement the electrodes on ductile; however, the preliminary prototype was fabricated on silicon substrates to simplify the fabrication process and verify the correctness of steps. Then the prototype will implemented on ductile substrates which overcome several challenges in mechanical analysis. Several techniques are used to tackle practical issues including interconnection and assembly of electrodes to be connected with measurement systems and implemented in vivo. This requires to design and fabricate customized components such as printed circuit boards.

### 6.1. Layouts

Layouts are designed with two different designs by Cadance tool. Figure 6. 1 shows the layout of the electrode with only one metal layer.

#### 6.1.1. One Metal Layer

The structural of the preliminary electrodes is made of Silicon, with only one metal layer which contains the pads and its tracks.

The steps of fabrication:

1. The wafer is prepared by RCA cleaning and dipping in BHF bath to remove the native oxide layer.
2. Metal thin film was deposited and patterned to create the pads and routing tracks.
3. Polyimide passivation layer was deposited. The passivation layer was patterned to expose the metal pads and form the electrode contour. Polyimide was patterned using dry etching and aluminum hard mask. Metallization layers were made of multiple thin films; chrome (or aluminum) provided the thickness required for achieving low DC resistance, and gold (or titanium) thin film was deposited to provide biocompatible contact.

The masks of the single shaft electrode presented in Figure 6. 2 and Figure 6. 3 provided 6 stimulation channels on 10mm shaft with a width of 500 $\mu$ m, and the pads were 110x110 $\mu$ m. The structural is thick enough to realize a mechanically competent structure. However, this design would not comply with the biomedical design constraints due to the exaggerated shaft dimensions which would yield remarkable tissue trauma.

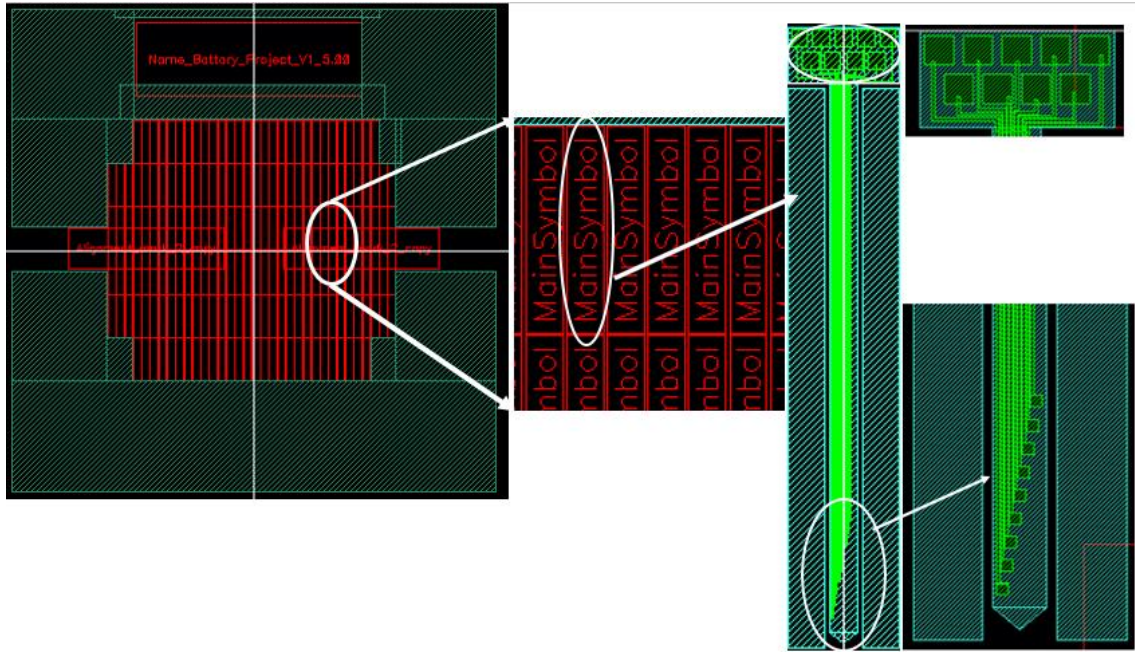


Figure 6. 1 The Layout of the electrode

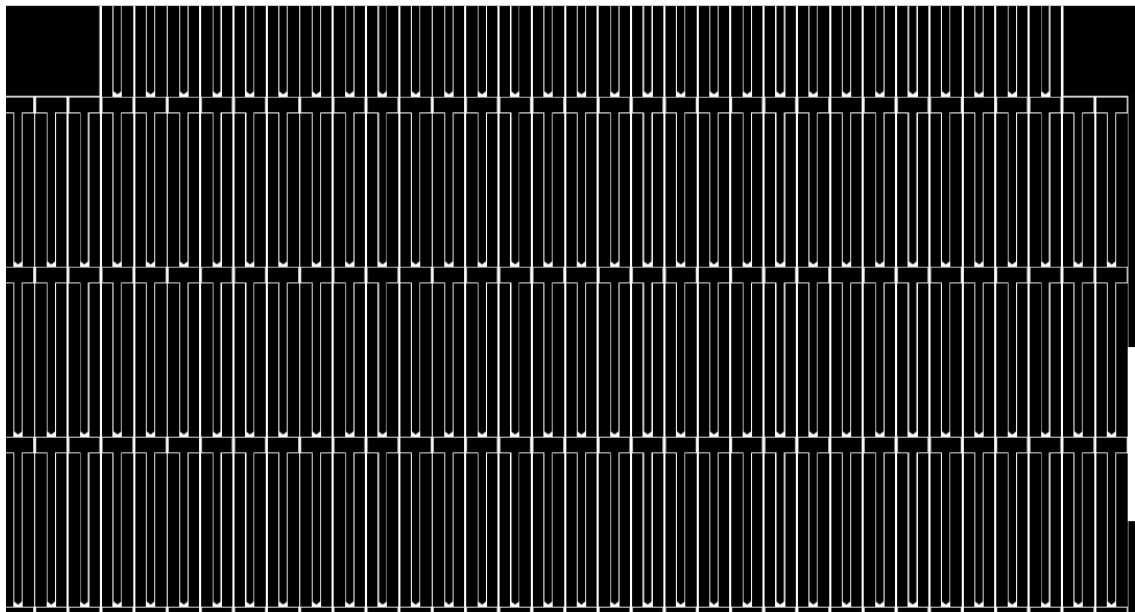
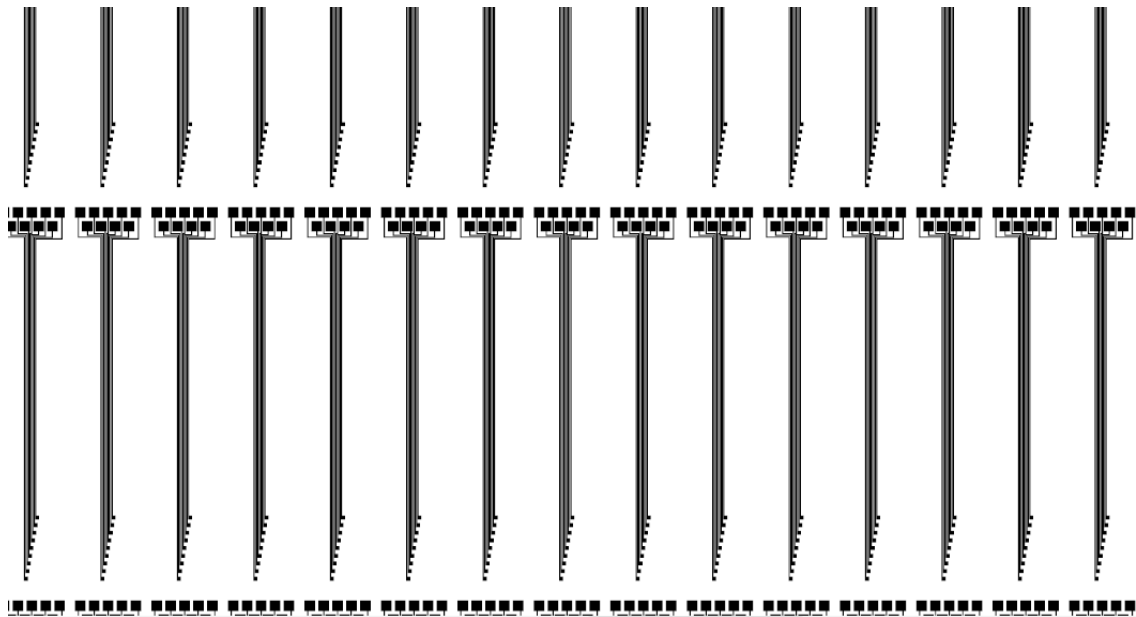


Figure 6. 2 Snapshot of Contour mask



**Figure 6. 3 Snapshot of Pads Mask**

#### **6.1.1.1. Fabrication Steps**

The fabrication process is made in the cleanroom of Yousef Jamel Science and Technology Research Center (YJ-STRC), in the School of Sciences and Engineering (SSE), in American University in Cairo.

##### *6.1.1.1.1. RCA cleaning*

Clean the wafer from the particles. There are 2 types of cleaning one is to use RCA1 this contain some chemical with certain concentration, and is made by next steps:

1. Solvent clean
2. Dionized (DI) water
3. RCA clean
4. The last step is DI rinse

If we talk about the first step “Solvent Clean”. This step takes 5 minutes as a setup time, but the all step takes 15 minutes. This step cleans organic residues and oils. Put the Acetone into a container of a glass and put the methanol in another container. Take the 1st container and put it on a hot plate with a temperature which is less than 55 deg C. Then put the Si wafer in this acetone container for 10 min. as a warm bath. Take off it from this container and then put it in the 2nd container for 2 to 5 min.

After that go to the 2nd step and rinse it by DI water. This step is optional so we can ignore it and jump to the next step of it “RCA cleaning”. Then blow the wafer by the nitrogen.

Step three has a setup time of 5 min. and the all process takes 20 min. This step is used to erase the organic residues from the wafers of Si. The recipe of the RCA-1 contains 3 materials: (H<sub>2</sub>O, NH<sub>4</sub>OH, H<sub>2</sub>O<sub>2</sub>). These materials are mixed together with a certain values as:

Put DI water with 325 ml and add NH<sub>4</sub>OH “ammonium hydroxide” with 65 ml and then add H<sub>2</sub>O<sub>2</sub> by 65 ml. The DI water should be put in a Pyrex container with the other 2 materials. The indication that the solution is ready is the bubble vigorously, and

this may take between 1 to 2 min. Put the wafer in RCA-1 solution and this may take 15 min. After this step go to the last step and put the Si wafer in a DI water container. Then change the water for a several times.

After RCA-1 clean, we may make a HF clean to remove the dielectric layer. HF is the Hydrofluoric acid. This bath contains 2 materials HF with 20 ml and reduce its concentration by water, the added water is of 480 ml.

The previous step is all the perfect clearance, but if needing to make a fast clean, use only the acetone bath then the IPA bath which can be considered as a type of Alcohol family. Then dry it by N<sub>2</sub> “nitrogen”.

#### *6.1.1.1.2. Dielectric Layer*

SiN “Silicon Nitride” is preferred than the SiO<sub>2</sub> “Silicon Oxide” because it has a best isolation than the SiO<sub>2</sub>.

In this step, the dielectric layer is deposited by using PECVD “Plasma Enhancement Chemical Vapor Deposition”. There are some steps to operate the device and to put the recipe of the procedure. The recipe depends on the brand of the device, the dielectric layer thickness, and the dilution of the gases. Figure 6. 4 shows the PECVD and its chamber pump and the wafer is in it window. This is the figure of the chamber after making plasma cleaning which should be done after each process and some mechanical cleaning. Manual cleaning should be made after the plasma cleaning to be sure that the chamber pump hasn’t any unwanted particles. Figure 6. 9 shows the chamber before plasma cleaning. Some problems appear, the first one is the arm of the device doesn’t work and hangs because there are three white pins in the plate inside the chamber pump should go up to rise the wafer and then the arm take this wafer and exits it to the loadlock pump, so that the wafer may be broken. Figure 6. 6 shows the broken wafer after the PECVD process. The second problem is the holder uses only 6 inch wafer and our wafer is 4 inch so the 4 inch wafer is put on a dummy 6 inch wafer with using a specific oil to fix it. Figure 6. 5 shows the 4inch wafer above the 6inch dummy wafer.





**Figure 6. 4 Opened chamber pump of PECVD**

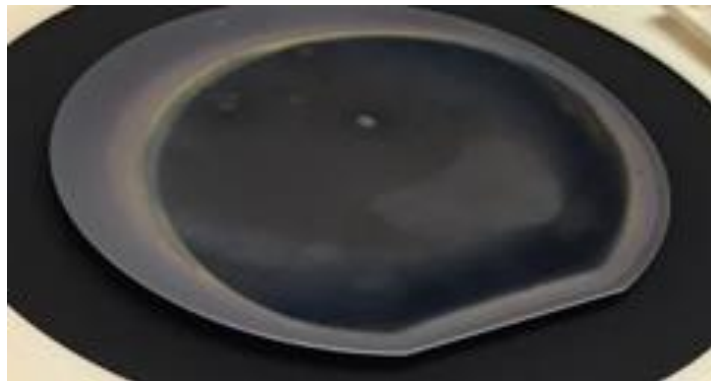


**Figure 6. 5 4inch wafer above 6inch dummy wafer**

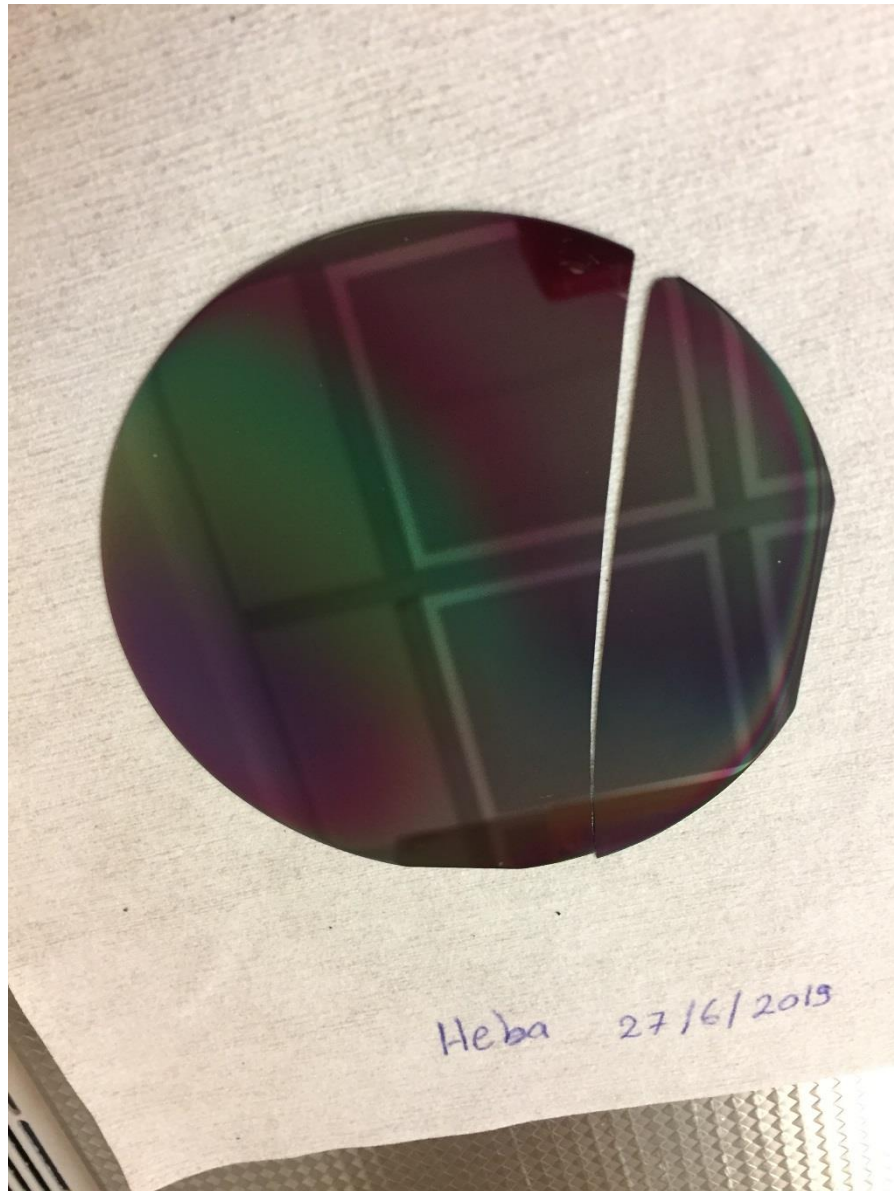


**Figure 6. 6 The broken wafer after PECVD process**

The recipe should be inserted to the PECVD but before this recipe there are many setup steps. The all steps are:

1. Open the needed gas from the exit boxes because these gases have a dangerous effects.
2. Rise the hand breaker of the PECVD and the Heater
3. Turn on the machine from green bottom
4. Turn on its PC
5. Turn on the software and put the name and the password
6. From system bare open pumping window and then in the part of chamber pump press (Figure 6. 7 illustrates the pump window in the software)
  - i. stop
  - ii. evacuate
  - iii. Vent (to check that the chamber is clean and if not we will make a plasma cleaning then mechanical cleaning).

- iv. The mechanical cleaning is done by using a small sponge and Acetone (red bottle) and alcohol (yellow bottle “IPA”) then after the previous steps make the last step to be sure that the holes of the chamber are clean use Vacuum Cleaner.
7. in the loadlock pump press the pump to run then
    - i. stop
    - ii. evacuate
    - iii. vent ( to load the wafer at the loadlock window)
  8. From process bar, find the recipe window and chamber window
  9. Recipe window will be put in it my recipe to deposit the dielectric layer that is needed
    - i. press load and select any old recipe
    - ii. change its name
    - iii. press save to save this new recipe

First step of recipe should be stabilization temperature to increase the temperature to approximate value (the process will need some time to reach to degree nearby the needed temperature).

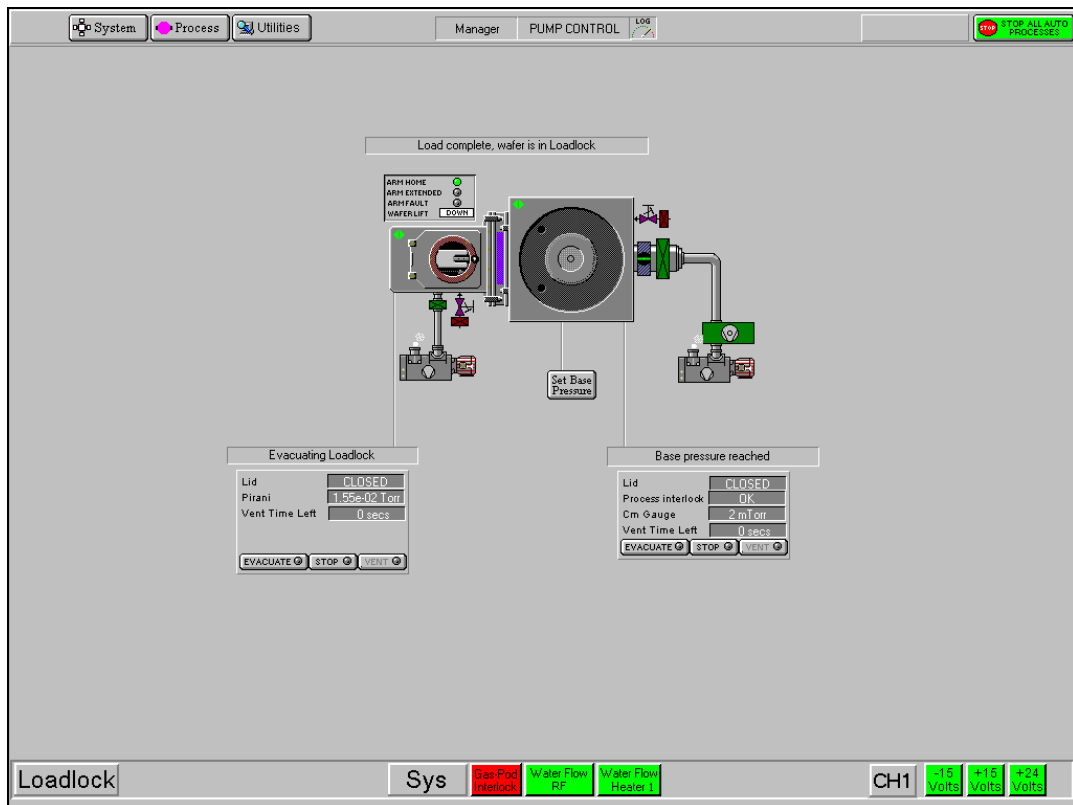


**Figure 6. 7 Pumping window**

The setup steps will be as follow:

1. the stabilization temperature, this step is done to increase the temperature of the chamber pump to a temperature near to the needed temperature in the recipe:
  - a. Put temperature with 200°C
  - b. No gas flow, all gases are 0 flow

- c. Time is for 5 min, to run this process for 5 min.
- 2. Pre-clean Step, this step is modified to reduce the pressure from 2000mTorr to 1500mTorr because the maximum pressure for this device is 2000mTorr.
  - a. Put the pressure = 1500 mTorr, this is considered a high pressure
  - b. No gas flow all gases are 0 flow
  - c. Time 5 min.
- 3. Pre-heat to exceed the temp to 350 deg C because the recipe put the Temp between 300 and 400 deg C
  - a. No gas flow
  - b. Temp. 350
  - c. Time is 2 min.
- 4. The main Recipe. Figure 6. 8 shows the window which has the amount of the gases:
  - a. SiH4 will be 20 Sccm
  - b. NH4 will be 20 Sccm
  - c. N2O will be 980 Sccm
  - d. Helium purger should be 5 mTorr as a minimum value to protect the pumps
  - e. pressure is between 650 and 850 mTorr “ in this case we can set the valve instead of the pressure and the parameter of this is the degree of the valve and this has a value between 0 and 90”
  - f. RF power = 20 Watt
  - g. Run the recipe for 15 min.
- 5. There are 3 steps for cooling the chamber pump
  - a. Enter a N2 by 2000 Sccm for 15 min. and set the valve by 90 degree instead of the pressure
- 6. To circumvent the arm problem:
  - a. load the wafer manually from the pumping window before running the recipe
  - b. open recipe menu and select manual from the left upper corner
  - c. load our recipe
  - d. After finishing the run. Unload the wafer manually from the pumping window and don't enter the service mode window at any time.

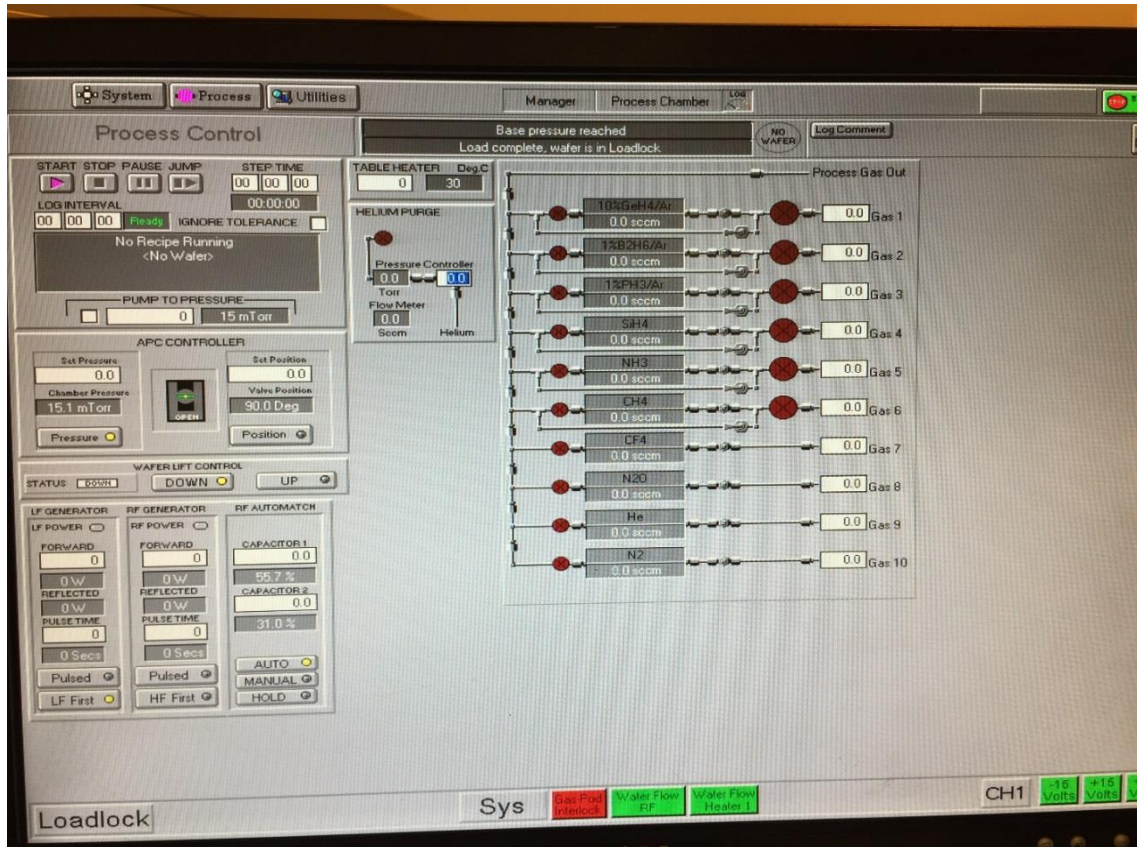


**Figure 6. 8 The window of the my recipe**

#### 6.1.1.1.3. Lithography

This step is a main step to deposit a metal layer, and is divided into:

1. Use a photoresist and put it on the wafer by using a spin coating device and should determine the acceleration and the speed to get a good surface of photoresist. Figure 6. 10 illustrates a wafer on the spin coater after fixed on a dummy 6 inch wafer and has an amount of photoresist on its surface. After run the process, the photoresist spreads on the surface of the wafer as shown in Figure 6. 11.



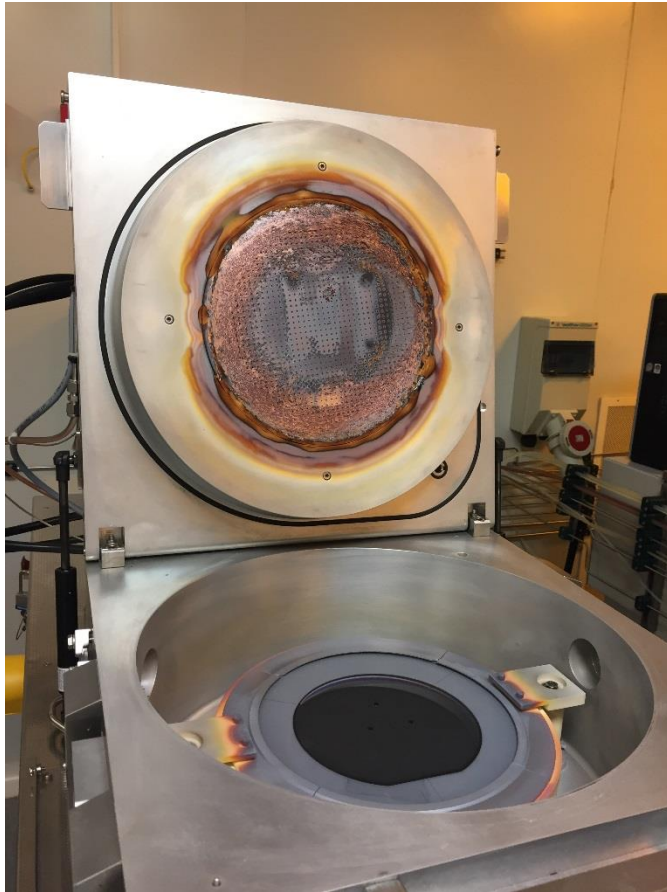


**Figure 6. 9 Chamber before plasma cleaning**

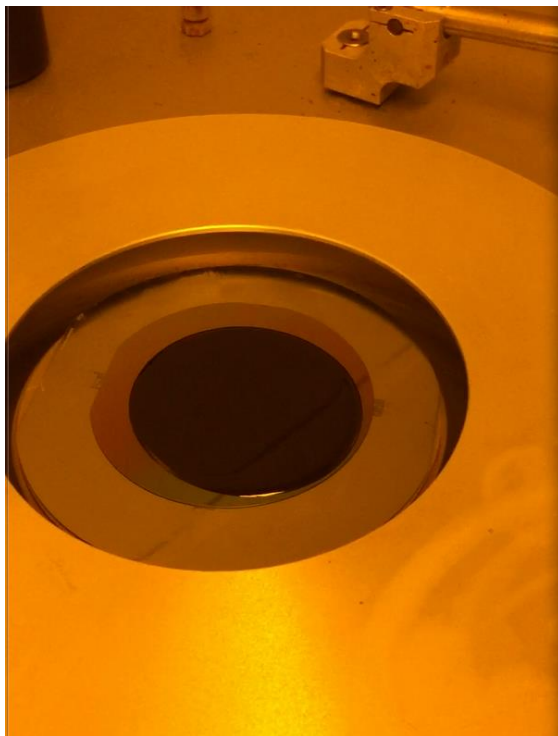


**Figure 6. 10 Wafer on Spin Coater**



**Figure 6. 11 Spread Photoresist**

2. Put the wafer on a hot plate for 45sec with temperature of  $110^{\circ}\text{C}$ . Figure 6. 12 shows the hot plate device and the wafer above its surface.

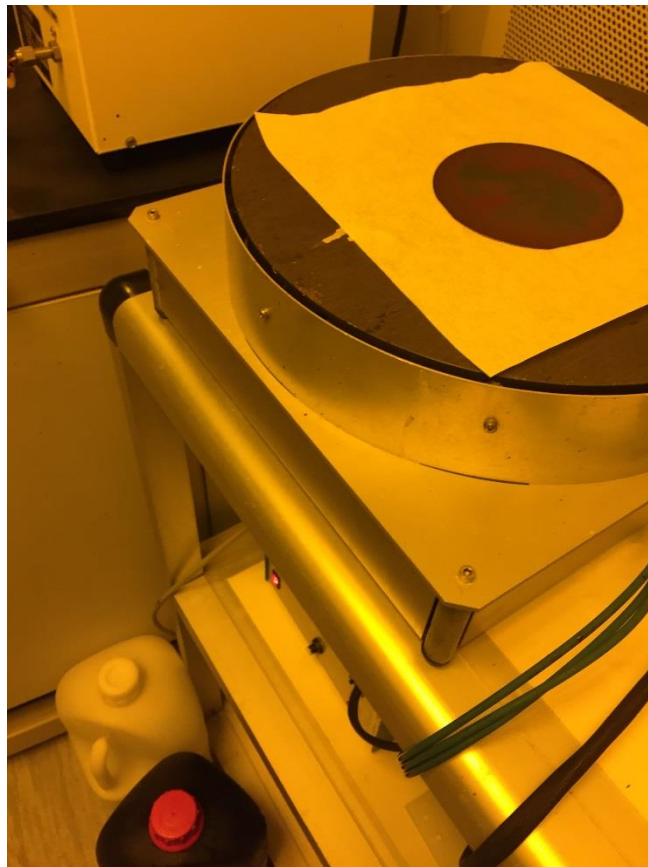


**Figure 6. 12 Wafer on Hot plate**

- Put the wafer on the UV exposure. In this device, the mask and the wafer are held for a certain time which is called exposure time. When using positive photoresist the UV will expose the places of the pattern. Figure 6. 13 shows the UV when hits the surface of the wafer through the mask.



**Figure 6. 13 UV process**

- The wafer will put in a developer of this photoresist to remove the parts which are exposed to the UV. Figure 6. 14 shows the pattern after developer bath.



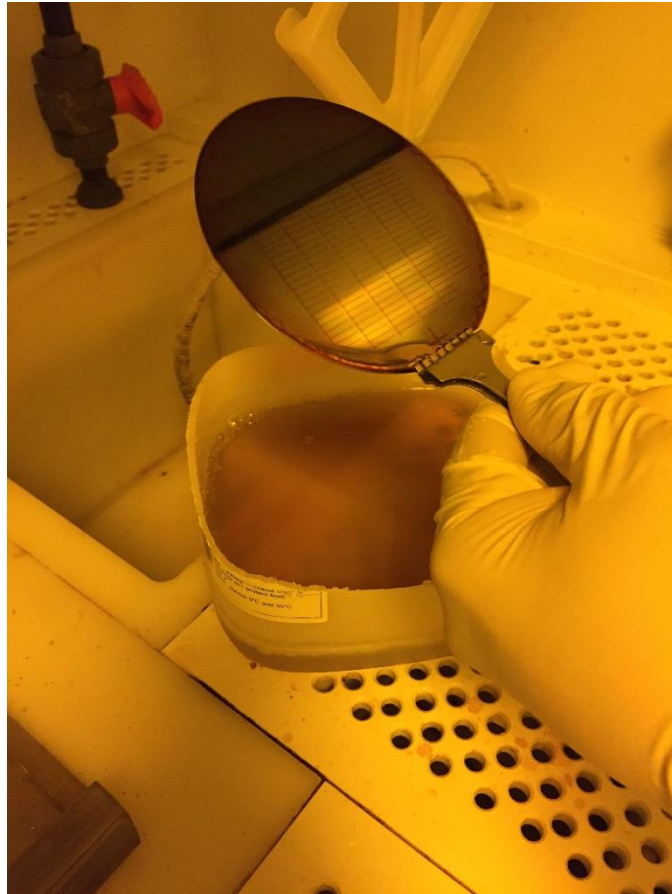


**Figure 6. 14 Wafer in developer**

5. Check the wafer under the microscope. Figure 6. 15 shows the wafer after the developer bath. This should be modified to improve the exposure process.

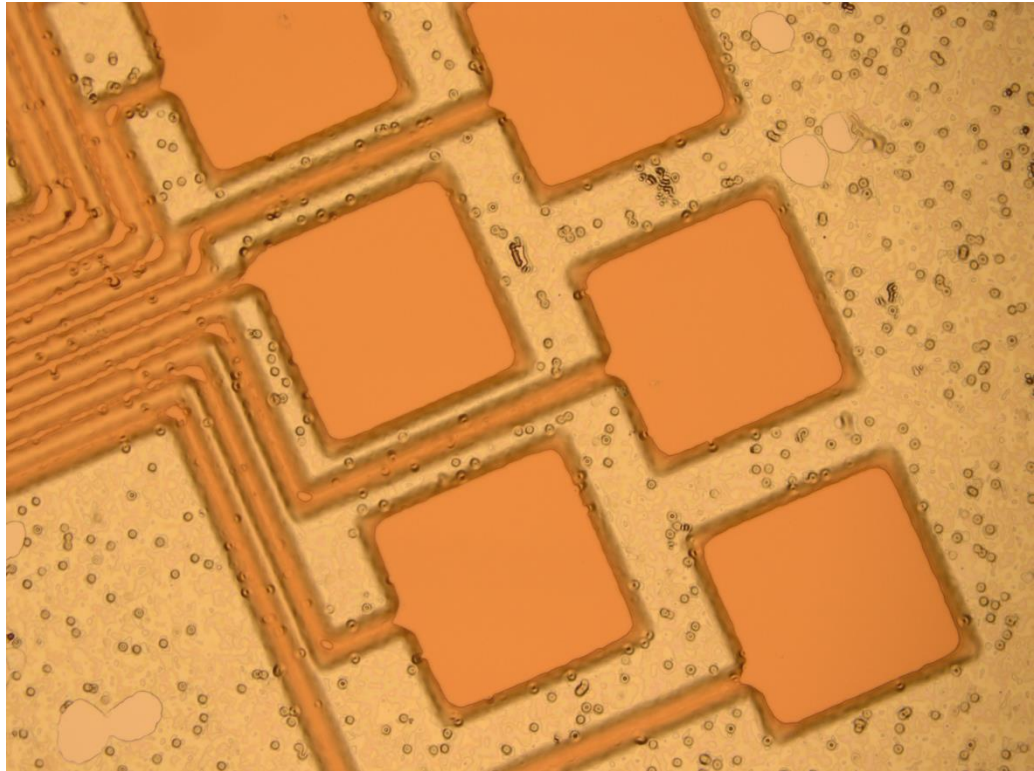


**Figure 6. 15 Pattern under microscope**

Note:

The step of photoresist should be done in any fabrication step for depositing any material or to etching certain places. Figure 6. 16 shows that if using positive photoresist the pattern will be as the figure after the process of UV exposure and developer bath. The negative photoresist has an opposite attitude.

6. After the developer, the wafer will be taken to deposition a metal layer on its surface by using RF sputtering for different materials like gold, Nickel, Titanium, or Platinum. Or using ALD to deposit Aluminum.

Figure 6. 17 shows the expected shape of metal after deposition or etching process.

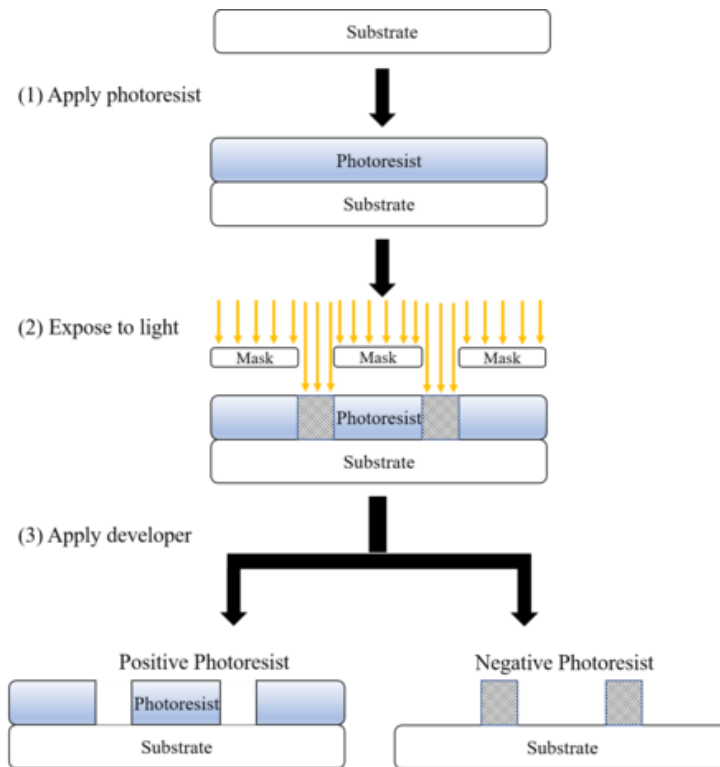


**Figure 6. 16 Photoresist [89]**

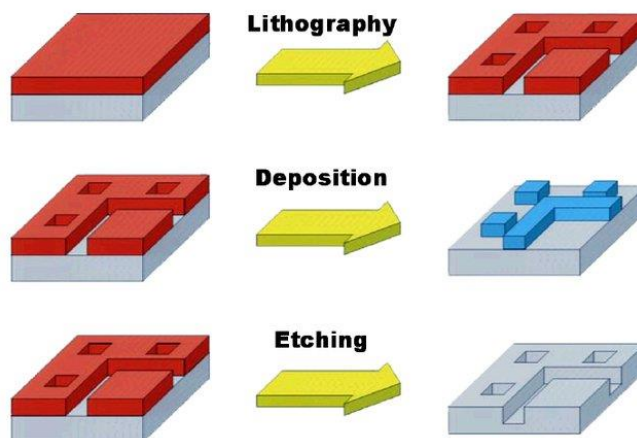


**Figure 6. 17 Lithography**

### 6.1.2. Two Metal Layer

The structure substrate is of Silicon material and contains two metal layers, one for tracks and the other for pads. Then replace the structure with ductile material “Nickel”. Figure 6. 18 illustrates the shape of the electrode with small dimensions than the previous design. Figure 6. 19 shows the mask of the tracks shape which forms the first metal layer. Figure 6. 20 has the shape of the vias to connect the tracks wires with the pads in the next metal layer.

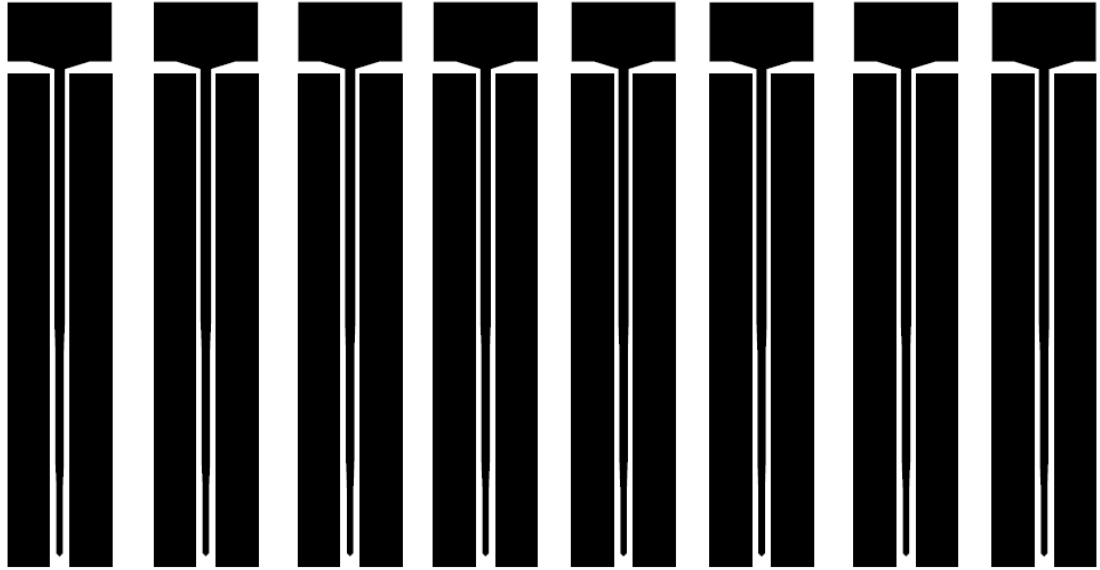


**Figure 6. 18 Snapshot of the contour mask**

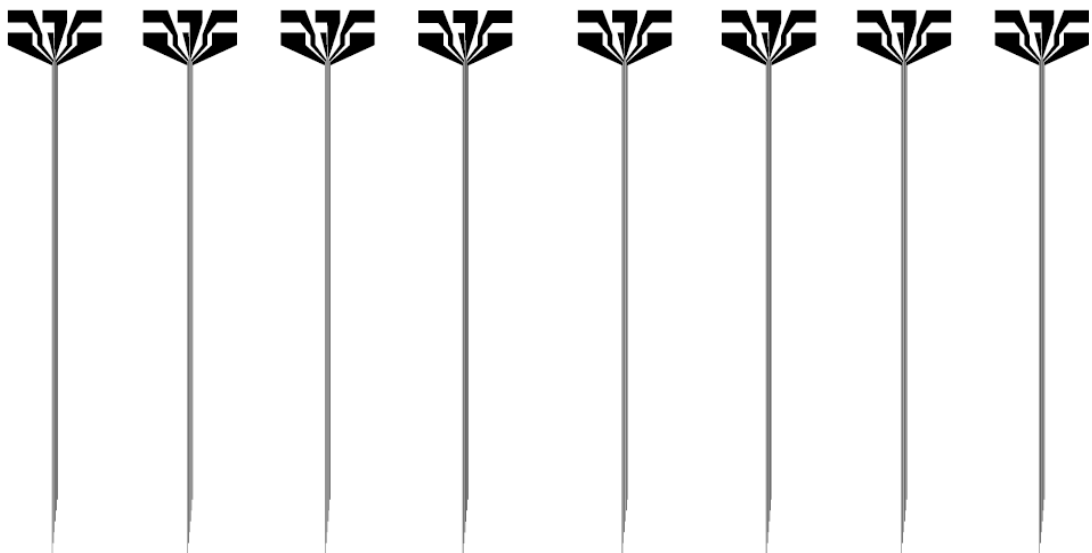


**Figure 6. 19 Mask of the first metal layer**

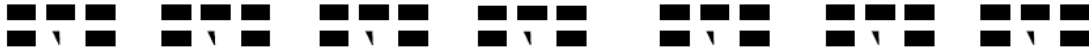


**Figure 6. 20 Vias of the layout**

#### **6.1.2.1. Fabrication Steps**

The fabrication steps and costs have been estimated for each material. It should be known that some steps might need further development in order to get the electrode properly with its required structure. The main fabrication steps implemented with copper and nickel are as follows:

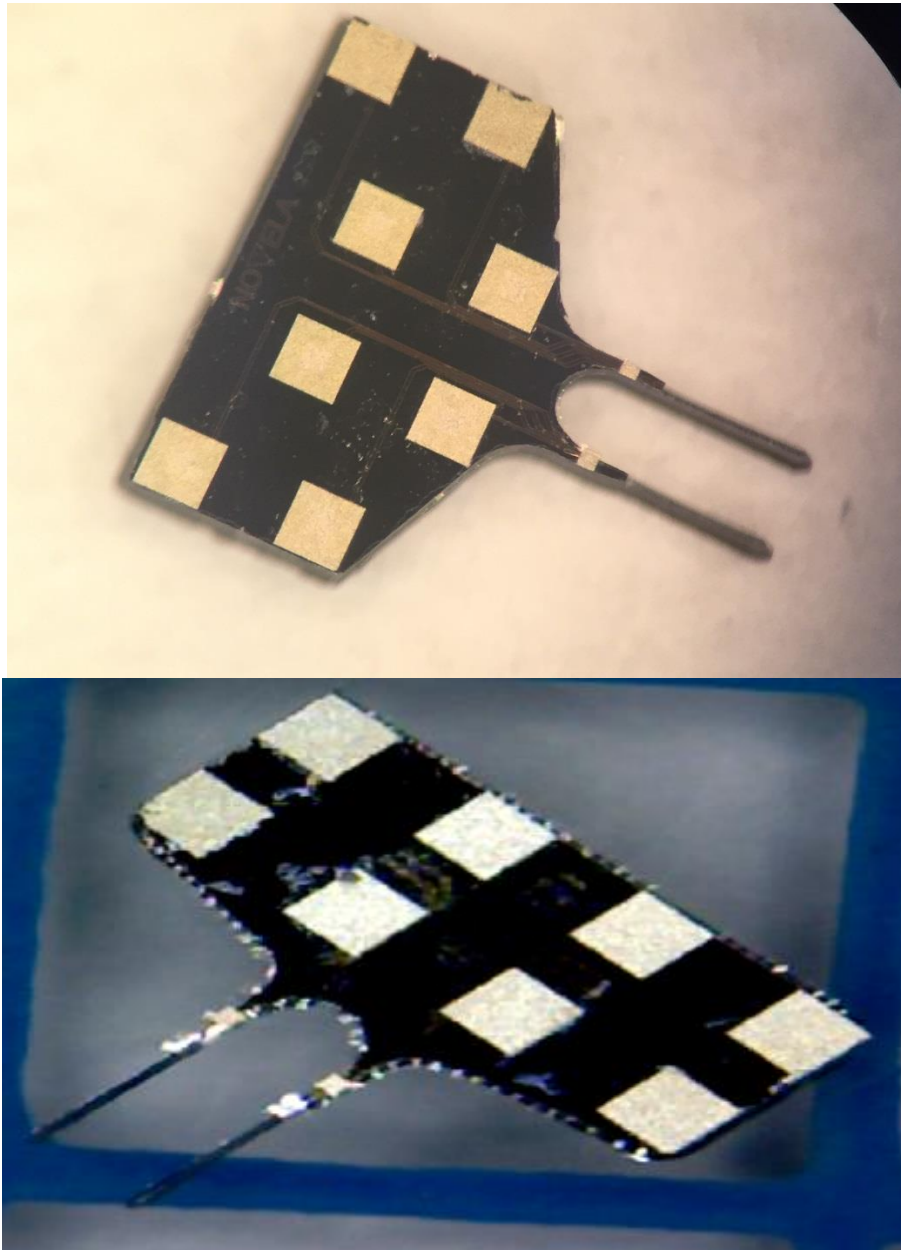
- RCA-1 Si Wafer Cleaning.
- Sputtering of thin layer of metal (Cu, Ni).
- Lithography and Spin Coating of more than 100µm thick Photoresist.
- Cu Electroplating.
- Performing Chemical Mechanical Polishing CMP to improve surface roughness.
- RCA-1 Cleaning and removing Photoresist.
- Gold Plating to make the structure bio-compatible, since Ni and Cu are poisonous materials.

However, Nickel is a high stress material, thus curvatures may be encountered during the structure release. As for Si material, SOI wafers will be used instead of Si wafers, thus there is no need for sputtering step. The fabrication steps are as shown:

- RCA-1 SOI Wafer Cleaning.
- Lithography and Spin-coating of Photoresist.
- Deep Reactive Ion Etching (DRIE) of the wafer.
- RCA-1 SOI Wafer Cleaning.
- Dicing of the SOI wafers to get individual electrodes.
- Back side etching of the Si handle wafer to release the structure using KOH.
- HF to remove oxide layer in the SOI wafer.

As for the Polyimide material, simpler steps are needed. The main step is lithography in order to achieve the required thickness and using the appropriate developer.

After finishing the fabrication and dicing the wafer by the laser, the DBS electrode will be ready as a product to be implanted in the brain and connected with a wires or PCB to provide the ability to expose the brain signal on an oscilloscope. Figure 6. 21 shows some graphs of electrodes one of this is good and the other have defects.



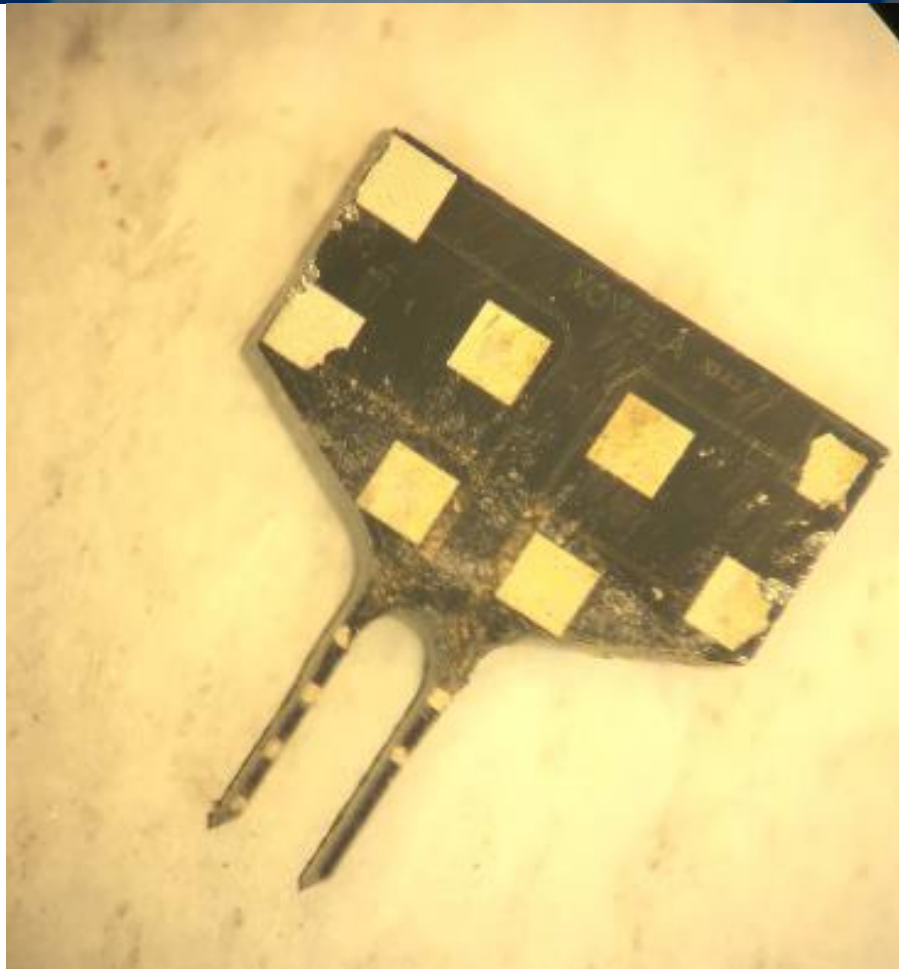
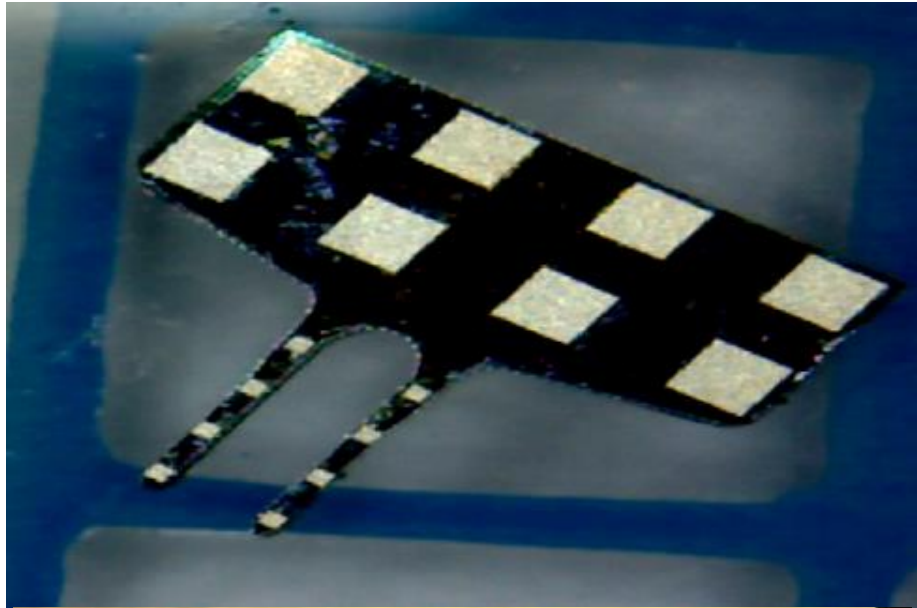


**Figure 6. 21 Some graphs of electrode device**

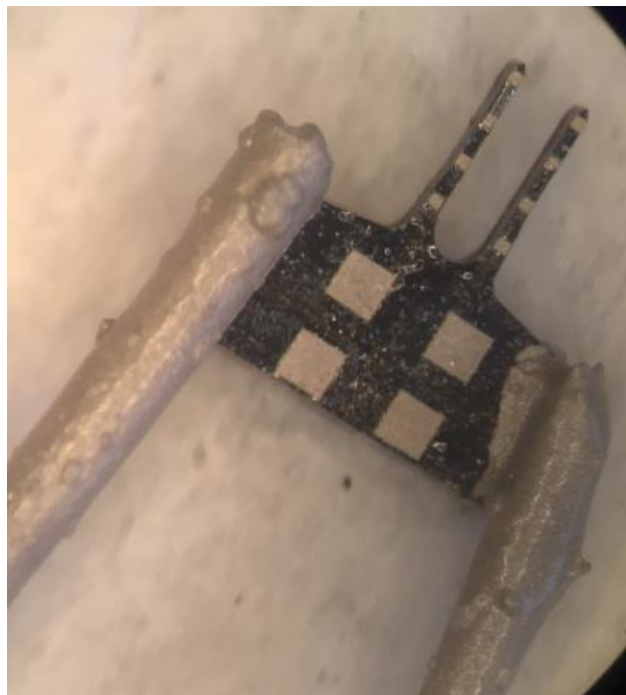


## 6.2. PCB

A (PCB) printed circuit board electrically connects electronic components or electrical components using conductive tracks, pads and other features etched from one or more sheet layers of copper laminated onto or between sheet layers of a non-conductive substrate. To connect the electrode with an oscillator device to expose the brain signals, there is a need to connect it with wires or PCB to simplify this process. The first trial is to adhere the wire with the electrode using conductive epoxy. Figure 6. 22 illustrates some trials to adhere wires with the base pads of the electrode, one with a thick wire, the second with 4 thin wires, and the last one with only one thin wire. A problem appears in this adhesion. The solder released after the adhesion process or if someone move it with some force. And it will be implanted in rat brain, so it should not be released with a large force to be suitable with the rat moves.

To solve this problem, there is a thinking to fabricate a PCB to connect the electrode with an external circuit. There are 2 designs which are drawn using Altium designer summer 09 as a design tool to make the layout of the PCB. One of them had one metal layer and the other had two metal layer. The fabrication was made in Banha Military Factory Electronic Industries, and when the design was made, its minimum feature was taken in concentration. Figure 6. 23 presents the design of the PCB with 2 metal layers, but to simplify and decrease the cost, the fabricated PCB is done only with one layer and if the process was completed with sufficient results, the PCB with 2 layer will be fabricated.

Figure 6. 24 illustrates another design of PCB, but it is not compatible with the fabrication facilities because the space between the wires and the pads is smaller than  $40\mu\text{m}$  and the minimum feature that the factory can fabricate, is  $40\mu\text{m}$ . And the thickness of the wires is too small. Figure 6. 25 presents the implemented layout of the PCB. Figure 6. 26 shows the fabricated PCB. PCB is fabricated from epoxy material and the wires are from Aluminum materials.





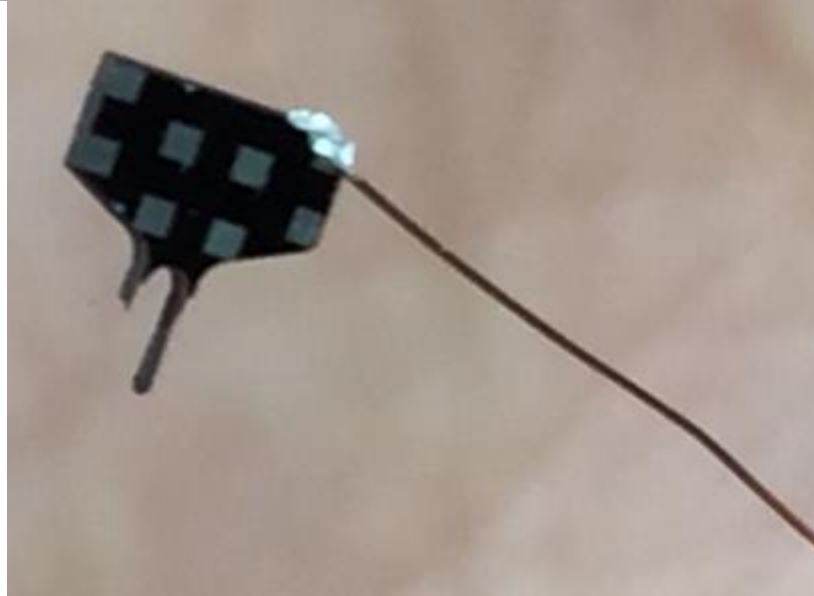
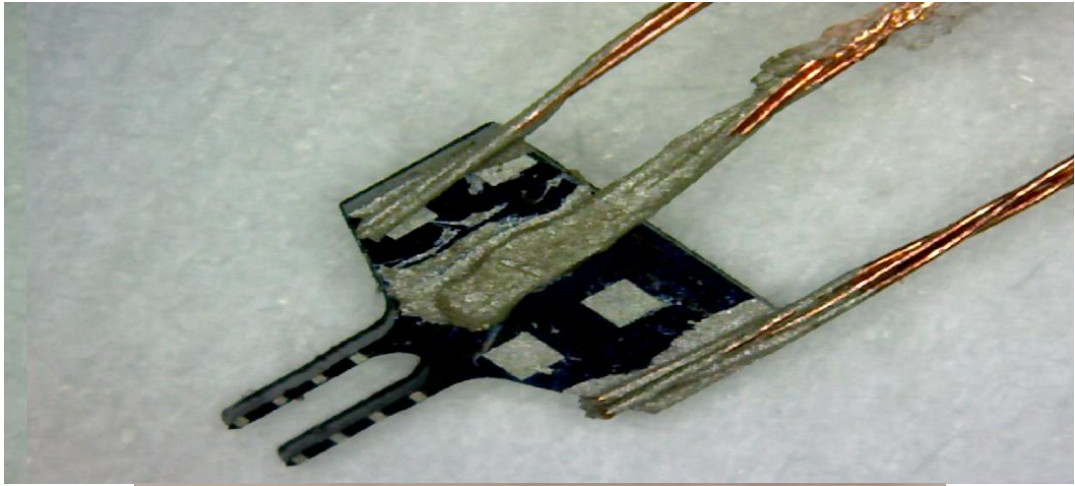
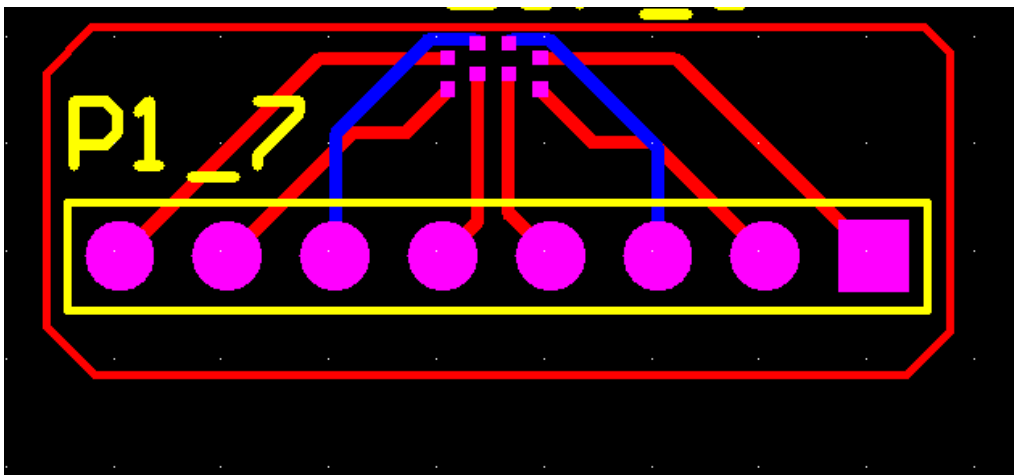


Figure 6. 22 Some trials to adhere wires



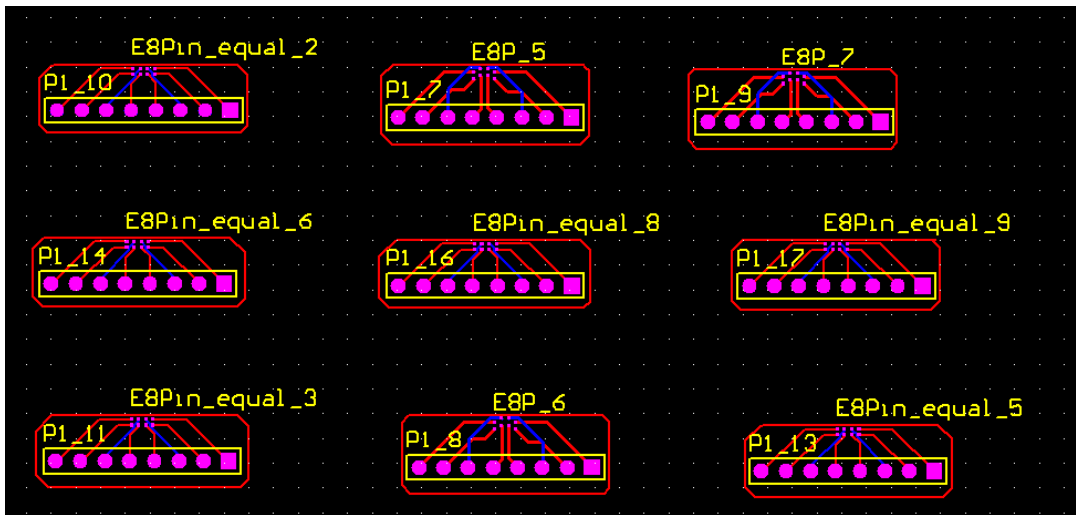
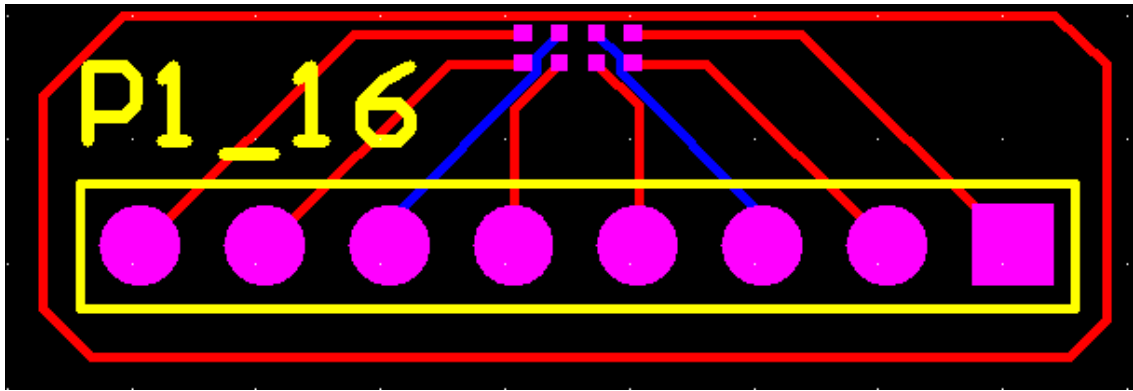
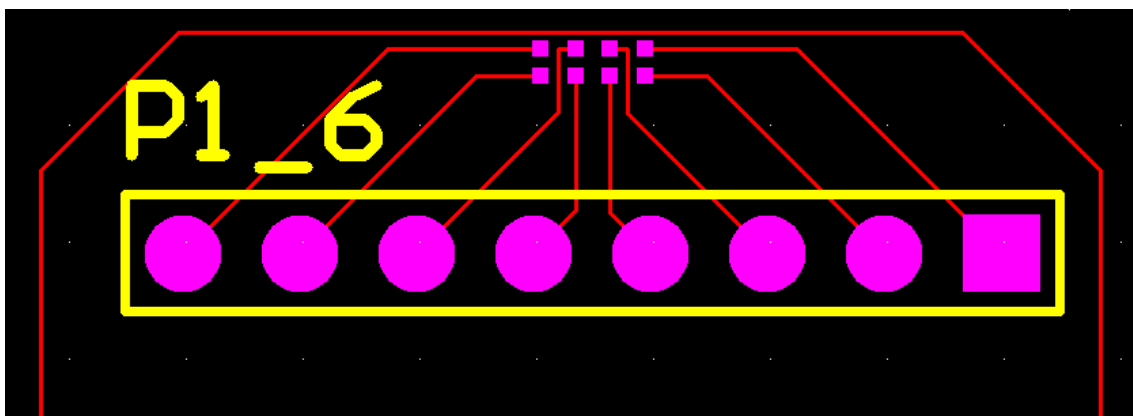


Figure 6. 23 The design of PCB with 2 Layers



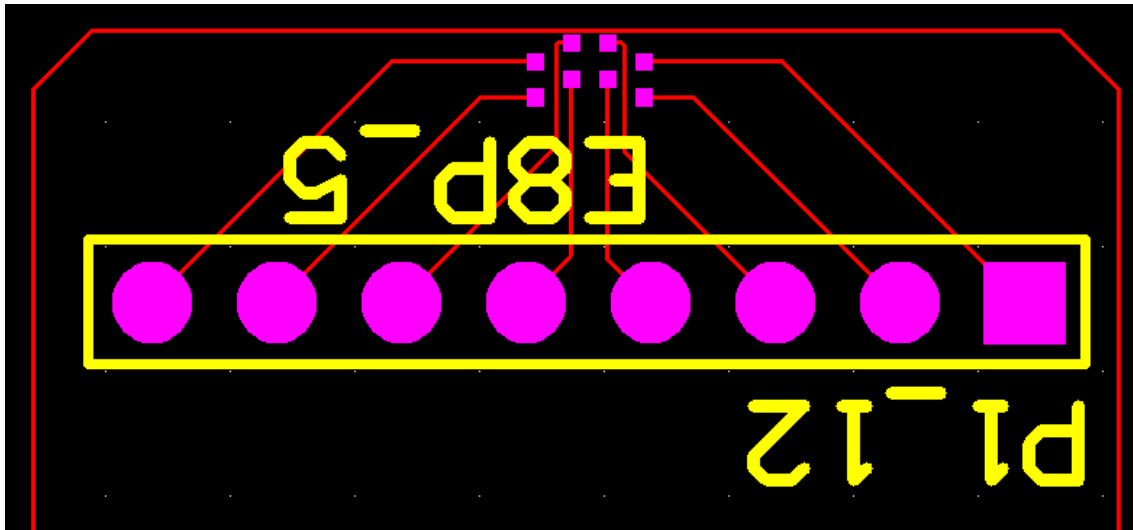


Figure 6. 24 PCB with one metal layer

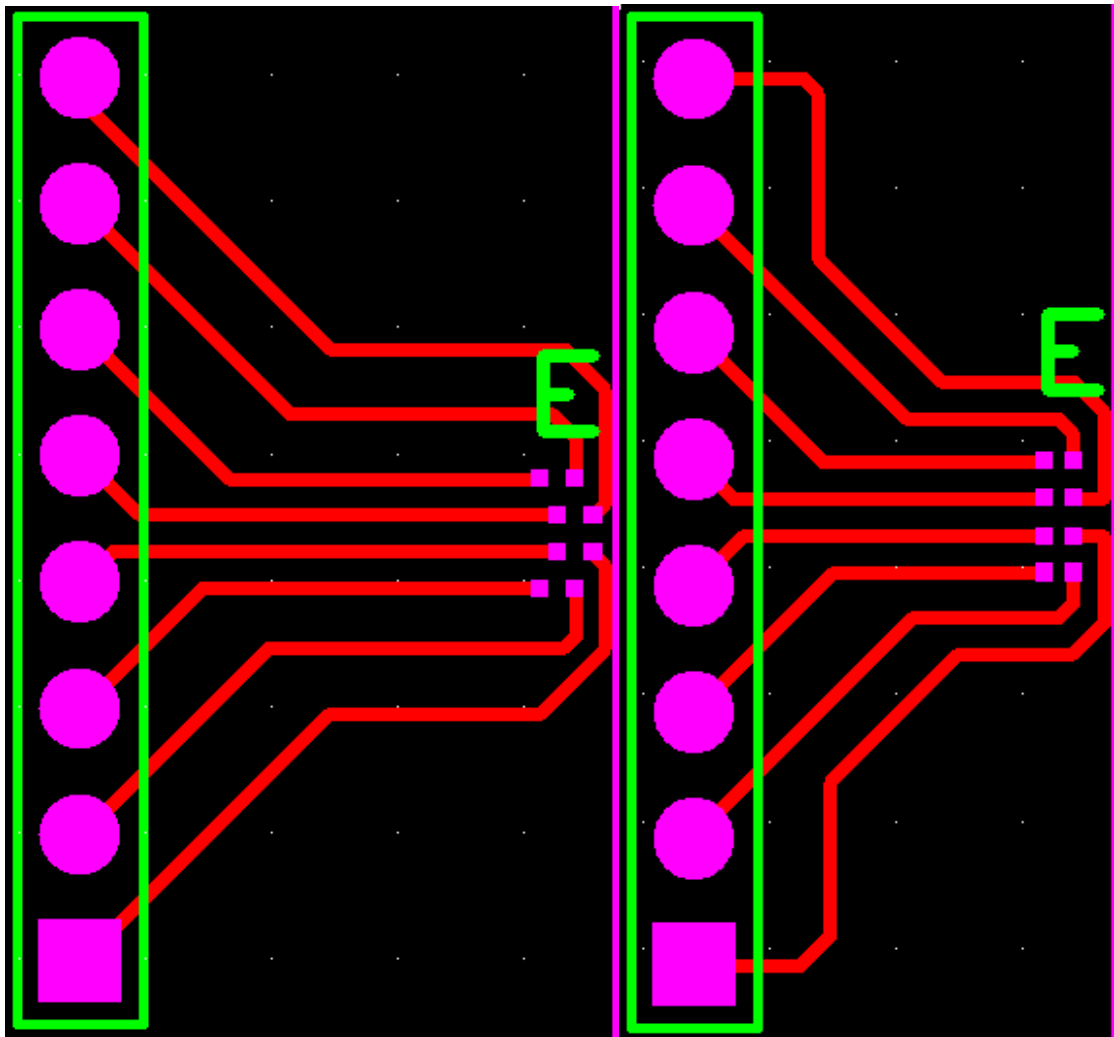
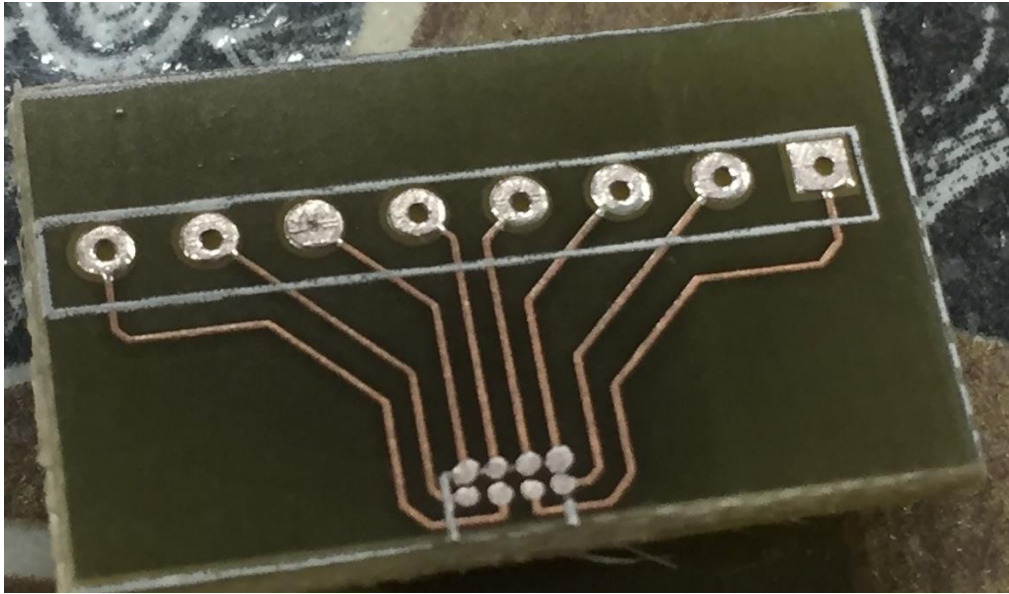


Figure 6. 25 The implemented design



**Figure 6. 26 Implemented PCB**

### **6.3. Test on Rat**

The test of the DBS electrode is made on a wistar rats which are considered the most frequently cited animal model in biomedical publications. In Egypt, wistar rats are the easier rats to get it and make the tests on it. Figure 6. 27 shows the rat through the surgery. Figure 6. 28 shows the rat after the implementation of the electrode then connected with the oscilloscope to read the brain signal. Figure 6. 29 illustrates the process to read the brain signal from the electrode.



**Figure 6. 27 Rat through the surgery**



**Figure 6. 28 Rat with cables**

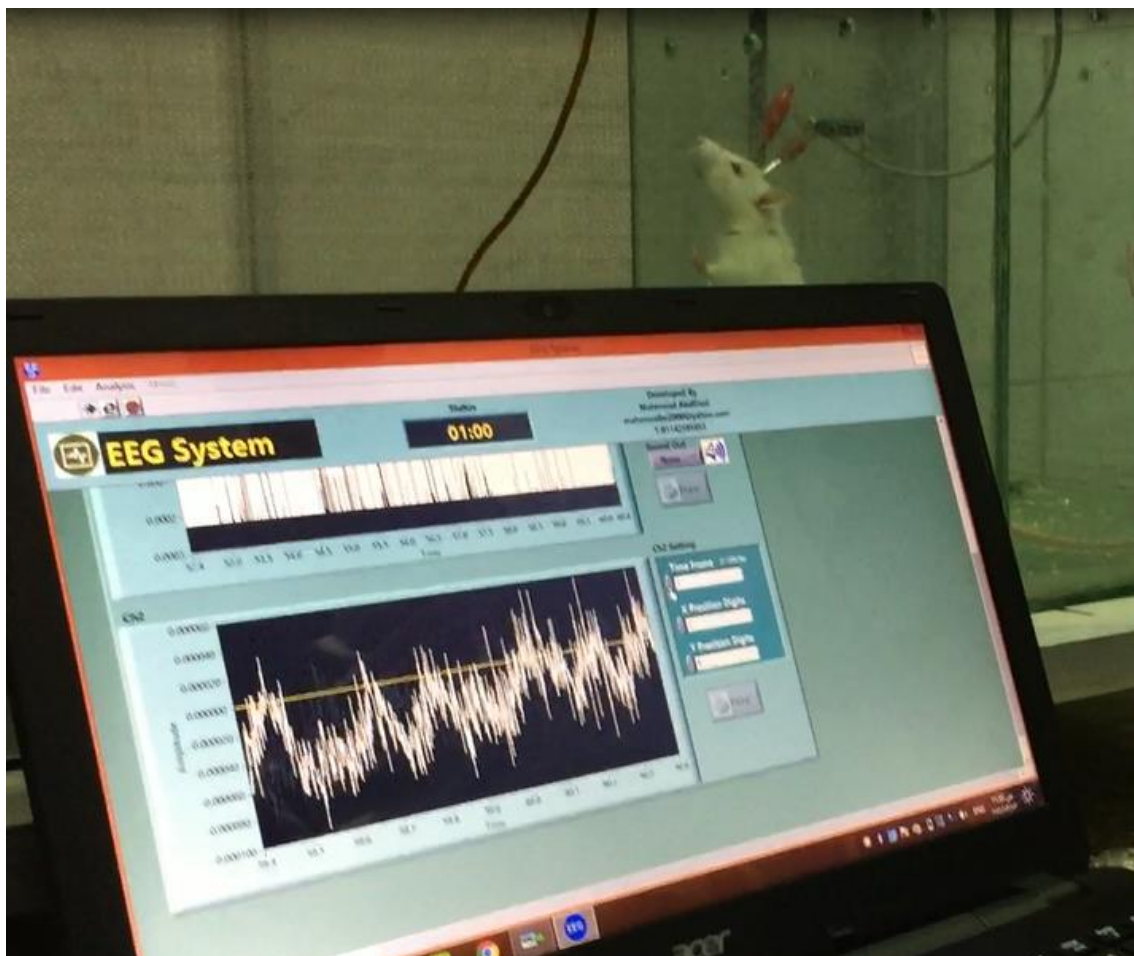


**Figure 6. 29 Brain signal from normal rat**

Figure 6. 30 shows the rat after injected with some chemicals that lead to seizure.



**Figure 6. 30 The rat with seizure**

## Discussion and Conclusions

In this research, there was an introduction of the intra-cortical electrodes and its different types and applications which included several stimulations such as deep brain stimulation (DBS), then the progress of intra-cortical electrodes in treating neurological disorders such as epilepsy, Parkinson's diseases, depression and etc.

Several designs of DBS electrode were exposed with its mechanical simulations and electrical simulations. From these results, the best design of the shape of DBS electrode could be decided and then fabrication. The quest for developing electrodes for neuro-interfacing applications motivated this work. The main objective was to investigate a structure and a material for intra-cortical microelectrodes to allow the implantation process without external assistant devices and maintain its functionality and biocompatibility, then fabricate it. This is required to modify and create new layouts and architectures which supported to satisfy the application requirements by reworking the conventional electrode technology. It showed several novelties and innovations improve the electrode renitency and biocompatibility.

Electrode development was executed by improving design methodology of the intra-cortical microelectrodes, and then creating mechanical models for the electrode to study its performance and to improve its design. There was also some electrical simulation to select the best material for the pads of electrode. This assisted in creating novel electrode architectures and layouts to implement proposed designs. The research introduced mechanical and electrical simulations of electrode designs that integrated simultaneous recording and stimulation.

It also illustrated the fabrication processes of the DBS electrode. The first design consists of only one metal layer. The other design is the optimal design which is fabricated with Silicon and then with Nickel. After the fabrication, the electrode will be implanted in the wister rat brain. Then to be able to connect the electrode with an external circuit, printed circuit board is needed.

Finally, it introduced some data about another type of Intra-Cortical Stimulation electrode which is called "Optrode". There were also some simulations of one type of optrode which had  $\mu$ LEDs on its shaft. The simulation included the change of temperature and electric field which appeared from the existing of the  $\mu$ LED. There is a suggestion of a new design of Optrode.

For future work,

1. There is an ability to implement other designs with other materials such as Nickel.
2. Improve the optrode design by increasing the number of  $\mu$ LEDs, decreasing its power, and implementing several  $\mu$ LEDs with different materials to generate different wavelengths of lights.
3. Implement optrode with using different materials which have a high thermal analysis to improve the temperature distribution.
4. Implement the  $\mu$ LED with our design and increase the recording sites

## References

- [1] B. M. J., “Cortical stimulation parameters for functional mapping,” *Br. Med. J.*, vol. PMC2295628, pp. 481--491, 1875.
- [2] X. Jia and A. Kohn, “Gamma Rhythms in the Brain,” vol. 9, no. 4, pp. 2–5, 2011.
- [3] M. Tudor, L. Tudor, and K. I. Tudor, “Hans Berger (1873-1941)--the history of electroencephalography.” 2005.
- [4] J. L. Stone and J. R. Hughes, “Early history of electroencephalography and establishment of the American Clinical Neurophysiology Society,” *J. Clin. Neurophysiol.*, vol. 30, no. 1, pp. 28–44, 2013.
- [5] R. H. Wurtz, “Recounting the impact of Hubel and Wiesel,” vol. 12, pp. 2817–2823, 2009.
- [6] S. Ja and T. Rs, “Spinal cord stimulation for chronic pain ( Review ),” no. 3, 2010.
- [7] C. B. Corbin, *Ergogenic aids and muscular performance*. Academic Press, 1972.
- [8] T. Mulder, “Motor imagery and action observation : cognitive tools for rehabilitation,” vol. 2, pp. 1265–1278, 2007.
- [9] M. I. Hariz, P. Blomstedt, and L. Zrinzo, “Deep brain stimulation between 1947 and 1987: the untold story,” *Neurosurg. Focus*, vol. 29, no. 2, p. E1, 2010.
- [10] “p950035.pdf.” FDA approval using electrode and stimulator, p. FDA approval, 1997.
- [11] J. Gardner, “A history of deep brain stimulation : Technological innovation and the role of clinical assessment tools,” 2013.
- [12] J. Adkins, “Michigan ’ s first patient treated with thalamic deep brain stimulation for epilepsy,” no. March, pp. 3–5, 2019.
- [13] Ms. Elaine Kiriakopoulos MD, “Deep Brain Stimulation (DBS),” <https://www.epilepsy.com/learn/treating-seizures-and-epilepsy/devices/deep-brain-stimulation-dbs>, vol. Online, 2019.
- [14] U. G. Hofmann *et al.*, “A novel high channel-count system for acute multisite neuronal recordings,” *IEEE Trans. Biomed. Eng.*, vol. 53, no. 8, pp. 1672–1677, 2006.
- [15] S. R. Gabran, “Intra-Cortical Microelectrode Arrays for Neuro-Interfacing,” *Phd Thesis from Univ. Waterloo*, vol. Electrical, 2012.
- [16] “Kit on Epilepsy What you can do,” *World Heal. Organ.*, vol. online "ht, 2019.
- [17] J. J. Mancuso *et al.*, “Integration of multiscale dendritic spine structure and



- function data into systems biology models,” vol. 8, no. November, pp. 1–15, 2014.
- [18] Y. Wang *et al.*, “Targeting analysis of a novel parietal approach for deep brain stimulation of the anterior nucleus of the thalamus for epilepsy,” vol. 153, no. October 2018, pp. 1–6, 2019.
- [19] E. PATRICK, “DESIGN, FABRICATION, AND CHARACTERIZATION OF MICROELECTRODES FOR BRAIN-MACHINE INTERFACES” *Univ. FLORIDA*, 2010.
- [20] D. R. McNeal, “2000 years of electrical stimulation,” *Funct. Electr. Stimul.*, pp. 3–35, 1977.
- [21] T. Witt *et al.*, “Long-term efficacy and safety of thalamic stimulation for drug-resistant partial epilepsy,” 2015.
- [22] “The concept of blinding in clinical trials,” *online* “<https://www.eupati.eu/clinical-development-and-trials/concept-blinding-clinical-trials/>,” 2015.
- [23] “Sham Stimulation,” *online* “[https://www.neuroelectrics.com/wiki/index.php/About\\_tCS](https://www.neuroelectrics.com/wiki/index.php/About_tCS),” 2018.
- [24] M. J. G.-M. M. D. P. S. N. M. Dileep Nair MD; William Bingaman and P. Andre Machado MD, “DBS for Epilepsy: An Important Expansion of Neuromodulatory Therapy for Intractable Seizures,” *online*, 2018.
- [25] T. A. Fofonoff, S. M. Martel, N. G. Hatsopoulos, J. P. Donoghue, and I. W. Hunter, “Microelectrode array fabrication by electrical discharge machining and chemical etching,” *IEEE Trans. Biomed. Eng.*, vol. 51, no. 6, pp. 890–895, 2004.
- [26] Y. Huang, H. Lane, and C. Lin, “Review Article New Treatment Strategies of Depression : Based on Mechanisms Related to Neuroplasticity,” vol., 2017.
- [27] O. Publications, “Po e t r n c i a o t,” vol. 2, 2019.
- [28] K. Kagoo, “Microelectrode Arrays for Neural Recording,” *Sch. Eng. UCSC*, 2005.
- [29] Y. Hanein, Y. V. Pan, B. D. Ratner, D. D. Denton, and K. F. Böhringer, “Micromachining of non-fouling coatings for bio-MEMS applications,” *Sensors Actuators B Chem.*, vol. 81, no. 1, pp. 49–54, 2001.
- [30] K. D. Wise, D. J. Anderson, J. F. Hetke, D. R. Kipke, and K. Najafi, “Wireless implantable microsystems: high-density electronic interfaces to the nervous system,” *Proc. IEEE*, vol. 92, no. 1, pp. 76–97, 2004.
- [31] H. H. Draz, S. R. I. Gabran, M. Basha, H. Mostafa, M. F. Abu-Elyazeed, and A. Zaki, “Comparative mechanical analysis of deep brain stimulation electrodes,” *Biomed. Eng. Online*, vol. 17, no. 1, pp. 1–14, 2018.

- [32] A. H. Bretag, N. Ling, R. Waldo, and G. Ling, "The glass micropipette electrode : A history of its inventors and users to 1950," vol. 149, no. 4, pp. 417–430, 2017.
- [33] N. Nath, J. Hyun, H. Ma, and A. Chilkoti, "Surface engineering strategies for control of protein and cell interactions," *Surf. Sci.*, vol. 570, no. 1–2, pp. 98–110, 2004.
- [34] C. Im and J.-M. Seo, "A review of electrodes for the electrical brain signal recording," *Biomed. Eng. Lett.*, vol. 6, no. 3, pp. 104–112, Aug. 2016.
- [35] B. Ghane-Motlagh and M. Sawan, "A review of microelectrode array technologies: design and implementation challenges," in *Advances in Biomedical Engineering (ICABME), 2013 2nd International Conference on*, pp. 38–41, 2013.
- [36] K. L. Drake, K. D. Wise, J. Farraye, D. J. Anderson, and S. L. BeMent, "Performance of planar multisite microprobes in recording extracellular single-unit intracortical activity," *IEEE Trans. Biomed. Eng.*, vol. 35, no. 9, pp. 719–732, 1988.
- [37] N. A. Blum, B. G. Carkhuff, H. K. Charles, R. L. Edwards, and R. A. Meyer, "Multisite microprobes for neural recordings," *IEEE Trans. Biomed. Eng.*, vol. 38, no. 1, pp. 68–74, Jan. 1991.
- [38] K. A. Moxon, S. C. Leiser, G. A. Gerhardt, K. A. Barbee, and J. K. Chapin, "Ceramic-based multisite electrode arrays for chronic single-neuron recording," *IEEE Trans. Biomed. Eng.*, vol. 51, no. 4, pp. 647–656, 2004.
- [39] M. Mojarradi *et al.*, "A miniaturized neuroprosthesis suitable for implantation into the brain," *IEEE Trans. neural Syst. Rehabil. Eng.*, vol. 11, no. 1, pp. 38–42, 2003.
- [40] B. G. Motlagh and M. Sawan, "High-density 3D pyramid-shaped microelectrode arrays for brain-machine interface applications," *IEEE 2014 Biomed. Circuits Syst. Conf. BioCAS 2014 - Proc.*, vol. 1, no. Corning 7070, pp. 364–367, 2014.
- [41] B. V Mech, "( 12 ) United States Patent," vol. 2, no. 12, 2017.
- [42] K. D. Wise, "Silicon microsystems for neuroscience and neural prostheses," *IEEE Eng. Med. Biol. Mag.*, vol. 24, no. 5, pp. 22–29, 2005.
- [43] J. Du, I. H. Riedel-kruse, J. C. Nawroth, M. L. Roukes, G. Laurent, and S. C. Masmanidis, "High-Resolution Three-Dimensional Extracellular Recording of Neuronal Activity With Microfabricated Electrode Arrays," pp. 1671–1678, 2009.
- [44] S. Negi, a Hogan, M. Leber, M. M. H. Shandhi, and R. Bhandari, "NOVEL DESIGN AND FABRICATION OF DOUBLE SIDE PENETRATING Department of Electrical and Computer Engineering , University of Utah , Salt Lake City , UT , USA Blackrock Microsystems , Salt Lake City , UT , USA," pp. 1731–1734, 2015.

- [45] T. Suzuki, K. Mabuchi, and S. Takeuchi, "A 3D flexible parylene probe array for multichannel neural recording," in *First International IEEE EMBS Conference on Neural Engineering, 2003. Conference Proceedings.*, pp. 154–156, 2003.
- [46] B. Ghane-Motlagh and M. Sawan, "Design and Implementation Challenges of Microelectrode Arrays: A Review," *Mater. Sci. Appl.*, vol. 04, no. 08, pp. 483–495, 2013.
- [47] C. Metallo, R. D. White, and B. A. Trimmer, "Flexible parylene-based microelectrode arrays for high resolution EMG recordings in freely moving small animals," *J. Neurosci. Methods*, vol. 195, no. 2, pp. 176–184, 2011.
- [48] Y.-C. Chen *et al.*, "An active, flexible carbon nanotube microelectrode array for recording electrocorticograms," *J. Neural Eng.*, vol. 8, no. 3, p. 34001, 2011.
- [49] X. Cui and D. C. Martin, "Electrochemical deposition and characterization of poly ( 3 , 4-ethylenedioxythiophene ) on neural microelectrode arrays," vol. 89, pp. 92–102, 2003.
- [50] K. H. Polasek and H. A. Hoyen, "NIH Public Access," pp. 1–24, 2010.
- [51] W. He and R. V Bellamkonda, "A molecular perspective on understanding and modulating the performance of chronic central nervous system (CNS) recording electrodes," 2008.
- [52] Trevor Haynes, "Shining A Light in the Brain\_ Optogenetics as a 'guiding light' for deep brain stimulation - Science in the News." Harvard University, 2018.
- [53] A. Zhang, "Remote Brain Stimulation\_ A new treatment for Parkinson's disease\_ - Science in the News." the Department of Chemistry & Chemical Biology at Harvard University, 2019.
- [54] I. E. Fields *et al.*, "Noninvasive Deep Brain Stimulation via Temporally Article Noninvasive Deep Brain Stimulation via Temporally Interfering Electric Fields," *Cell*, vol. 169, no. 6, pp. 1029-1041.e16, 2019.
- [55] "Comsol Manual," *Comsol.software*, vol. Online "ww, 2019.
- [56] C. Multiphysics, "Introduction to COMSOL Multiphysics®," URL <https://cdn.comsol.com/documentation/5.2>, vol. 1, 1998.
- [57] I. Datta *et al.*, "Composite photonic platform based on 2D semiconductor monolayers," in *CLEO: QELS\_Fundamental Science*, pp. FTu3C--2, 2019.
- [58] Y.-Z. Deng, S.-F. Tang, H.-Y. Zeng, Z.-Y. Wu, and D.-K. Tung, "Experiments on Temperature Changes of Microbolometer under Blackbody Radiation and Predictions Using Thermal Modeling by COMSOL Multiphysics Simulator," *Sensors*, vol. 18, no. 8, p. 2593, 2018.
- [59] M. S. Kamarudin, N. H. Radzi, A. Ponniran, and R. Abd-Rahman, "Simulation of electric field properties for air breakdown using COMSOL multiphysics," in *4th IET Clean Energy and Technology Conference (CEAT 2016)*, pp. 1–5, 2016.

- [60] B. Sezgin, D. G. Caglayan, Y. Devrim, T. Steenberg, and I. Eroglu, "Modeling and sensitivity analysis of high temperature PEM fuel cells by using Comsol Multiphysics," *Int. J. Hydrogen Energy*, vol. 41, no. 23, pp. 10001–10009, 2016.
- [61] S. Makridis, "COMSOL-1st." p. Materials and Energy Course,ng University of Weste, 2015.
- [62] J. T. Rubinstein, F. A. Spelman, M. Soma, and M. F. Suesserman, "Current density profiles of surface mounted and recessed electrodes for neural prostheses," *IEEE Trans. Biomed. Eng.*, no. 11, pp. 864–875, 1987.
- [63] S. R. Gabran, "Design and Optimization Methodology of Sub-dermal Electroencephalography Dry Spike-Array Electrode," University of Waterloo, 2006.
- [64] K. R. Rajagopal and A. R. Srinivasa, "Mechanics of the inelastic behavior of materials. Part II: Inelastic response," *Int. J. Plast.*, vol. 14, no. 10–11, pp. 969–995, 1998.
- [65] S. R. I. Gabran *et al.*, "3-D Flexible Nano-Textured High-Density Microelectrode Arrays for High-Performance," *IEEE Trans. Neural Syst. Rehabil. Eng.*, vol. 22, no. 5, pp. 1072–1082, 2014.
- [66] H. Kim, "Fabrication and analysis of plastic hypodermic needles by micro injection molding," Georgia Institute of Technology, 2004.
- [67] M. Salcman and M. J. Bak, "A new chronic recording intracortical microelectrode," *Med. Biol. Eng.*, vol. 14, no. 1, pp. 42–50, 1976.
- [68] S. D. Senturia, *Microsystem design*. Springer Science & Business Media, 2007.
- [69] S. R. Gabran, "Intra-Cortical Microelectrode Arrays for Neuro-Interfacing," 2012.
- [70] E. H. Chudler, "Brain facts and figures," *Visit. en septiembre*, 2003.
- [71] F. Kölbl and A. Demosthenous, "A figure of merit for neural electrical stimulation circuits," in *Engineering in Medicine and Biology Society (EMBC), 2015 37th Annual International Conference of the IEEE*, pp. 2075–2078, 2015.
- [72] A. C. Hoogerwerf and K. D. Wise, "A three-dimensional microelectrode array for chronic neural recording," *IEEE Trans. Biomed. Eng.*, vol. 41, no. 12, pp. 1136–1146, 1994.
- [73] D. Kil, P. De Vloo, B. Nuttin, and R. Puers, "A Foldable Neural Electrode for 3D Stimulation of Deep Brain Cavities," *Procedia Eng.*, vol. 168, no. 0, pp. 137–142, 2016.
- [74] H. Y. Lai *et al.*, "Design, simulation and experimental validation of a novel flexible neural probe for deep brain stimulation and multichannel recording," *J. Neural Eng.*, vol. 9, no. 3, 2012.

- [75] J. Wang, *COMBINED OPTICAL STIMULATION AND ELECTRICAL RECORDING IN IN VIVO NEUROMODULATION BY PROVIDENCE, RHODE ISLAND*, no. May. 2008.
- [76] K. Kampasi, J. Seymour, E. Stark, G. Buzsaki, K. D. Wise, and E. Yoon, “Efficient assembly of multi-color fiberless optoelectrodes with on-board light sources for neural stimulation and recording,” *Proc. Annu. Int. Conf. IEEE Eng. Med. Biol. Soc. EMBS*, vol. 2016-Octob, pp. 4479–4482, 2016.
- [77] M. Welkenhuysen *et al.*, “An integrated multi-electrode- optrode array for in vitro optogenetics,” *Nat. Publ. Gr.*, no. October 2015, pp. 1–10, 2016.
- [78] J. Zhang, “A Microelectrode Array Incorporating An Optical Waveguide Device for Stimulation and Spatiotemporal Electrical Recording of Neural Activity,” no. September, 2009.
- [79] J. Dai and T. B. Cognition, “Behavioral Manipulation by Optogenetics in the Nonhuman Primate,” no. September, 2017.
- [80] K. Kampasi *et al.*, “Fiberless multicolor neural optoelectrode for in vivo circuit analysis,” *Nat. Publ. Gr.*, no. May, pp. 1–13, 2016.
- [81] C. Goßler *et al.*, “GaN-based micro-LED arrays on flexible substrates for optical cochlear implants,” vol. 205401, 2014.
- [82] B. Fan, K. Kwon, R. Rechenberg, M. F. Becker, A. J. Weber, and W. Li, “TECHNOLOGY A hybrid neural interface optrode with a polycrystalline diamond heat spreader for optogenetics,” vol. 4, no. 1, pp. 15–22, 2016.
- [83] K. L. Montgomery *et al.*, “Wirelessly powered , fully internal optogenetics for brain , spinal and peripheral circuits in mice,” vol. 12, no. 10, pp. 3–5, 2015.
- [84] N. Mcalinden, E. Gu, M. D. Dawson, S. Sakata, and K. Mathieson, “Optogenetic activation of neocortical neurons in vivo with a,” vol. 9, no. May, pp. 1–8, 2015.
- [85] B. F.- Ieee, S. Member, K. Y. Kwon, I. S. Member, A. J. Weber, and W. Li, “An Implantable , Miniaturized SU-8 Optical Probe for Optogenetics-Based Deep Brain Stimulation,” pp. 450–453, 2014.
- [86] F. Wu, E. Stark, and P. Ku, “Monolithically Integrated m LEDs on Silicon Neural Probes for High-Resolution Optogenetic Studies in NeuroResource Monolithically Integrated m LEDs on Silicon Neural Probes for High-Resolution Optogenetic Studies in Behaving Animals,” pp. 1136–1148, 2015.
- [87] C. Multiphysics, C. Software, and L. Agreement, “InGaN / AlGaN Double Heterostructure LED,” vol. www.comsol, 2018.
- [88] V. K. Peddinti, “Light Emitting Diodes ( LEDs ),” vol. Online, no. (material.eng.usm.my/stafhome/zainovia/EBB424e/LED1.ppt, 2019.
- [89] “Positive Photoresist Market Size, Share, Trends Analysis by Workflow and End User to 2025 – Spot Herld.”,2016 .

## Appendix A: One Appendix

**Table A.1: Mechanical Properties of materials**

Material	Young's modulus (GPa)	Poisson ratio	Density ( $\text{Mg m}^{-3}$ )	Ultimate tensile stress (MPa)	Shear modulus (GPa)	Yield stress (MPa)
Copper Alloy	135	0.35	8.3	720	50	510
Nickel Alloy	180	0.31	8.5	1200	70	900
Polyamide (nylon)	3	0.42	1.1	55	0.76	40
Silicon	185	0.28	2.33	35	79.9	7000

## Appendix B:

Color	Wavelength	Frequency	Photon energy
Violet	380–450 nm	680–790 THz	2.95–3.10 eV
Blue	450–485 nm	620–680 THz	2.64–2.75 eV
Cyan	485–500 nm	600–620 THz	2.48–2.52 eV
Green	500–565 nm	530–600 THz	2.25–2.34 eV
Yellow	565–590 nm	510–530 THz	2.10–2.17 eV
Orange	590–625 nm	480–510 THz	2.00–2.10 eV
Red	625–740 nm	405–480 THz	1.65–2.00 eV

Following is a list of semiconductor materials and the corresponding colors:

- Aluminium gallium arsenide (AlGaAs) — red and infrared
- Aluminium gallium phosphide (AlGaP) — green
- Aluminium gallium indium phosphide (AlGaInP) — high-brightness orange-red, orange, yellow, and green
- Gallium arsenide phosphide (GaAsP) — red, orange-red, orange, and yellow
- Gallium phosphide (GaP) — red, yellow and green
- Gallium nitride (GaN) — green, pure green (or emerald green), and blue also white (if it has an AlGaN Quantum Barrier)
- Indium gallium nitride (InGaN) — 450 nm - 470 nm — near ultraviolet, bluish green and blue
- Silicon carbide (SiC) as substrate — blue
- Silicon (Si) as substrate — blue (under development)
- Sapphire (Al<sub>2</sub>O<sub>3</sub>) as substrate — blue
- Zinc selenide (ZnSe) — blue
- Diamond (C) — ultraviolet
- Aluminium nitride (AlN), aluminium gallium nitride (AlGaN), aluminium gallium indium nitride (AlGaInN) — near to far ultraviolet (down to 210 nm)

## Appendix C:

Process Parameters	HF only process	Pulsed HF/LF process
-100% SiH <sub>4</sub>	20 sccm	20sccm
-NH <sub>3</sub> flow	20 sccm(adjust for index)	20sccm (adjust for index)
-N <sub>2</sub> flow	980sccm	980sccm
-Pressure	650-850 mTorr	650-850mTorr
-R.F. power (13.56MHz)	20 Watts	20 Watts 13seconds
-R.F. power (100-300kHz)	-	20 Watts 7seconds
-Temperature	300-400°C	300-400°C

(low frequency pulses are added to reduce film stress and improve film quality)

### Film Characteristics

-Deposition rate >10 nm/min.

### Typical100 PECVD sequence

Step 1: Brief pumpdown 0-1 minutes (optional)

Step 2: Pre-heat/purge 1 minute for wafers, 5minutes for wafers on carrier plate

(e.g. 710sccm N<sub>2</sub> or N<sub>2</sub>O, 2Torr)

Step 3: Pre-clean plasma 1 minute (optional) (e.g. 710sccm N<sub>2</sub>O, 1Torr, 20Watts or 100sccm N<sub>2</sub>, 40sccm NH<sub>3</sub>, 0.2Torr, 20Watts)

Step 4: PECVD process



## Appendix D:

Figure D. 1 illustrates the model of design A on Comsol. There are two ways to make the model:

1. Draw it by the geometry tool bar as done for these models
2. Import it from CAD tools or from the Comsol library.

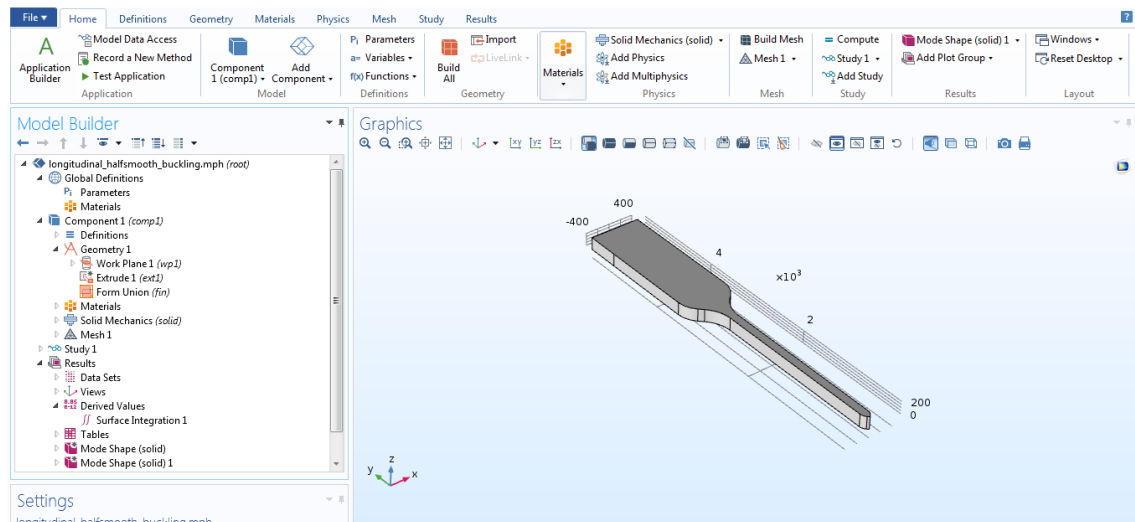
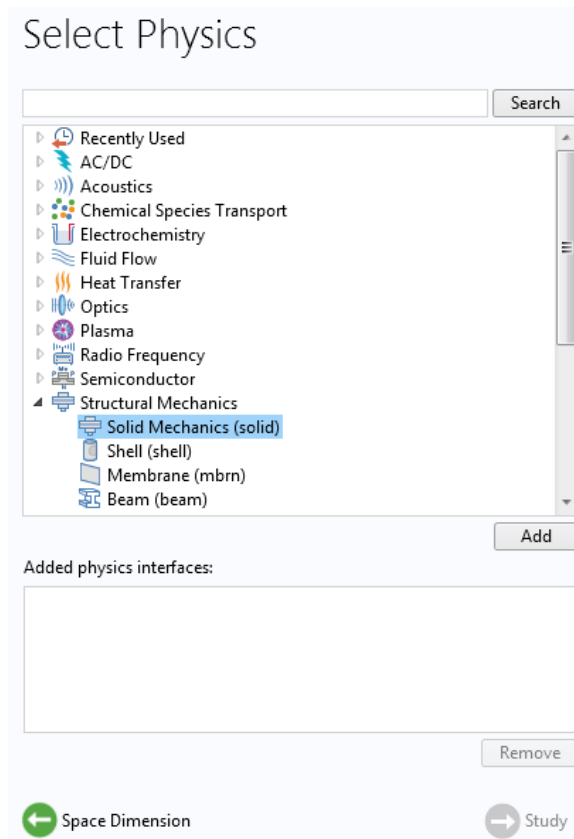


Figure D. 1 Comsol model

The Steps to establish a model:

1. Open Comsol Multiphysics.
2. Choose the model Wizard.
3. Choose 3D.
4. From select physics list as Figure D. 2, select Structural  $\longrightarrow$  Mechanics Solid Mechanics (solid)  $\longrightarrow$  Add  $\longrightarrow$  Study.
5. From select study list, select Linear Buckling  $\longrightarrow$  Done.
6. A new model is ready to put the data. Right click on Global definition as illustrated in Figure D. 3  $\longrightarrow$  Parameters then in the setting window of parameters put all the dimensions that will be used in drawing the model.
7. The parameters value of the dimensions of the model are illustrated at Figure D. 4.



**Figure D. 2 Select Physics window**

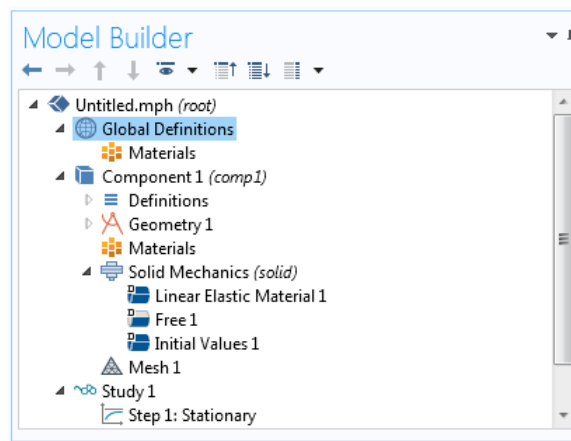


**Figure D. 3 Model Builder bar**

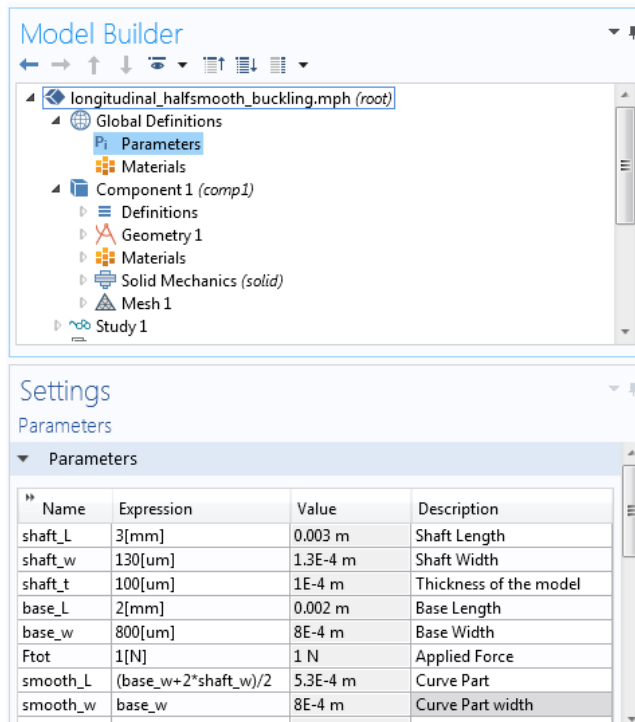


**Figure D. 4 The values of the model**

When using the geometry tools to draw 3D model with the same thickness for all parts of the model, it is preferred to choose work plane to make all the drawing part on 2D then extrude it to the purposed design. Figure D. 5 shows the work plane to draw the model as the first step on 2D. To do that, in the first choose the model geometry as 3D then from geometry tool bar select work plane. From work plane go to plane geometry and then use the suitable figures to draw the model. Figure D. 6 shows the model before using the 2D options such Chamfer and fillet.

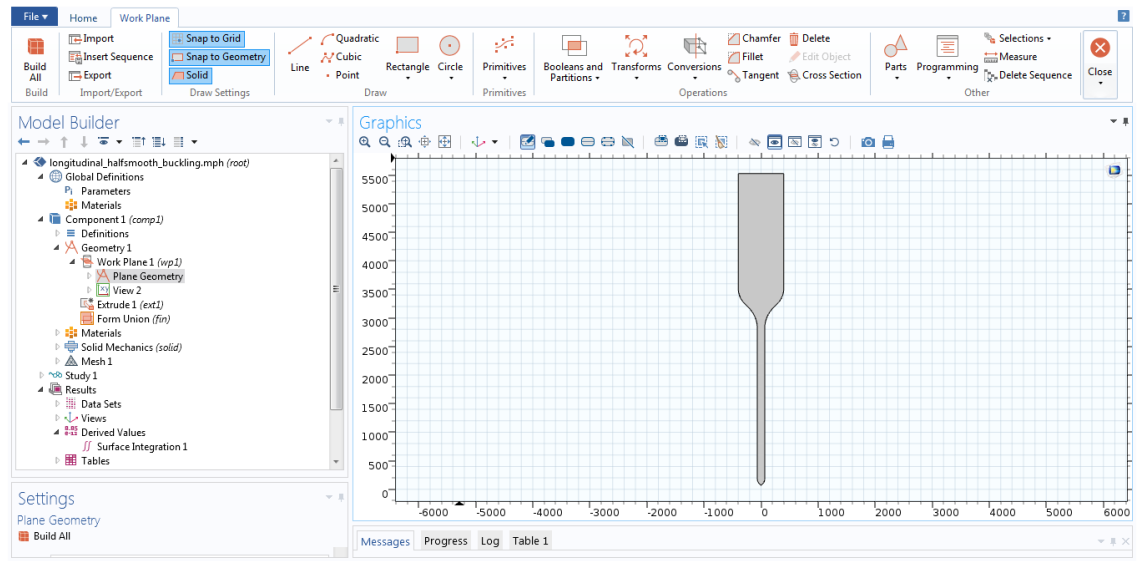


**Figure D. 5 Plane Geometry**

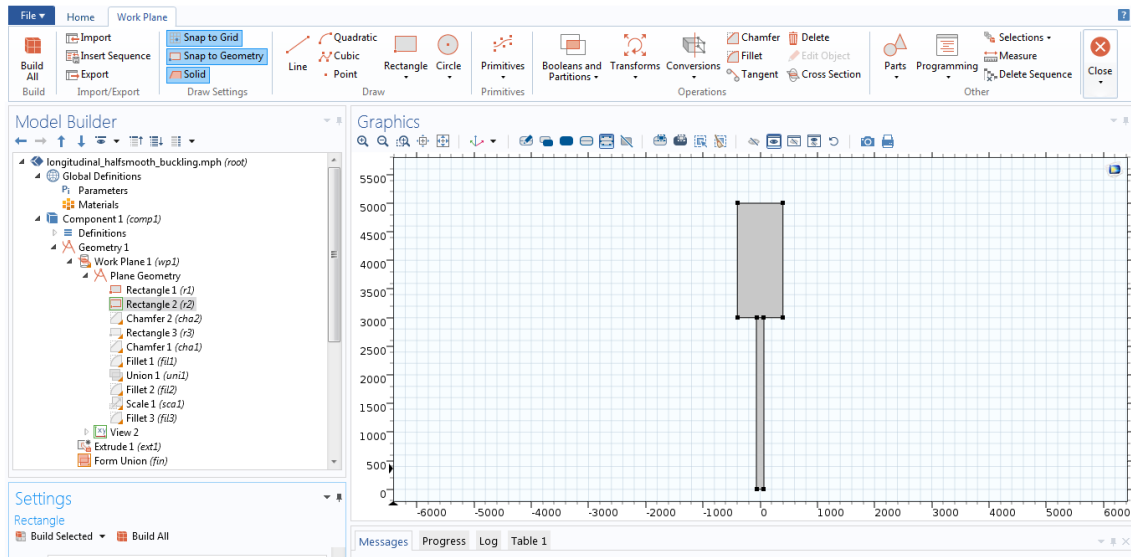


**Figure D. 6 First step**

Figure D. 7 shows the model after select Chamber option to make a sharp tip of the shaft of the electrode.

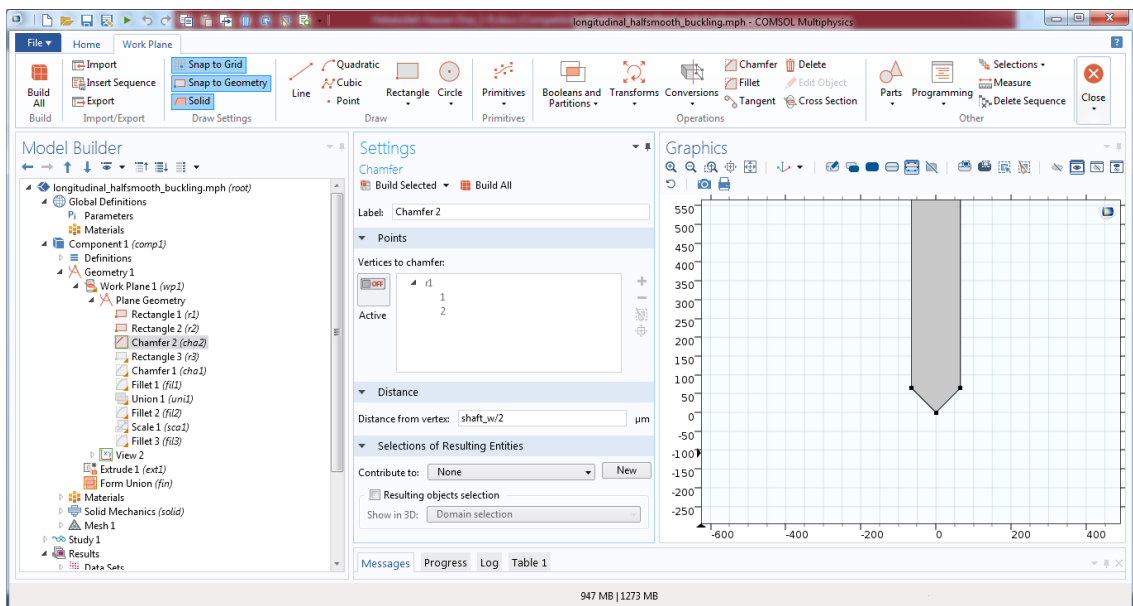


**Figure D. 7 the tip of shaft**

After finishing the shape, from Geometry bar press right click on work plane1 and select Extrude as illustrated in Figure D.8.

The next step is inserting the material. From tool bar select material then Add Material then from the list select MEMS → Semiconductors → Si-Polycrystalline Silicon then select Add to component.

Go to physics then press right click on solid mechanics and select boundary load and then select the face which we will add the force on it as Figure D.9.

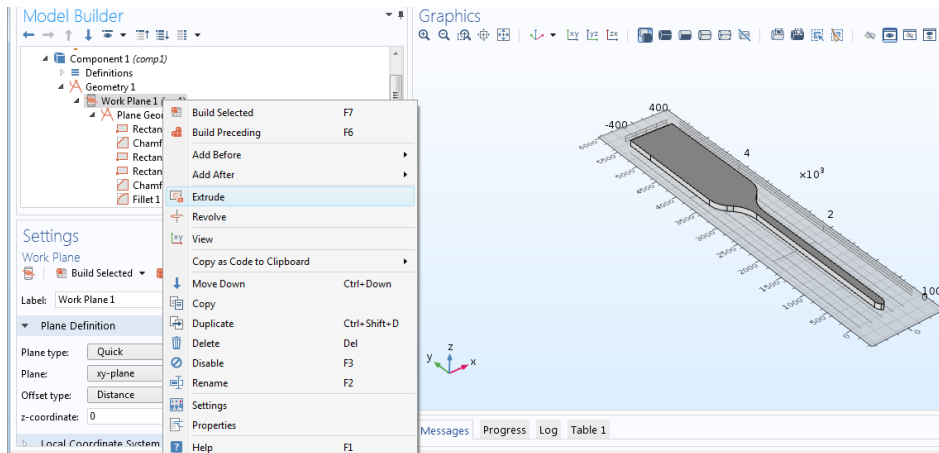


**Figure D. 8 insert the thickness**

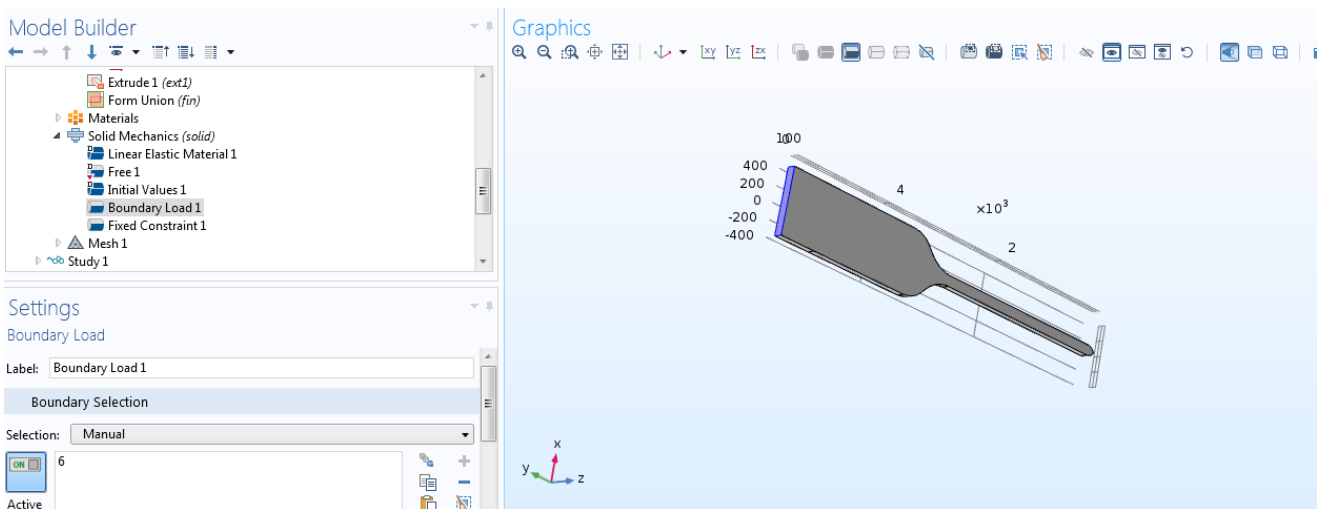


**Figure D. 9 Boundary Load**

In the setting of the Boundary Load go to force and at load type select total force and in Y add 1[N]. Then go to solid mechanics with right click and add fixed constrain then select the tip of the shaft as Figure D.10.

Then at Mesh in Predefined select Extra Fine to get accurate results.

Then go to study and press right click then select parametric sweep to simulate the model with different thickness from 20 $\mu$ m to 200 $\mu$ m. At the setting of Parametric sweep select Parameter name then choose shaft\_t (thickness of the electrode) and at parameter value list put range(20[um],10[um],200[um]). Then press Compute.

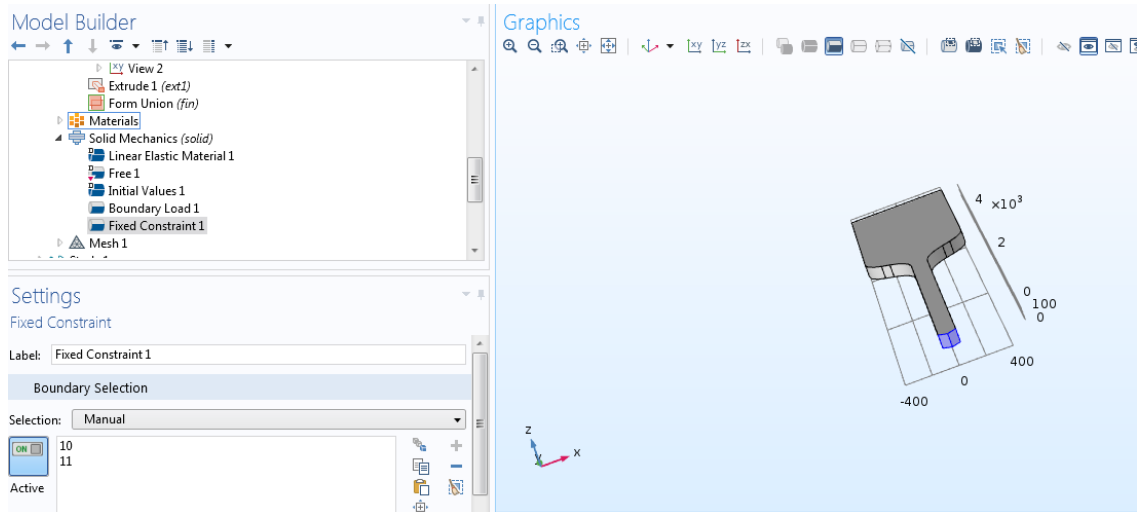


**Figure D. 10 Fixed Constraint**

## المخلص

الهندسة العصبية هي أحد أنواع مجالات الدراسة و الاهتمامات الاكاديمية التي تبحث في الانشطة الكهربائية للجهاز العصبي و بعض الاجراءات والتقنيات التي تستخدم لاكتشاف وتوصيف وتحليل العديد من وظائف الجهاز العصبي. كما أنها تطور تقنيات علاجية غير تقليديه لعلاج عدة أنواع من الاضطرابات العصبية وتساعد في استعادة الوظائف الحسية أو الحركية المفقودة. تستخدم الأقطاب الكهربائية الدقيقة كعناصر رئيسية في أنظمة التحفيز الكهربائي الوظيفي (FES) في الاجراءات الفيزيولوجية الكهربائية. حيث يتم عمل واجهه للاتصال مع الخلايا العصبية الفردية وتسجيل أنشطة الدماغ ، ومن ثم يقومون بتعديل سلوك الخلايا العصبية من خلال التحفيز الكهربائي. يتم اجراء العديد من التعديلات والابتكارات على الاقطاب الكهربائية لتحسين وظائفها ولتيسير استخدامها.

في هذا البحث، يتم تقديم تصميمات مبتكرة من الاقطاب الكهربيه الدقيقة المحفزه للمخ والتي يتم زراعتها داخل القشرة الدماغيه مع الاخذ في الاعتبار متطلبات وتطبيقات زراعه هذه الاقطاب. يتم تصنيع هذه الاقطاب باستخدام تقنيه الانظمه الميكرووالكتروميكانيكية والتي يتم استخدامها في كثير من المجالات الطبية لعلاج بعض الأمراض العصبية مثل الشلل الرعاش والصرع والصداع المزمن والاضطرابات الوهمية وغيرها.

الفصل الاول من رساله يحتوي على مقدمه عن مرض الصرع وتطورات العلاج المستخدم مع التقدم التكنولوجي. وفي الفصل الثاني قدمت الرساله تاريخ ظهور الاقطاب الكهربيه وتطورات استخدامها في علاج الامراض العصبية المختلفه وفي رصد اشارات المخ ثم متطلبات تحسينها وبعض برامج الحاسب المستخدمه لعمل محاكاة لهذه النماذج. ثم يقدم هذا الفصل أيضاً مقدمه تاريخيه عن التقنيه المستخدمه في تصنيع الاقطاب الكهربيه وهي الانظمه الميكرووالكتروميكانيكية. ثم يأتي في الفصل الثالث توضيح لبعض النماذج المقترحه لتقليل الاثار الجانبية الناتجه عن زراعه هذه الاقطاب في المخ مع اختبار لهذه الاقطاب لمقاومه القوه المؤثره وقياس قوه تحملها لهذه الضغوط ومن ثم الوصول لمعرفة أي هذه النماذج يكون أفضل وذلك من خلال برنامج المحاكاه Comsol. وفي الفصل الرابع يتم اجراء نفس الاختبارات ولكن علي اقطاب تكون مناسبه للانسان مع المحاولة للوصول لافضل تصميم. في الفصل الخامس يتم توضيح نوع من الاقطاب حديثه الظهور وهو Optrode والذي يستخدم أيضاً في تحفيز خلايا المخ العصبية ولكن باستخدام الضوء مع وضع تصميم مقترح لهذا القطب. ثم يأتي توضيح لخطوات التصنيع المستخدمه لتصنيع أحد هذه الأقطاب وبعض النماذج الأوليه ثم خطوات تصنيع دوائر مطبوعه لاستخدامها في توصيل هذ الاقطاب مع دوائر خارجيه للقياس منها او للتحفيز بها لاخبارها عملياً على فئران التجارب.

ضع صورتك هنا

مهندس: هبة الله حسن محمد دراز  
تاريخ الميلاد: 1984\9\21  
الجنسية: مصريه  
تاريخ التسجيل: 2014\10\1  
تاريخ المنح: 2019  
القسم: الالكترونيات والاتصالات الكهربيه.  
الدرجة: دكتوراه الفلسفة  
المشرفون:

ا.د. محمد فتحي أبو اليزيد  
ا.د. أمال زكي  
د. حسن مصطفى

المتحنون:

أ.د. محمد فتحي أبو اليزيد (المشرف الرئيسي)  
د. حسن مصطفى (عضو)  
أ.د. محمد رياض الغنيمي (المتحن الداخلي)  
أ.د. السيد مصطفى سعد (المتحن الخارجي)  
استاذ دكتور بقسم الالكترونيات بجامعة حلوان

عنوان الرسالة:

## تصميم وتصنيع الاقطاب الكهربائية المحفزه للمخ بتقنية الأنظمة الميكروالكتروميكانيكية

الكلمات الدالة:

الأقطاب الكهربيه المحفزه للمخ، أنظمة التحفيز الكهربائي الوظيفي ، الانظمه الميكروالكتروميكانيكية .

ملخص الرسالة:

تستخدم الأقطاب الكهربائية الدقيقة كعناصر رئيسية في أنظمة التحفيز الكهربائي الوظيفي (FES) في الاجراءات الفيزيولوجية الكهربيه. حيث يتم عمل واجهه للاتصال مع الخلايا العصبية الفردية وتسجيل أنشطة الدماغ ، ومن ثم يقومون بتعديل سلوك الخلايا العصبية من خلال التحفيز الكهربيه. يتم اجراء العديد من التعديلات والابتكارات على الاقطاب الكهربيه لتحسين وظائفها ولتيسير استخدامها. في هذا البحث، يتم تطوير وتصميم وتصنيع بعض انواع الاقطاب الكهربيه الدقيقه لزراعتها داخل قشرة المخ مع الاخذ في الاعتبار متطلبات وتطبيقات زراعه هذه الاقطاب.



# تصميم وتصنيع الاقطاب الكهربية المحفزه للمخ بتقنية الأنظمة الميكروالكتروميكانيكية

اعداد

هبة الله حسن محمد دراز

رسالة مقدمة إلى كلية الهندسة – جامعة القاهرة  
كجزء من متطلبات الحصول على درجة الدكتوراه  
في  
هندسة الالكترونيات والاتصالات الكهربية

يعتمد من لجنة الممتحنين:

الاستاذ الدكتور: محمد فتحي أبو اليزيد      المشرف الرئيسي

الاستاذ الدكتور: حسن مصطفى      مشرف

الاستاذ الدكتور: محمد رياض الغنيمي      الممتحن الداخلي

الاستاذ الدكتور: السيد مصطفى سعد      الممتحن الخارجي  
استاذ دكتور بقسم الالكترونيات بجامعة حلوان

كلية الهندسة - جامعة القاهرة  
الجيزة - جمهورية مصر العربية

2019

# تصميم وتصنيع الاقطاب الكهربية المحفزة للمخ بتقنية الأنظمة الميكروالكتروميكانيكية

اعداد

هبة الله حسن محمد دراز

رسالة مقدمة إلى كلية الهندسة – جامعة القاهرة  
كجزء من متطلبات الحصول على درجة الدكتوراه

في

هندسة الاكترونيات والاتصالات الكهربية

تحت اشراف

أ.د. أمال زكي

أستاذ

بمعهد بحوث الاكترونيات

أ.د. محمد فتحى ابو اليزيد

استاذ

بكلية الهندسة جامعة القاهرة

د. حسن مصطفى

أستاذ مساعد

بكلية الهندسة جامعة القاهرة

كلية الهندسة - جامعة القاهرة

الجيزة- جمهورية مصر العربية

2019



## تصميم وتصنيع الاقطاب الكهربائية المحفزة للمخ بتقنية الأنظمة الميكروالكتروميكانيكية

اعداد

هبة الله حسن محمد دراز

رسالة مقدمة إلى كلية الهندسة – جامعة القاهرة  
كجزء من متطلبات الحصول على درجة الدكتوراه  
في  
هندسة الالكترونيات والاتصالات الكهربائية

كلية الهندسة - جامعة القاهرة

الجيزة - جمهورية مصر العربية

2019